UNCLASSIFIED
SECURITY CLASSIFICATION OF THIS PAGE

DOCUMENTATION PAGE

Form Approved
OMB No. 0704-0188

AD-A199 961

	1b. RESTRICTIVE MARKINGS: None
	3. DISTRIBUTION/AVAILABILITY OF REPORT: Distribution unlimited; approved for public release
2b. DECLASSIFICATION/DOWNGRADING SCHEDULE	
4. PERFORMING ORGANIZATION REPORT NUMBER(S): 88SRD012	5. MONITORING ORGANIZATION REPORT NUMBER(S): AFOSR-TR- 88-0935
6a. NAME OF PERFORMING ORGANIZATION: GE Research and Development Center; 6b. OFFICE SYMBOL (If applicable):	7a. NAME OF MONITORING ORGANIZATION: AFOSR/NA
6c. ADDRESS (City, State, and ZIP Code): P.O. Box 8, Schenectady, NY 12301	7b. ADDRESS (City, State, and ZIP Code): Building 410, Bolling AFB, DC 20332-6448
8a. NAME OF FUNDING/SPONSORING ORGANIZATION: AFOSR/NA; 8b. OFFICE SYMBOL (If applicable): NA	9. PROCUREMENT INSTRUMENT IDENTIFICATION NUMBER: F49620-85-C-0035
8c. ADDRESS (City, State, and ZIP Code): Building 410, Bolling AFB, DC 20332-6448	10. SOURCE OF FUNDING NUMBERS: PROGRAM ELEMENT NO. 61102F; PROJECT NO. 2308; TASK NO. A2; WORK UNIT ACCESSION NO.

DTIC ELECTE OCT 06 1988 E

11. TITLE (Include Security Classification)
Carbon Monoxide and Turbulence-Chemistry Interactions: Blowoff and Extinction of Turbulent Jet Diffusion Flames (Unclassified)

12. PERSONAL AUTHOR(S): Dr. S.M. Correa

13a. TYPE OF REPORT	13b. TIME COVERED	14. DATE OF REPORT (Year, Month, Day)	15. PAGE COUNT
Final Report	FROM 85 May 1 TO 88 Jun 01	1988, 08, 31	73

16. SUPPLEMENTARY NOTATION

17. COSATI CODES			18. SUBJECT TERMS (Continue on reverse if necessary and identify by block number)
FIELD	GROUP	SUB-GROUP	
21	01		turbulence-chemistry interactions, extinction, turbulent diffusion flames, superequilibrium, laser diagnostics.
21	02		

19. ABSTRACT (Continue on reverse if necessary and identify by block number)

Turbulence/chemistry interactions have been studied experimentally and theoretically in the context of turbulent diffusion flames. The goal is a quantitative understanding of these interactions under a wide range of conditions. These range from low Reynolds number conditions ("weak" interactions, affecting primarily the levels of intermediate species, pollutants and combustion efficiency) to high Reynolds number conditions, where the flame can be extinguished by intense turbulent straining. Jet flames in coflowing air have been emphasized, with a coannular pilot burner used where necessary for stabilization at the burner lip. Fuels have consisted of CO/H_2 mixtures with the fraction of H_2 successively reduced to promote extinction. Reynolds numbers have been increased to the point of blowoff. Major species and temperature have been measured by Raman scattering, and velocity and turbulence have been measured by laser velocimetry. These experiments have provided a comprehensive set of data on CO/H_2 flames, extending to conditions conducive to localized extinction. The data show significant temperature decrements due to finite-rate chemistry but no evidence of localized extinction.

(Continued on back)

20. DISTRIBUTION/AVAILABILITY OF ABSTRACT	21. ABSTRACT SECURITY CLASSIFICATION
X UNCLASSIFIED/UNLIMITED ☑ SAME AS RPT ☑ DTIC USERS	Unclassified
22a. NAME OF RESPONSIBLE INDIVIDUAL: Julian M. Tishkoff	22b. TELEPHONE (Include Area Code): (202)767-0463 / 22c. OFFICE SYMBOL: AFOSR/NA

DD Form 1473, JUN 86 — Previous editions are obsolete. SECURITY CLASSIFICATION OF THIS PAGE: UNCLASSIFIED

19. (Cont'd)

Finally, in the quest for higher Reynolds numbers without macroscopic blowoff, preliminary experiments have been performed on bluff-body stabilized flames; conditions which appear promising have been identified.

The computational effort has identified difficulties with the popular "laminar flamelet" model. These difficulties occur because the flame is not thin, compared with turbulence length scales. On the other hand, the partial equilibrium (p.e.) class of model is shown to be successful for moderate Reynolds number turbulent flames, using both averaged Navier-Stokes and joint pdf/Monte-Carlo implementations. It cannot, however, account for extinction due to assuming p.e. in the radical pool regardless of the turbulence field. A new computational model for a jet flame under the full span of conditions has been developed. In the model, combustion chemistry is represented by two-body shuffle reactions and three-body recombination reactions. The scalar dissipation field is examined for critical values, below which the two-body reactions are assumed to be in p.e. and above which they are assumed to be frozen and the gas therefore unburned. The kinetics of the recombination reactions are activated for the former fraction of the gas. This approach has been implemented in a shear-layer finite-volume averaged-Navier-Stokes model with k-ϵ assumed shape pdf submodels for turbulence. Comparisons with the data obtained in the experiments are very encouraging. In particular, it appears incontrovertible that localized extinction does not occur in CO/H_2 flames because of the ability of radicals to exist over spatially large regions violating the concepts of thin flamelets. The new model is more universal than predecessors, being useful for moderate to high Reynolds number turbulent flames.

Two other computational studies have been completed. Firstly, the p.e. approach for CO/H_2 flames has been extended to include finite rate CO chemistry, so requiring a third scalar for mathematical description. This has shown that the CO chemistry is fast enough that CO reaches equilibrium with radical species relatively rapidly, after which the simpler p.e. model is adequate. Secondly, the compressible strain field and flow about a cylinder have been examined because higher velocities required for blowoff place the flow in the compressible regime; the principal finding is an unexpected alleviation of strain, and therefore an unexpected stabilization of the flame.

These studies have led to an experimentally substantiated theoretical understanding of turbulent diffusion flames under conditions ranging from weak to strong turbulence-chemistry interactions.

TABLE OF CONTENTS

LIST OF ILLUSTRATIONS

LIST OF ILLUSTRATIONS (Cont'd)

LIST OF TABLES

1. INTRODUCTION AND SUMMARY

This report summarizes work performed in the period May 1, 1985 to June 1, 1988 for the Air Force Office of Scientific Research under Contract F-49620-85-C-0035. Dr. Julian Tishkoff was the Project Monitor. The work was performed and the report has been prepared by the Engineering Systems Laboratory at the GE Research and Development Center.

This section summarizes the technical problem that was considered and the state of understanding of turbulence-chemistry interactions, outlines present results, and suggests directions for future work as developed in the course of the program.

1.1 Problem

Non-premixed turbulent combustion occurs in practical equipment ranging from aircraft and industrial gas-turbine engines to relatively simple domestic units. Although the traditional fast chemistry or "mixed-is-burned" [Libby and Williams (1980)] model for combustion is useful for understanding the gross aerodynamics in many of these combustion systems, there is an increasingly important range of phenomena that cannot be so accounted for. For example, finite-rate radical pool chemistry has been shown to produce excess radicals during combustion. Consequently, it is very influential in thermal NO_x and CO emissions from atmospheric flames [Drake et al. (1987)] and degrades combustion efficiency in supersonic combustion systems [Correa and Mani (1987)]. Localized turbulence effects may be strong enough to induce extinction, and are due to the chemistry not being fast compared with the turbulent microscales, as has been demonstrated in laminar CH_4 flames [Miller et al. (1984)]. High-altitude blowout limitations on aircraft combustors are caused, in part, by slow kinetics due to the low densities. It seems clear that, as the limits of combustion equipment are expanded, it is more and more important to account fundamentally for finite-rate chemical kinetics and for the increasingly strong interaction with turbulence.

Kinetic mechanisms are known for only the simple fuels and even those are rather lengthy. Hydrogen combustion in air involves at least eight species (H_2, O_2, H_2O, N_2, O, OH, H, HO_2, and so forth) and associated reactions. Hydrocarbon combustion involves about 30 species and 100 reactions [Westbrook and Dryer (1981)]. These mechanisms add too many transport equations to kinetics models to be usable in other than laminar flame calculations. Even in laminar flames, the mathematical stiffness of the resulting set of equations requires special numerical methods.

Simpler models of the chemical kinetics are required for *turbulent* flames, where closure of turbulent flux and chemical source terms would increase the difficulties caused by a large set of species. Such models can be formulated by sacrificing a complete description of the chemistry. Examples are the partial-equilibrium models used for H_2 [Janicka and Kollman (1979)] and CO/H_2 [Correa et al. (1984)] flames and the multistep (three or four step) schemes for CH_4 [Bilger and Kee (1987)].

The development of nonintrusive laser-based diagnostics has permitted an in situ examination of turbulent flames. Laser Doppler Velocimetry (LDV), Raman scattering (for correlated measurements of major species and temperature), and pointwise and planar fluorescence (of OH radicals) have been used in this laboratory and in other laboratories for quantitative, time-resolved measurements in turbulent reacting flows. Significant contributions to the understanding of turbulent combustion have resulted, such as superequilibrium free radical formation; enhanced thermal NO_x; CO/H_2 partial equilibria; and a start on the problems of local extinction and fuel-bound nitrogen.

The geometry of a fuel jet in a coflowing air stream has received much attention for both experimental and computational reasons. Experimentally, the apparatus is simple, optically accessible, and results in a volume of heated gas not large enough to cause laser beam-steering problems. Computationally, the turbulence is describable by semiempirical models (such as the two-equation class), and the flow is dominated by axial convection leading to *parabolic* governing equations (thus greatly simplifying the problem of discretization of differential operators). Because of these advantages, studies in jet flames have contributed much to turbulent combustion.

Turbulent transport in axisymmetric or "round" jets is worth further mention. While it is now clear that gradient diffusion does not hold in the near field of a planar mixing layer, such models can explain to a large extent turbulent transport in fully developed jets. In the mixing layer, the primary vortex-pairing instability leads to growth of large-scale periodic structures and inviscid entrainment into their cores [Koochesfahani and Dimotakis (1986)]. Except for homogenization within these cores, no significant transport is effected by small-scale structures. In round jets, however, the additional instability mechanisms present, e.g., circumferential waves, lead to fully developed three-dimensional turbulence, with a spectrum of length scales. Random large-scale structures ("intermittency") can be accounted for with conditional modeling. Recent experiments in water jets have indicated the presence of unmixed ambient fluid at the centerline, which has been held up as proof that periodic large-scale structures do exist in jets [Dahm and Dimotakis (1987)]. Such structures are not seen in gaseous jets. Moreover, the structures were imaged using a concentration-sensitive technique, i.e., relying on diffusion and thus dependent on the Schmidt number, Sc. Since $Sc \simeq 600$ in water, it is likely that the supposedly "unmixed" fluid had transferred momentum albeit not mass. In gaseous jets, $Sc \simeq 1$ and such behavior would not occur. Therefore, we must conclude that round gaseous jets do not exhibit periodic large-scale structures in the fully developed regions and that gradient-diffusion models, which assume that transport is due to small scales, are at least useful.

As the Reynolds number of the jet flow is increased, the flame blows off the lip at the exit of the nozzle. Thus strong turbulence-chemistry interactions leading to turbulent extinction cannot be studied in the region well downstream of the exit, which is relatively free from the influence of the initial conditions. A coannular pilot flame burning a small amount of premixed fuel and air has been used in our laboratory to stabilize the flame in this initial region without influencing the downstream region significantly. Turbulent extinction effects have been looked for in the region 10 to 20 jet diameters downstream of the exit, using temperature-mixture fraction scattergrams based on Raman measurements. Mixtures of CO and H_2 were used as the fuel because the chemistry is known reasonably well and the extinction limits approach those of hydrocarbons, which are the fuels of practical relevance.

This work has shown that it is overly simplistic to consider turbulent flames as ensembles of laminar flames subjected to strain. Essentially, the reason for this oversimplification is that the different kinetic steps in a combustion mechanism have widely disparate time-scales (e.g., chain-branching reactions are much faster than recombination reactions). The fastest reactions can interact with the local turbulence in a "flamelet" manner while, for the slow reactions, the Damkohler numbers are relatively small and the flame is more akin to a well-distributed zone of reaction. This has led us to a new model for turbulent flames in which the fast reactions are described by a strained flamelet theory, while the radicals they produce are considered to be transported, and react according to the theory used for lower Reynolds number flames.

To increase the interaction between turbulence and chemistry and the probability of localized extinction, the jet velocity in the pilot-stabilized burner has been increased; however, only a small increase is possible before the flame blows off the lip. Preliminary experiments with a non-premixed

bluff-body-stabilized flame have been far more successful. The flame appears stretched and extinguished in a region well away from the inlet plane. Moreover, even with methane fuel, the flame is blue, which allows Raman scattering diagnostics to be used.

1.2 Statement of Work

A. Improve and expand the database for turbulent $CO/H_2/N_2$ jet flames utilizing pulsed Raman spectroscopic measurements.

B. Use experimental results to evaluate assumptions made in formulating prediction methods based on probability density functions and on laminar flamelets.

C. Modify the experimental facility to conduct turbulent jet combustion tests at Reynolds numbers greater than 9000 without blow-off at nozzle. Use PLIF* to visualize extent of extinction.

D. Model a $CO/H_2/N_2$ jet flame at the 8500 Reynolds number using two-scalar and flamelet approaches.

E. Conduct experiments on two $CO/H_2/N_2$ jet flames at Reynolds numbers above 9000 under conditions of local extinction.

F. Formulate alternatives to the partial equilibrium chemical kinetics model previously used to predict the chemistry of carbon monoxide flames.

G. Extend laminar flamelet model for hydrocarbon flames

1.3 Project Accomplishments

The goal of this three-year research program was a quantitative understanding of turbulence-chemistry interactions in non-premixed turbulent flames. These turbulence-chemistry interactions are responsible for excess radical formation, which leads, for example, to incomplete combustion in scramjet engines and to increased pollutant formation in conventional combustors. In very intense turbulence, these interactions can lead to flame extinction.

Specific accomplishments of the program include:

1. Reanalysis of preexisting Raman data using high-temperature correction factors. Reassessment (favorably) of partial equilibrium/joint p.d.f. Monte-Carlo models.
2. Development of Raman scattering system for fuels containing enough carbon to make chemiluminescence an issue.
3. Experimental identification of a CO/H_2 fuel mixture with Rayleigh cross section matched between products and reactants in diffusion flame situation, and with critical strain rate for extinction approaching that of methane.
4. Development of an analytical theory for the effect of compressibility on critical strain rate for flamelet extinction.

---

* PLIF: Planar Laser-Induced Fluorescence

5. Development of a three-variable model for CO/H_2 flames including finite-rate CO kinetics.
6. Development of a pilot-stabilized turbulent diffusion flame burner for combustion at high Reynolds number, approaching extinction.
7. Space- and time-resolved Raman scattering measurements of temperature and concentrations of major species in flames of CO/H_2 mixtures at conditions approaching extinction.
8. Development and application of a new class of flamelet models for turbulent diffusion flames. Comparison of results of new model with data in high Reynolds number flame.
9. Preliminary experiments with a bluff-body stabilized burner used to increase the Reynolds number of the flame.

2. TECHNICAL DISCUSSION

This section describes experimental and modeling studies of turbulent combustion, performed under this contract, in more detail.

2.1 Reanalysis of Prior Data and Comparison with Joint pdf/Monte Carlo Model

A significant improvement in the analysis of the raw Raman data for the Re = 8500 flame of 40% CO, 30% H_2, 30% N_2 fuel ("medium-Btu gas" or "syngas") was made by correcting for the fraction of Raman signal in the Raman band pass of the major species (O_2, N_2, H_2, H_2O, CO) at elevated temperatures. This correction factor was inadvertently set to unity in prior analyses of the raw Raman signals [Drake et al. (1984)]. The significance of this correction to the measured Raman signal at elevated temperatures arises from the fact that the Raman exit slits have a finite width caused by space limitations and noise considerations; therefore significant portions of the hot Raman bands at higher temperatures do not fall within the finite exit slit and are not measured. The correction factors required to account for the limited Raman spectral band pass are a function of the species involved, temperature, width of the exit slit, and the wavelength region covered by the physical Raman band pass. They were calculated by determining the fraction of the predicted Raman vibrational contour in the Raman bandpass using codes developed by Lapp et al. (1983). Table 1 lists typical values of the correction factors for the major species involved. As can be seen, the correction factors for H_2 and H_2O are significantly in excess of unity, whereas those for CO, O_2, and N_2 are less than unity. Tables 2 and 3 compare typical mean values of temperature, mixture fraction, and mole fractions of major species obtained at $x/d = 25$ in the Re = 8500 syngas flame for two cases: in Table 2, all correction factors have been set to unity, while in Table 3, the correction factors assume proper values (listed in Table 1). The mean temperature values are less sensitive to nonunity correction factors since temperature is based upon the sum-of-mole-fraction method, which is not significantly affected by the corrections. However, the mole fractions of some major species – including CO, H_2O, and H_2 – are found to differ by as much as 20%. The mixture fraction values, which are based on the hydrogen element, are found to increase by 20%, corresponding to the increase in the mole fractions of H_2 and H_2O.

Because CO_2 has a particularly complicated Raman contour caused by flame resonance interactions between the relevant vibrational transitions, its concentration was determined initially by assuming that the atomic ratios of carbon and hydrogen are invariant throughout the flame and are equal to the carbon-to-hydrogen ratio in the fuel, i.e.,

$$\frac{(CO) + (CO_2)}{(H_2) + (H_2O)} = \left[\frac{(CO)}{(H_2)}\right]_{initial} = \frac{4}{3} \qquad (1)$$

Since the mole fractions of CO, H_2, and H_2O are known from their measured Stokes vibrational Raman scattering intensities, instantaneous mole fractions of CO_2 could be calculated. This approach was not totally satisfactory because (1) it ignores preferential diffusion effects that have been observed in turbulent H_2 jet diffusion flames [Drake et al. (1982)], and (2) it does not permit a totally independent measure of temperature from the sum of the mole fractions of all major species.

Because of the reasons mentioned above, this approach for measuring CO_2 was abandoned. Instead, a laminar, premixed porous plug burner was used for a series of calibration experiments. Temperatures were measured in the center of the flame 1 cm downstream from the burner in stoichiometric H_2-air mole% in the burnt gas. Flame temperatures were independently controlled by

Table 1
High-temperature correction factors for vibrational Raman scattering used to correct fraction of hot bands of various species falling outside their respective exit slits.

Temp. (K)	O_2	CO	N_2	H_2O	H_2
300	1.00	1.00	1.00	1.000	1.000
600	0.975	0.994	1.019	1.001	1.014
900	0.914	0.966	1.009	1.011	1.060
1200	0.848	0.922	0.982	1.058	1.133
1500	0.799	0.876	0.953	1.141	1.229
1800	0.769	0.839	0.932	1.270	1.345
2100	0.756	0.812	0.922	1.440	1.479
2400	0.757	0.796	0.922	1.650	1.629
2700	0.768	0.790	0.932	1.900	1.795
3000	0.787	0.792	0.950	2.159	1.976

Table 2
Temperature and mole fraction of major species at x/d = 25, obtained without correcting for high-temperature effects (correction factors set to unity).

(30% H_2, 40% CO, 30% N_2) Re = 8500, x/d = 25

Position (r/a)	Temperature T/2000 K	Mole Fraction CO_2	O_2	CO	N_2	H_2O	H_2	Mixture Fraction Conv.	Favre
.63	0.600	0.084	0.007	0.233	0.489	0.105	0.075	0.443	0.448
1.89	0.687	0.099	0.012	0.189	0.530	0.114	0.049	0.385	0.39
3.15	0.722	0.110	0.034	0.127	0.587	0.109	0.024	0.297	0.293
4.39	0.647	0.101	0.084	0.054	0.655	0.090	0.008	0.199	0.176
5.66	0.478	0.061	0.139	0.021	0.706	0.062	0.002	0.117	0.081
6.92	0.333	0.035	0.175	0.010	0.733	0.037	0.001	0.059	0.033
8.18	0.229	0.017	0.194	0.004	0.757	0.019	0.001	0.023	0.011
9.44	0.159	0.005	0.208	0.001	0.770	0.007	0.000	0.004	0.001
10.69	0.146	0.004	0.209	0.001	0.772	0.004	0.000	0.001	0.000

Table 3
Temperature and mole fraction of major species at $x/d = 25$ corrected for high-temperature vibrational bands using the correction factors listed in Table 1.

Position (r/a)	Temperature $T/2000$ K	Mole Fraction CO_2	O_2	CO	N_2	H_2O	H_2	Mixture Fraction Conv.	Favre
0.63	0.638	0.080	0.005	0.193	0.505	0.122	0.090	0.541	0.541
1.89	0.739	0.093	0.007	0.144	0.545	0.141	0.062	0.504	0.506
3.15	0.785	0.104	0.025	0.085	0.605	0.141	0.032	0.408	0.396
4.39	0.699	0.096	0.072	0.025	0.676	0.113	0.010	0.267	0.225
5.66	0.504	0.059	0.129	0.004	0.725	0.072	0.003	0.145	0.093
6.92	0.343	0.034	0.169	0.000	0.746	0.040	0.001	0.067	0.036
8.18	0.231	0.016	0.191	0.000	0.763	0.019	0.001	0.024	0.011
9.44	0.159	0.005	0.207	0.000	0.771	0.007	0.000	0.004	0.001
10.69	0.146	0.004	0.209	0.000	0.773	0.004	0.000	0.001	0.000

inserting a series of stainless steel screens upstream of the measurement zone to increase the radiative heat loss. Figure 1 shows the comparison of temperature measurements with radiation-corrected silica-coated fine wire (0.176 mm-coated bead diameter) Pt/PtRh thermocouples with temperatures measured by pulsed Raman scattering using the N_2 Stokes/anti-Stokes ratio method. The results show excellent agreement – deviations are equal to the expected error in the Raman measurements (+50 K). Figure 2 shows the calculated apparent CO_2 mole fraction calculated from the measured CO_2 Stokes vibrational Raman intensity, assuming that the percentage of CO_2 vibrational Raman band in the spectrometer bandpass is independent of temperature. Thus, for the spectral bandpass used, the calculated apparent CO_2 mole fraction was constant from 300 to 1000 K and then slowly increased with temperature. However, the total variation was less than 20% from 300 to 1700 K. Apparent correction factors for CO_2 were then added to the Raman data reduction program, and the previous Raman data for the Re = 8500 turbulent $CO/H_2/N_2$ jet diffusion flame were reanalyzed.

Figure 3 shows the mean temperature obtained using two methods, viz., SAS and sum of mole fraction. Figure 4 shows the radial variation of major species H_2O, CO, CO_2, and O_2 at $x/d = 10$. These data are compared with model calculations in detail and are reported next; see also Correa et al. (1988).

The results of the partial-equilibrium/Monte Carlo model [Pope and Correa (1986)] have again been compared with data on the non-premixed 40% CO, 30% H_2, 30% N_2 "syngas" jet flame in coflowing air [Correa et al. (1988)]. The Raman data on major species, density, and temperature are those of Drake et al. (1984) corrected here for high-temperature effects as described above. The Raman data are compared at three axial locations, (x/d = 10, 25, and 50); $x/d = 50$ corresponds approximately to the visible length of the flame.

Radial profiles of the Favre-averaged mean mixture-fraction ($\tilde{\xi}$) agree quite well at $x/d = 10$ (Figure 5) except that the jet is predicted to have decayed too slowly on the centerline, and $\tilde{\xi}$ is slightly overspread at the boundary. These differences are exaggerated in the mean density normalized by that of air (Figure 5). The central region of the jet is hotter (lower density) than indicated by the data. Temperature profiles (Figure 6) further confirm this discrepancy and also indicate a difference of about 100 K in the off-axis peaks. Nitrogen concentrations plotted in Figure 6 show better agreement. It should be recalled that the mixture fraction data are based on the measured H_2 and H_2O concentrations. More will be said below about this. Some of the other mean major species concentrations are shown in Figure 4 as discussed earlier. Compared with the data, CO is underpredicted by 12% at worst, H_2 is overpredicted by about 10%, and CO_2 is overpredicted, which is consistent with a carbon balance. The jet spread is again slightly overpredicted. The discrepancies in the core seem consistent with overpredicting the amount of CO burned and therefore the temperature. The oxygen profiles also appear to agree reasonably well.

Mean mixture fraction and density at $x/d = 25$ show that the jet spread is predicted quite well, but the centerline mixture fraction is about 10% too low (Figure 7). Correspondingly, since the gas is predicted to be closer to stoichiometric, the temperature is higher by about 150 K than measured in the central region (Figure 8). The spread rate appears to be quite reasonable. Once again, the nitrogen profiles (Figure 8) agree well, except in the central region, i.e., $r/a < 4$.

Mean major species concentrations at $x/d = 25$ are shown in Figure 9. The agreement is much better than presented in Pope and Correa (1986) because of the changes in the Raman data. Here CO is underpredicted by at worst 10%, and O_2, H_2, and CO_2 are predicted very well.

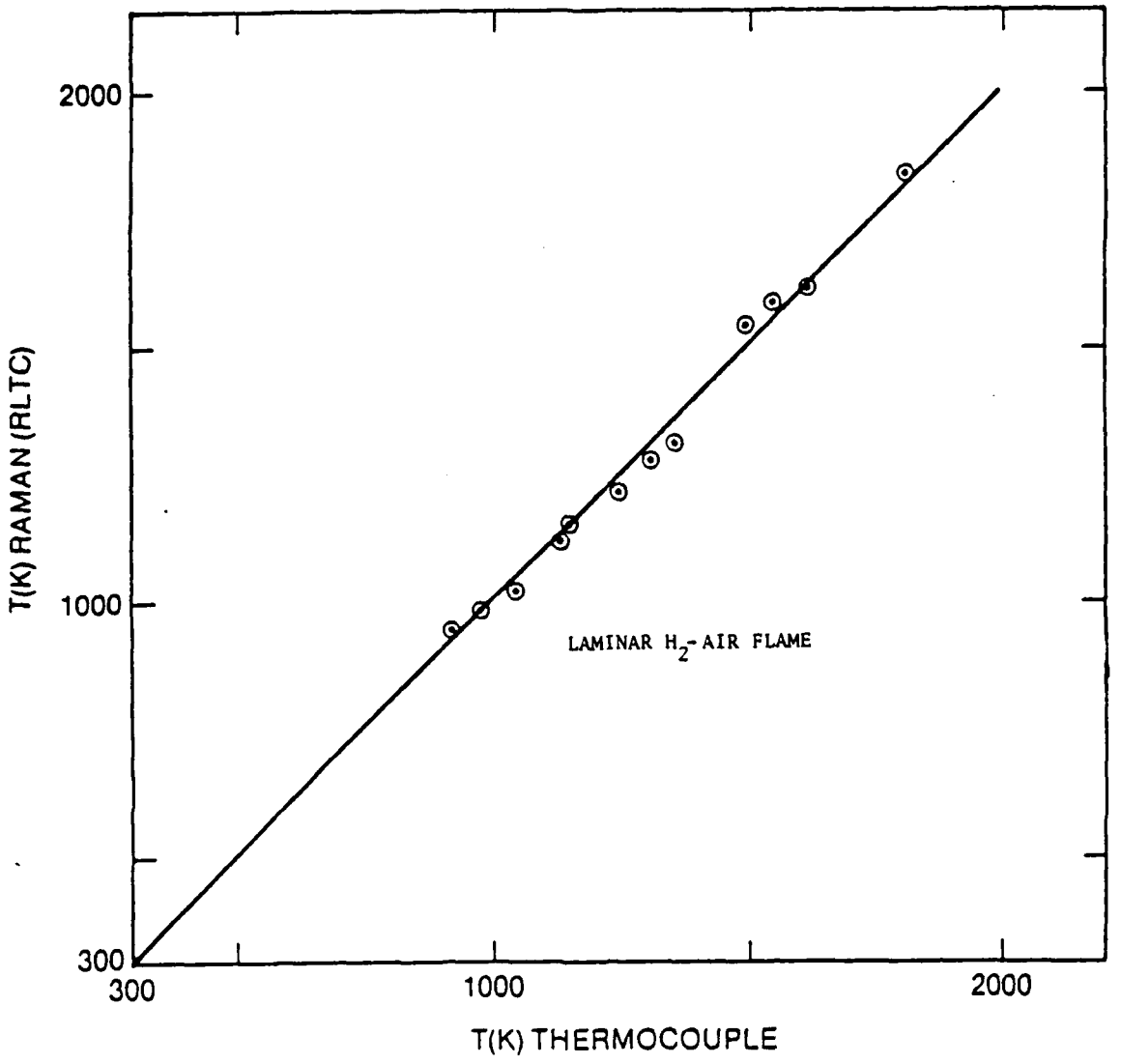

Figure 1. Comparison of temperatures measured by radiation-corrected thermocouples and by pulsed Raman scattering.

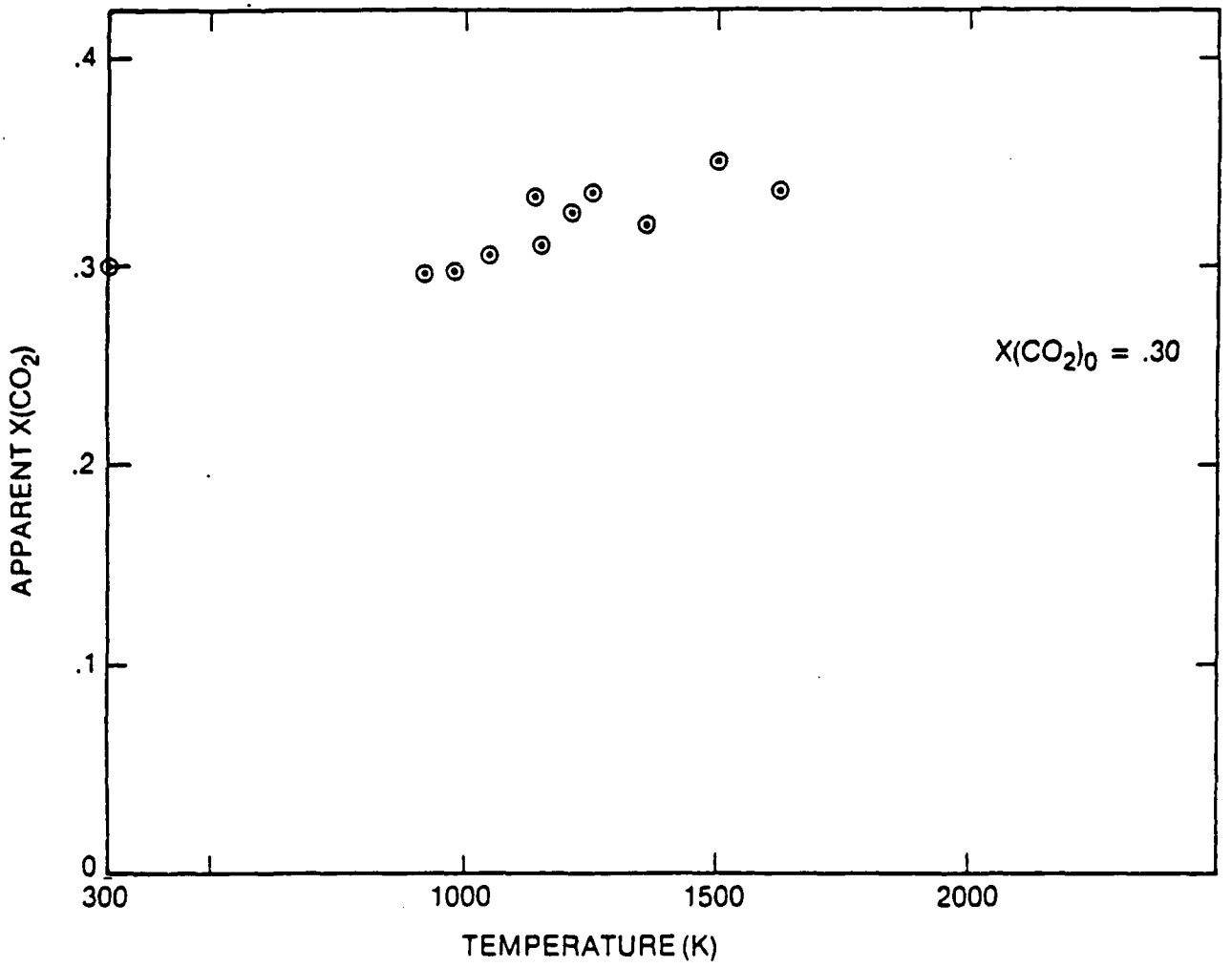

Figure 2. Apparent CO_2 mole fraction from measured CO_2 Stokes vibrational Raman intensity.

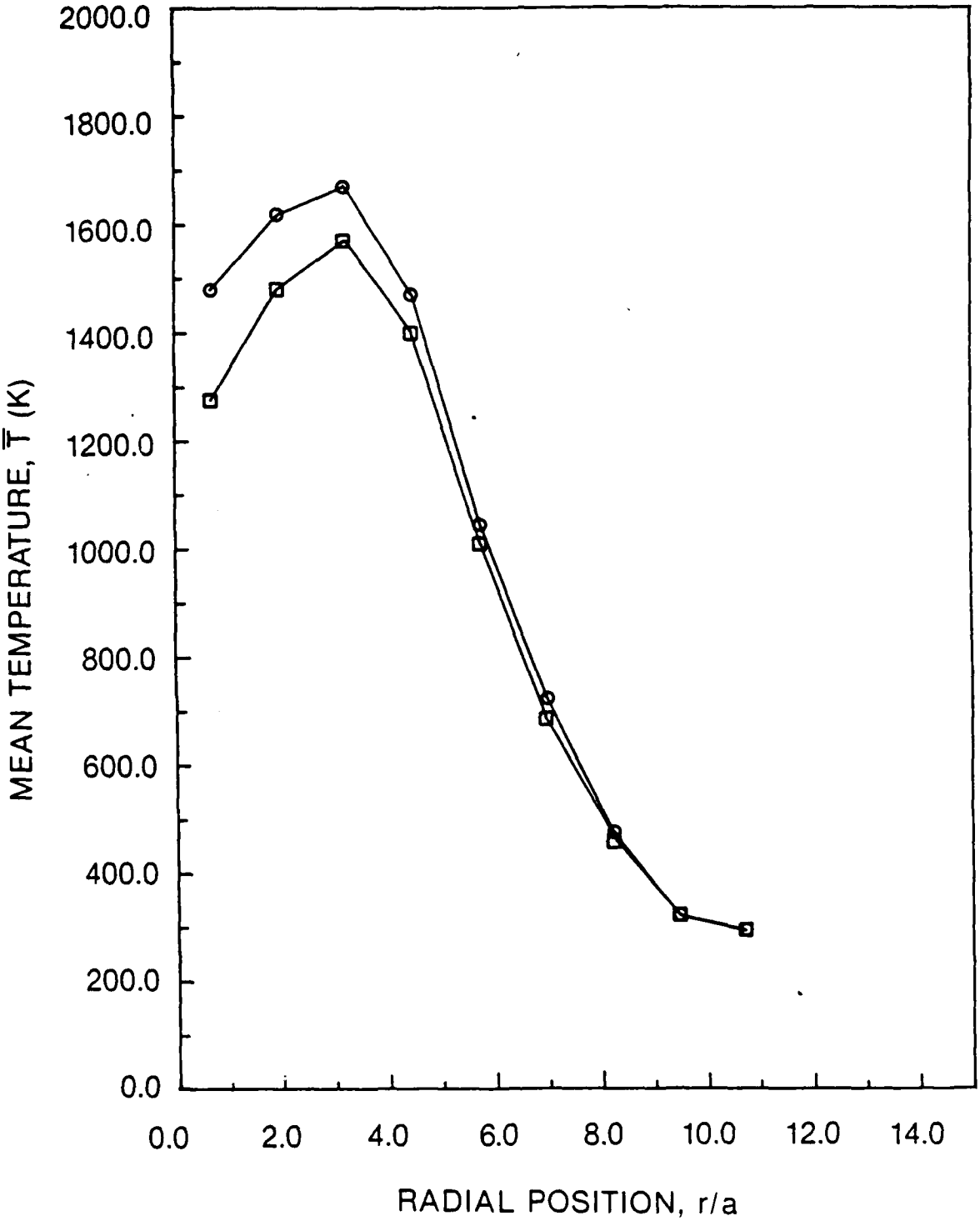

Figure 3. Comparison of radial temperature profiles using SAS method (○) and sum-of-mole fraction method (□) at $x/d = 25$.

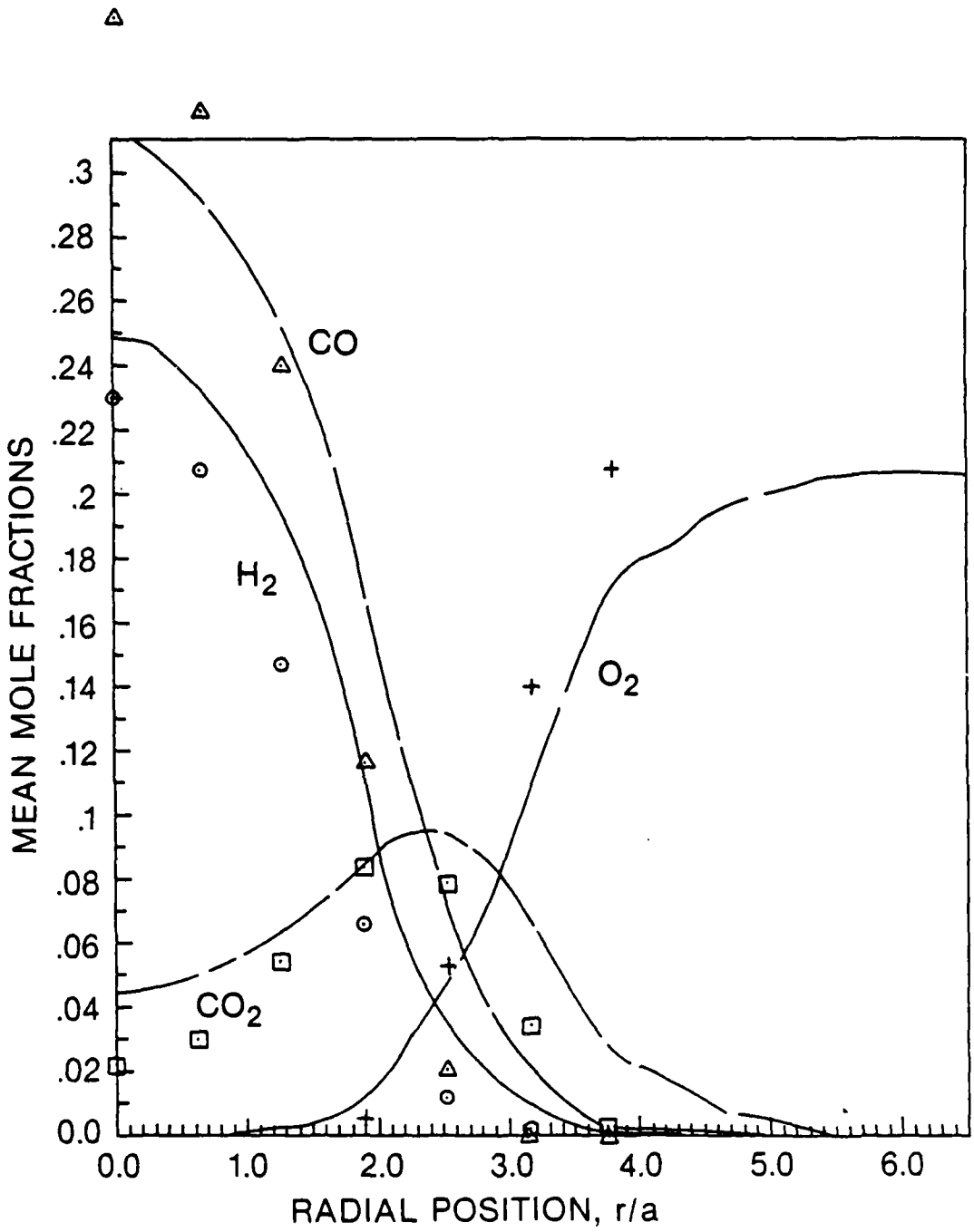

Figure 4. Mean concentrations of major species ($\overline{X_i}$) at $x/d = 10$.

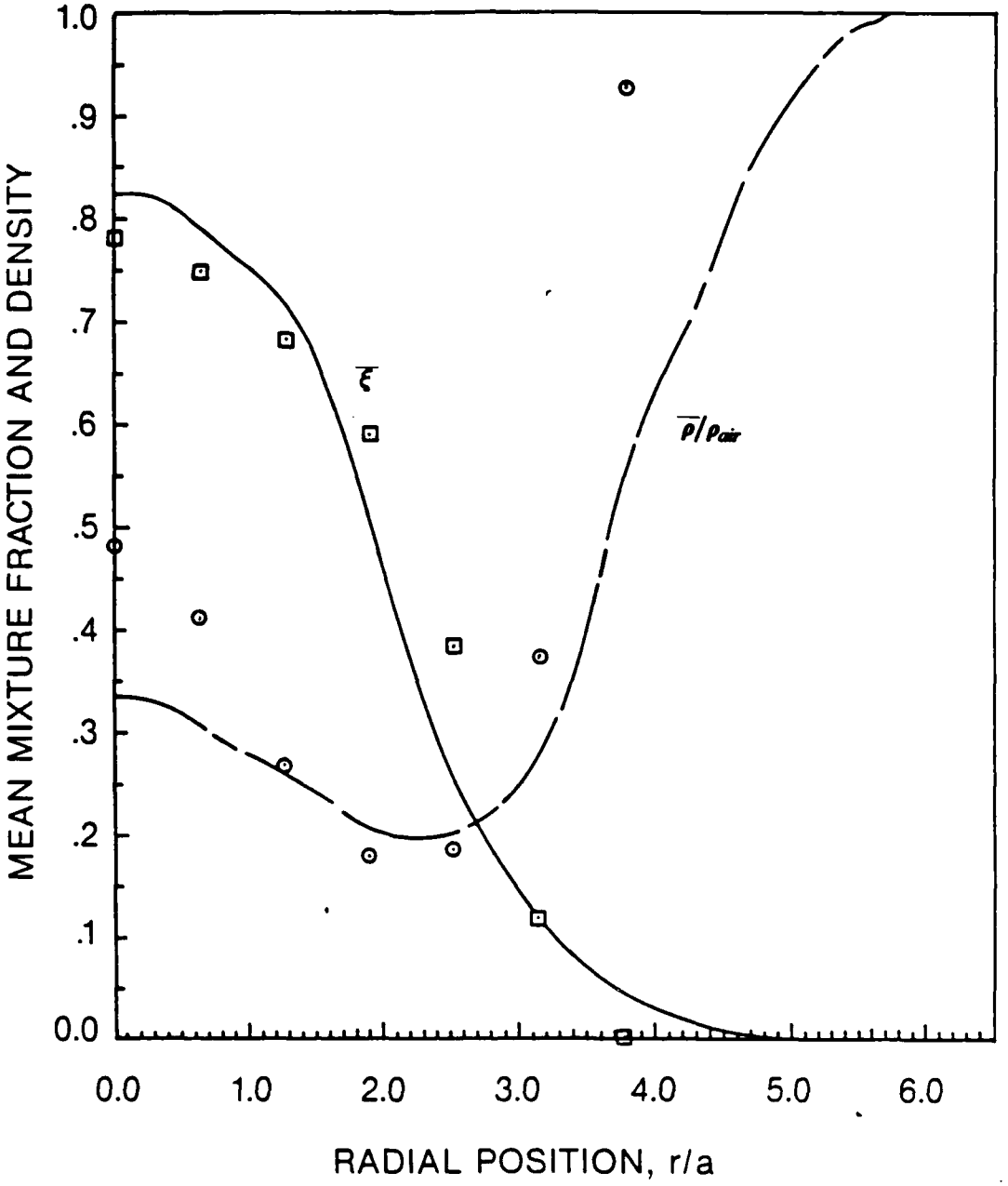

Figure 7. Mean mixture fraction ($\bar{\xi}$) and density ($\overline{\rho}/\rho_{air}$) at x/d = 10.

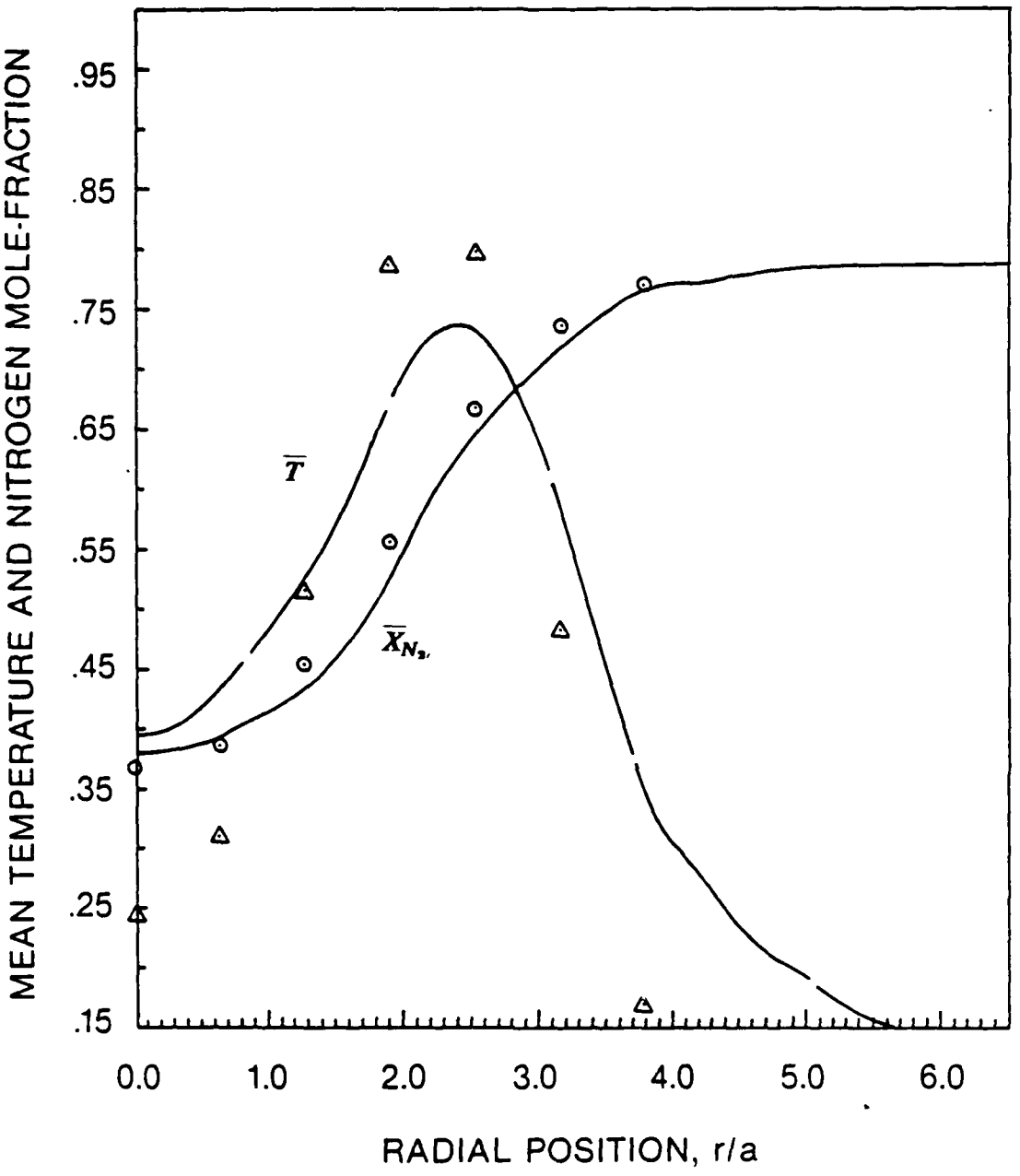

Figure 6. Mean temperature ($\overline{T}$) and nitrogen mole-fraction ($\overline{X}_{N_2}$) at $x/d = 10$.

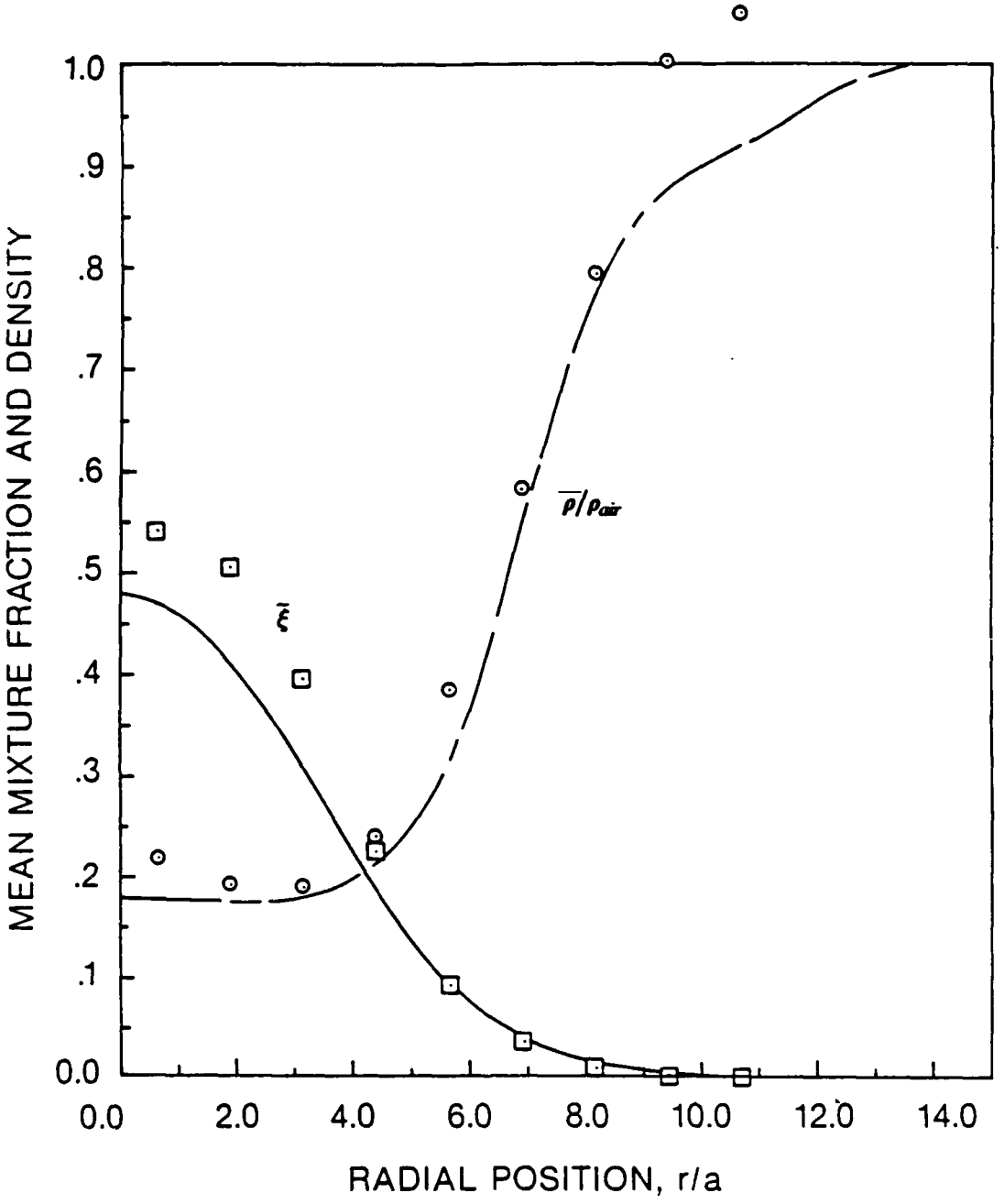

Figure 7. Mean mixture fraction ($\tilde{\xi}$) and density ($\overline{\rho}/\rho_{air}$) at $x/d = 25$.

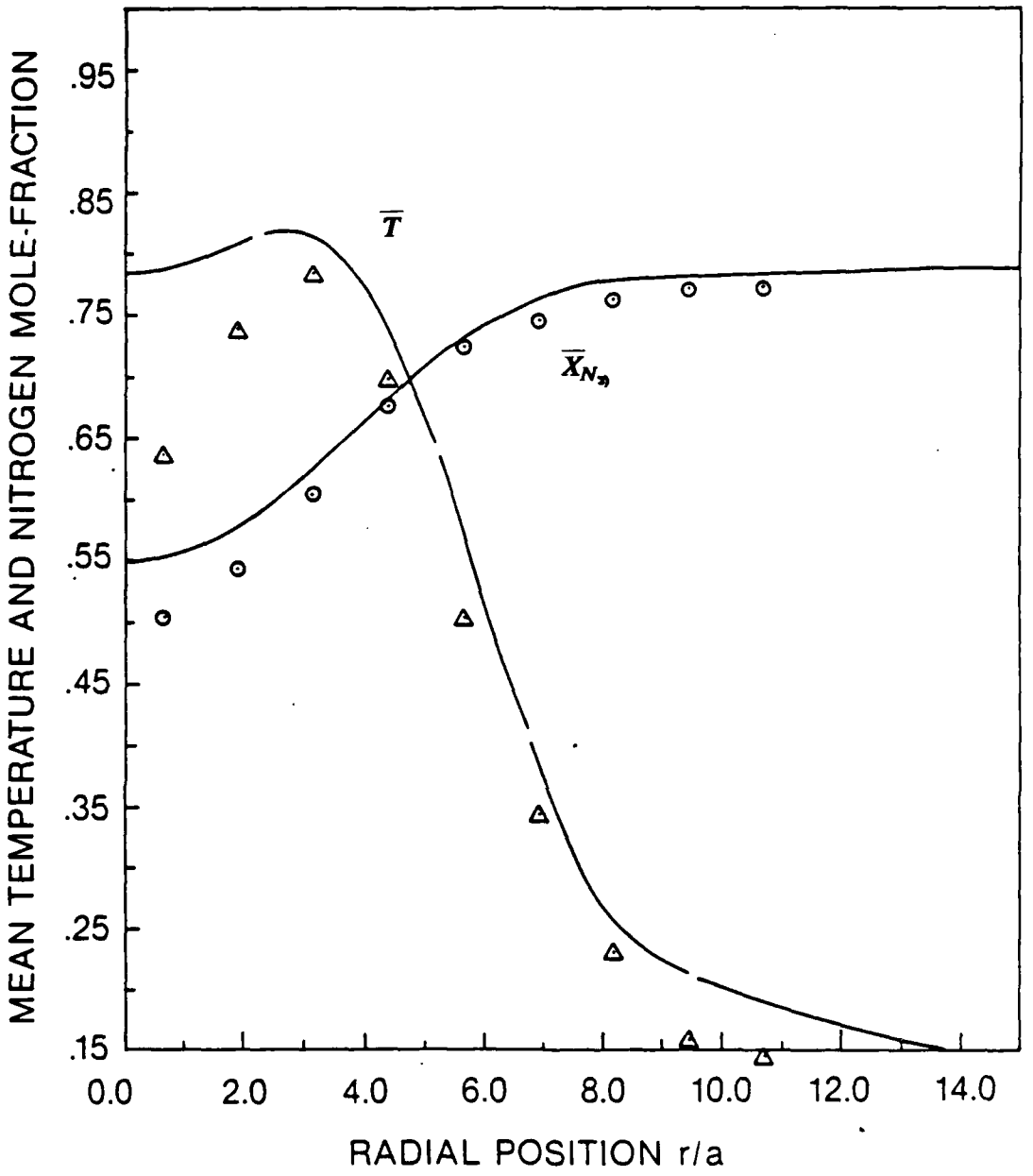

Figure 8. Mean temperature ($\overline{T}$) and nitrogen mole-fraction ($\overline{X}_{N_2}$) at x/d = 25.

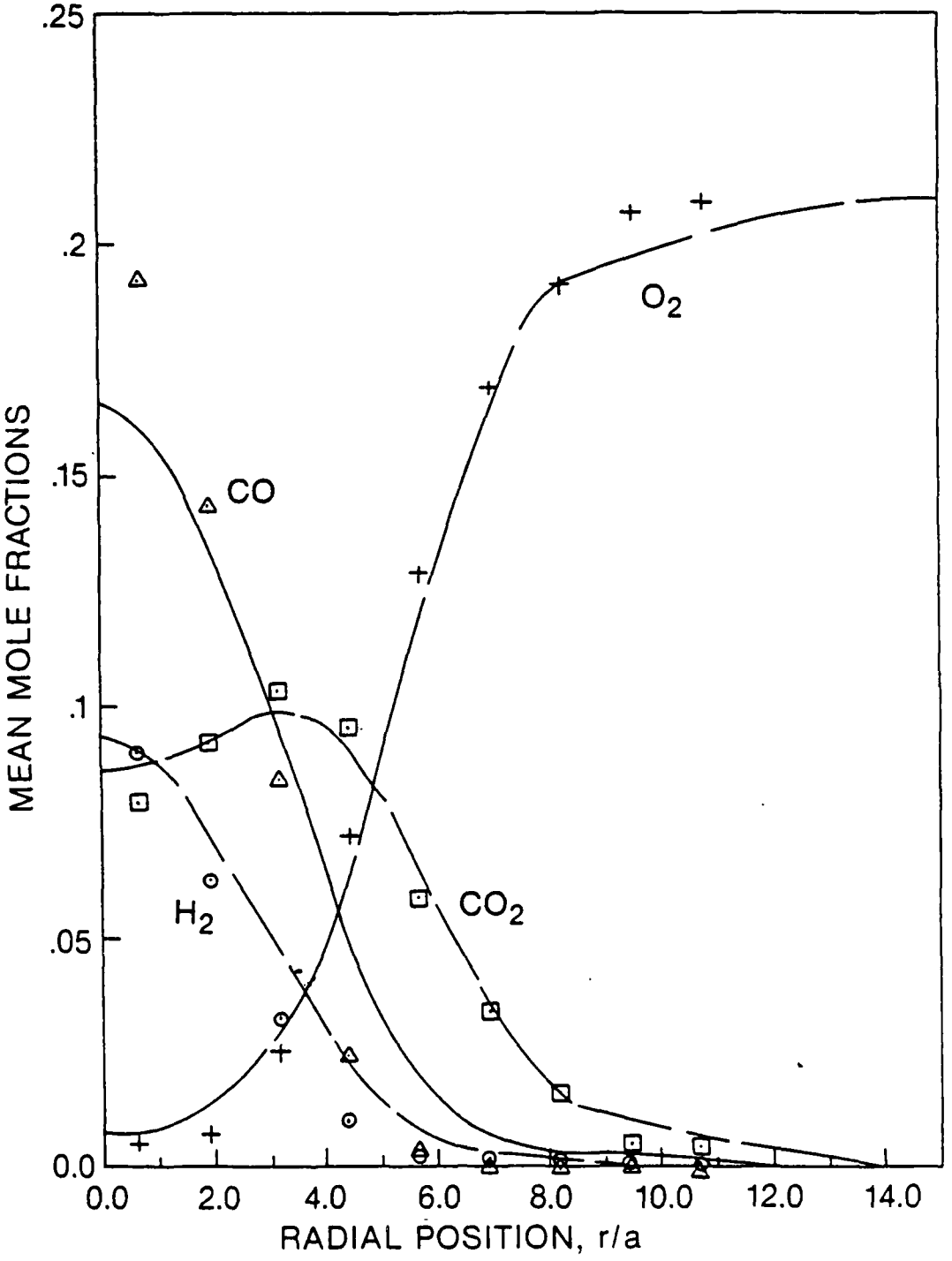

Figure 9. Mean concentrations of major species ($\overline{X_i}$) at $x/d = 25$.

Mean mixture fraction profiles at $x/d = 50$ show significant disagreement, whereas the mean density (Figure 10) agrees well with the data. Mean temperature and N_2 concentrations also agree fairly well, as seen in Figure 11. The good agreement in N_2 mole fraction is, at first glance, surprising, given the relative lack of agreement in ξ. N_2 is essentially an inert species (only trace quantities are converted to NO_x) and therefore should follow a conserved scalar distribution.

This apparent contradiction can be resolved. The measurement of the mole fraction of N_2 is independent of the systematic errors involved in the measurement of other species, whereas the mixture fraction is a derived quantity involving errors in measurements of all major species. The instantaneous value of fraction, ξ, can, for example, be defined as

$$\xi = \frac{X_{N_2}/(\Sigma X_i w_i)\ \text{mixture} - X_{N_2}^{air}/w_{air}}{X_{N_2}^{jet}/w_{jet} - X_{N_2}^{air}/w_{air}} \tag{2}$$

Hence, the systematic errors in ξ are due to (a) errors in measurement of all major species, and (b) neglecting all radicals and other minor species because they are not measured by Raman scattering. These errors affect the "measured" molecular weight $\Sigma X_i W_i$ used in Equation 2. In fact, a change in mean molecular weight of the gas mixture from 27.86 to 28.8, for the same measured mole fraction of nitrogen ($X_{N_2} = 0.711$) results in the mixture fraction changing from 0.15 to 0.22. Thus, "measurements" of the mixture-fraction are very sensitive to the molecular weight of the mixture, especially at low values of ξ (as at $x/d = 50$). It should be noted that all the data for ξ are based on hydrogen element, but the same argument holds since, as Table 4 shows, the values of ξ based on three elements (C,H, and N) agree well. This latter agreement is expected because the effects of differential diffusion, observed in flames at lower Reynolds numbers [Drake et al. (1982)] should be negligible in this (Re = 8500) flame. Systematic errors in the measurement of ξ discussed above are common to the three cases.

The comparison between data and the model predictions shows that, with the addition of two variables to describe the nonequilibrium kinetics and thermochemistry, it now appears that finite-rate radical pool kinetics can be predicted with reasonable accuracy in the context of turbulent non-premixed syngas flames. Results plotted here show better agreement with (reanalyzed) data on major species than previously thought. Thus, this study shows that the partial-equilibrium model for the oxyhydrogen radical pool including CO is more useful than was concluded by Correa (1985) and Pope and Correa (1986). Although there are unresolved discrepancies between the predictions and the data, these are perhaps the result of obtaining and interpreting Raman data to a greater extent than previously thought. The reanalyzed data do not show large amounts of CO present where H_2 is absent, which would have been a strong indication of the breakdown of partial equilibrium. Generally good agreement on the minor species (OH) in this flame obtained earlier [Correa et al. (1984)] further supports the partial-equilibrium model and emphasizes the importance of the relatively slow radical-recombination chemistry.

2.2 High Reynolds Number Flame: Selection of Fuel

One of the primary goals was to obtain a better understanding of nonequilibrium chemistry effects in non-premixed turbulent jet flames at high strain rates. Such flames may have regions of locally extinguished eddies embedded in the flame, which may be a precursor to flame liftoff and blowoff. The probability of finding large regions of local extinction in the flame is a strong function of the fuel being used. The choice of the fuel was motivated primarily by the desire to increase this probability. However, there were other considerations involved in the choice of the fuel, which are discussed below.

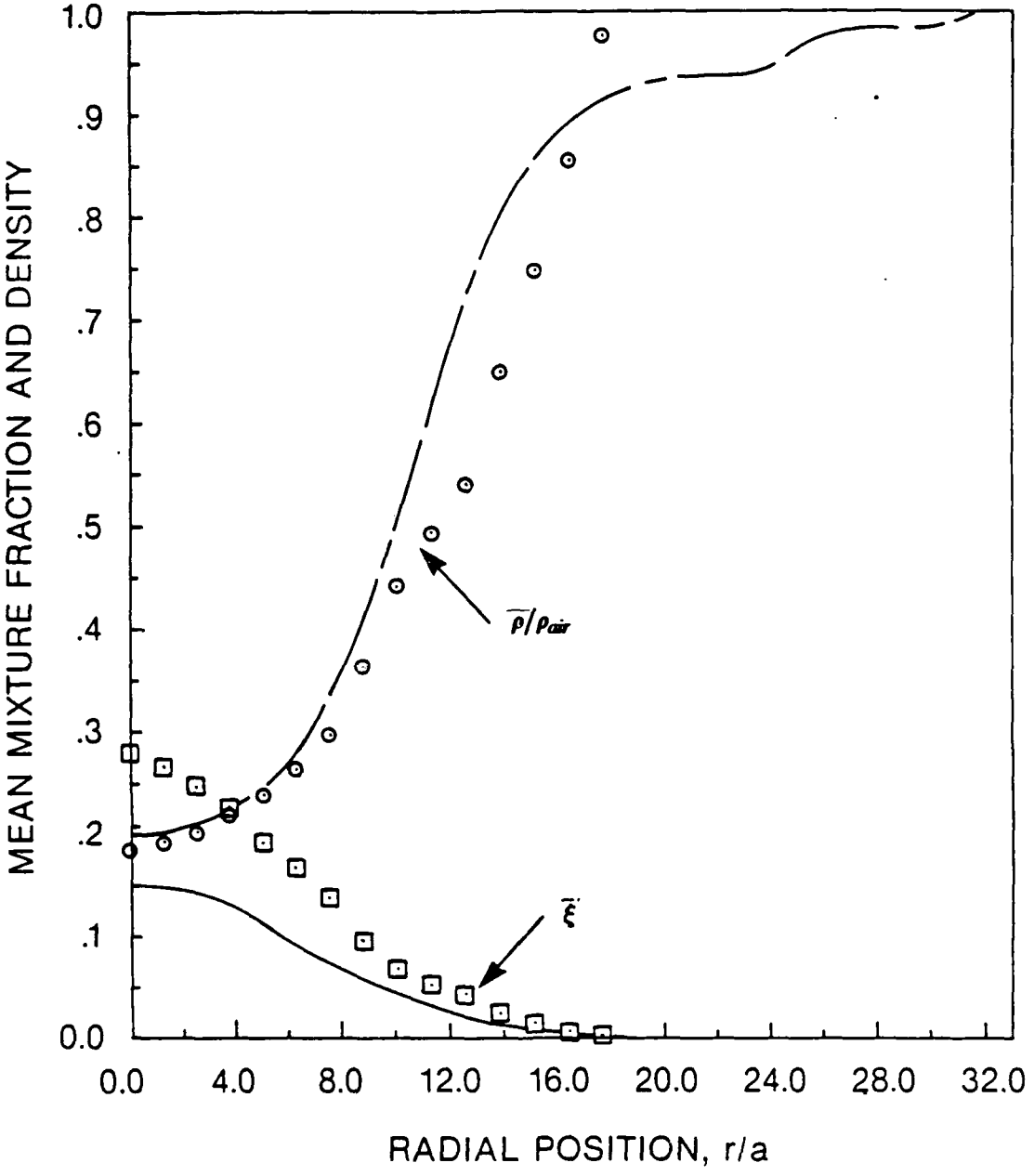

Figure 10. Mixture fraction $\tilde{\xi}$ and density $\overline{\rho}/\rho_{air}$ at $x/d = 50$.

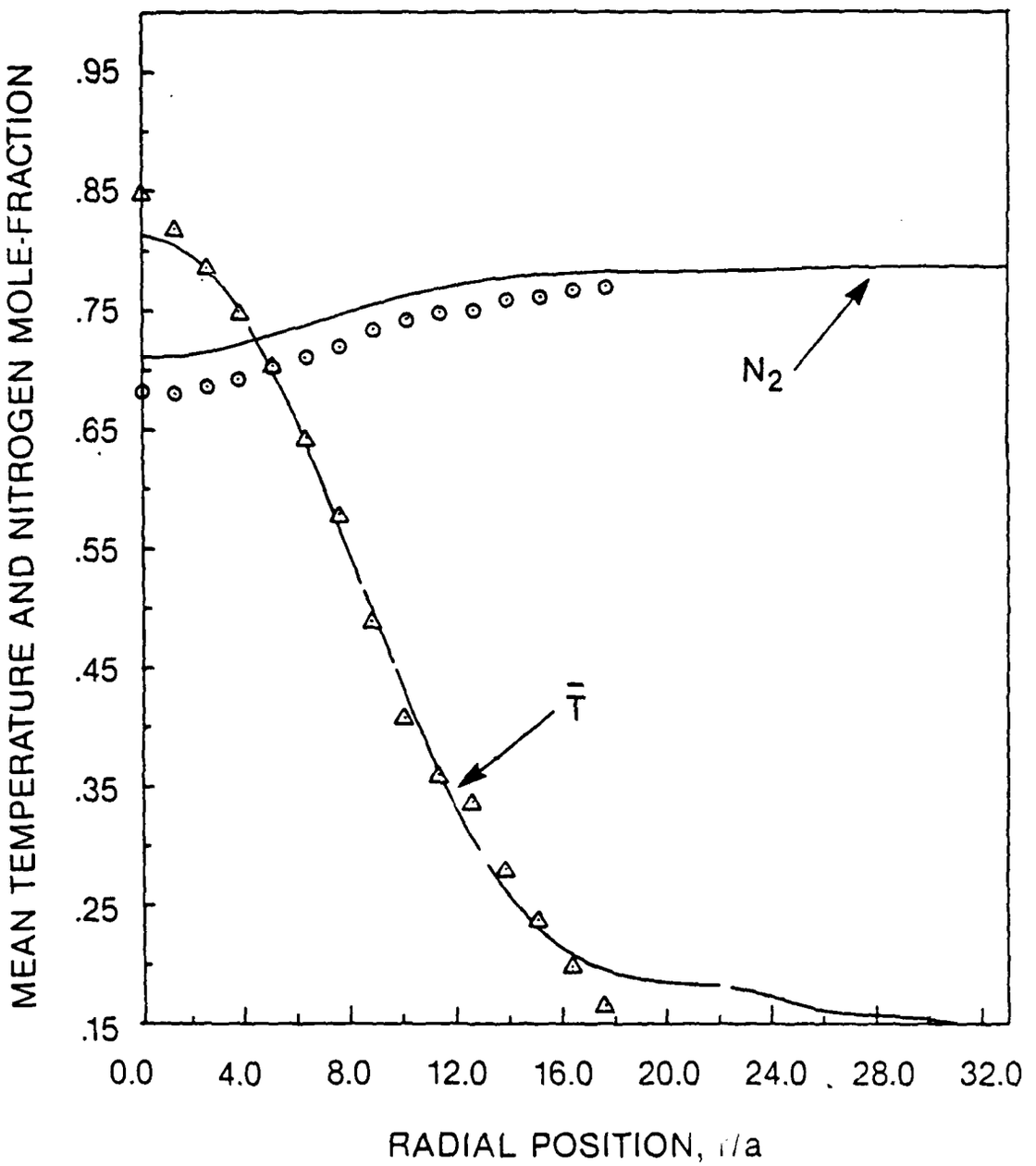

Figure 11. Mean temperature and nitrogen mole-fraction at $x/d = 50$.

Table 4
Mean mixture fraction at $y = 0$, based on the Carbon, Hydrogen, and Nitrogen elements.

x/d	Based on N	Based on H	Based on C	Predicted Values Pope and Correa (1986)
10	0.85	0.78	0.85	0.83
25	0.59	0.54	0.52	0.48
50	0.27	0.28	0.23	0.15

The fuel chosen for detailed study consists of 10% H_2, 40% CO, and 50% N_2 (by volume) and hereafter is referred to as low hydrogen content (LHC) gas. The prime considerations in the selection of the fuel were:

1. The probability of extinction in the turbulent flame should be sufficiently high to warrant detailed measurements. To estimate the probability of extinction, a simple experiment was conducted to estimate the value of the critical strain rate parameter ($\alpha_c = 2\,V/R$); see Section 2.5 for derivation and explanation. A counterflow diffusion flame burner of the type used by Tsuji and Yamaoka (1970) and described in Drake (1985) was used to estimate the value of α_c for various fuel compositions. The burner consists of a 5-cm diameter cylinder (5 cm long) with a 60 ° sector porous plug, which is used to stabilize a flame 2 to 5 mm away from the surface of the porous burner. The burner is installed in the subsonic low turbulence variable-free-stream velocity tunnel such that the 60 ° sector is symmetric about the stagnation stream line. As the free-stream air velocity is increased, the flame is pushed closer to the burner surface and eventually blows off abruptly at a critical strain rate, for which the characteristic mixing time τ_m evidently exceeds the characteristic reaction time τ_c.

   Figure 12 shows α_c as a function of percentage of hydrogen in the fuel, which consists of 50% N_2 and the rest of CO. In these measurements, the fuel velocity ratio was held constant to avoid excessive heat loss from the flame when it is close to the burner. As can be seen in the figure, the value of α_c increases from 400 s^{-1} corresponding to 2% H_2 to 1350 s^{-1} corresponding to 15% H_2. The value of α_c is 950 s^{-1} for the LHC gas chosen for this study. This value is much lower than the estimate (12,000 s^{-1}) for hydrogen and the estimate (greater than 2000 s^{-1}) for medium Btu gas (40% CO, 30% H_2, 30% N_2), and is of the order of α_c for methane flames ($\approx$330 s^{-1}).

   The probability of local extinction thus decreases very rapidly as the hydrogen content is increased. For a pure hydrogen flame, it is almost impossible to achieve extinction. Even though data presented by Dibble and Magre (1987) show existence of eddies that are lean mixtures of air-fuel and have very low temperatures, these eddies could be the result of large holes in the flame through which air has penetrated into the main jet and mixed with fuel without burning. In fact, that flame was visually unsteady. In hydrocarbon flames there is evidence of local extinction at relatively low strain rates (as suggested by the low value of α_c), but hydrocarbon flames have the complications of involving complex chemistry, which is not well understood, and of not being particularly amenable to Raman measurement because of fluorescence interferences [Dibble et al. (1987)]. These measurements of α_c indicate that for the LHC gas chosen for this study the probability of extinction is fairly significant.

2. The fuel should have relatively simple chemistry. The finite rate chemistry mechanisms in $H_2/CO/N_2$ flames are fairly well understood. Both H_2 and H_2/CO turbulent flames at lower Reynolds numbers have been studied in detail in the past [Drake and Kollmann (1985)]. The study of H_2/CO flames is also important because most hydrocarbon fuels undergo pyrolysis and form H_2 and CO as intermediate constituents before burning out.

3. The resulting flame should be amenable to Raman diagnostics. Even though it is advantageous to reduce the H_2 content of the fuel, it was found that for less than 10% H_2 content, the amount of CO had to be increased significantly to obtain a stable flame. Excessive amounts of CO present in the flame seriously interfere with Raman diagnostics because of chemiluminescent interference from the $CO + O \rightarrow CO_2$ reaction. This chemiluminescence is fairly broad-banded and extends all the way to the far red. Even though flame luminescence can be subtracted on a

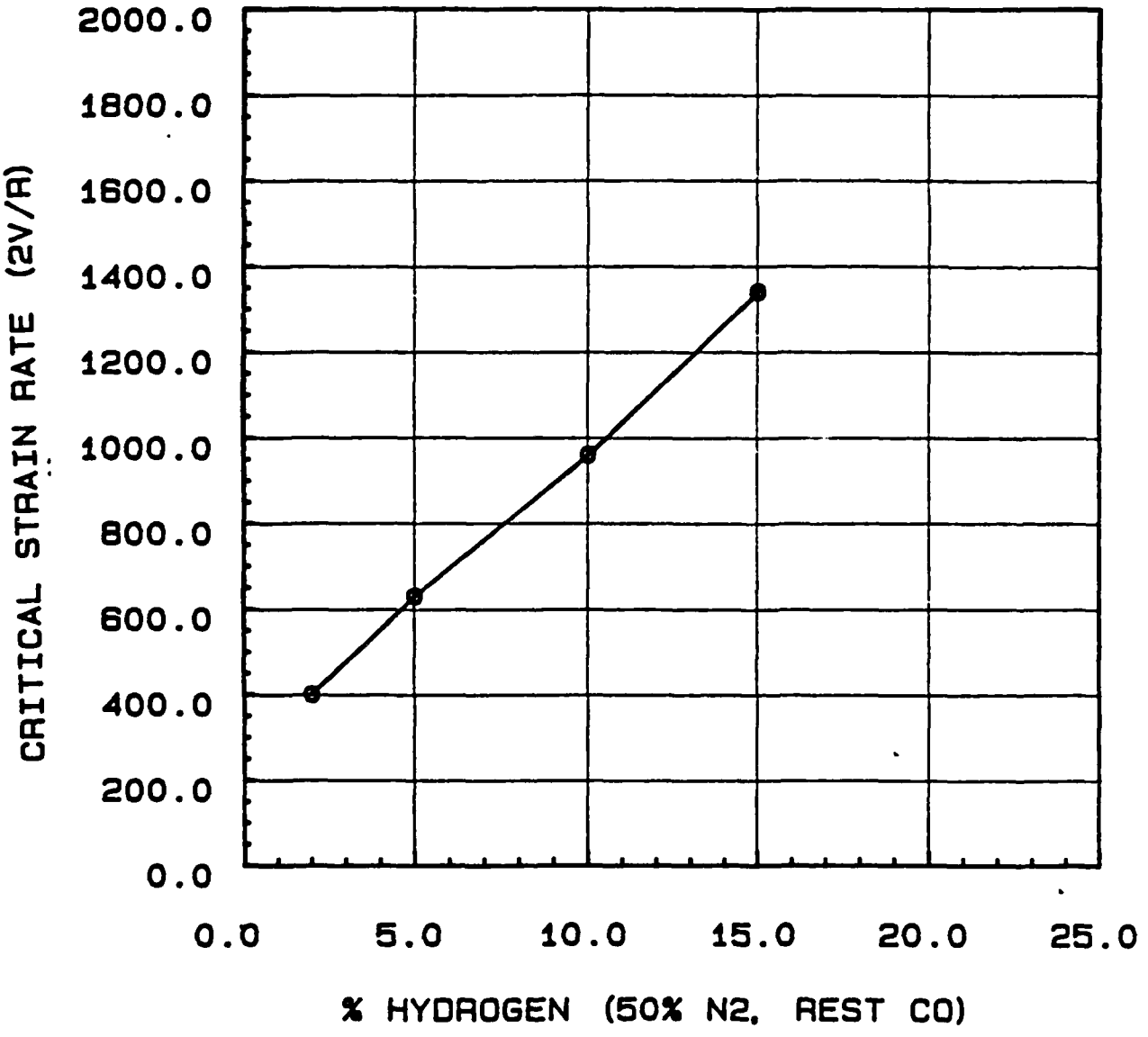

Figure 12. Plot of critical strain rate α_c ($S.^{-1}$) vs. percent H_2 in fuel (50% nitrogen, the rest carbon monoxide).

shot-to-shot basis during Raman data collection, the change in the chemiluminescence during the time interval can result in spurious Raman signals. Thus, it was necessary to reduce both the CO and H_2 content of the flame as much as possible by diluting it with nitrogen. For nitrogen dilution more than 50%, a stable flame at high Reynolds number could not be obtained even with the aid of a pilot. The LHC flame at 15,000 Reynolds number was fairly stable with the premixed pilot. Thus, the Raman feasibility, the stability of the flame, and the probability of localized extinction required a compromise in the choice of the fuel composition.

4. A final consideration regarding the choice of the fuel was the ability to use Rayleigh scattering to obtain 2D images of density in the flame by matching the Rayleigh cross section of air, fuel, and products. With a fuel composed of 10% H_2, 40% CO, 25% N_2, and 25% Ar, it is estimated that the change in Rayleigh cross section between the fuel, air, and products is less than 7%. This important property of the modified LHC gas will facilitate the measurement of strain rate in the future.

2.2.1 Pilot-Stabilized Burner

As the Reynolds number of the unpiloted jet flame is increased, the flame blows off. It was found that medium-Btu and H_2 gas flames could not be stabilized beyond Reynolds numbers of 8500 and 17,000, respectively, without additional modifications. Therefore, the main jet in the tunnel was modified to obtain a pilot-stabilized flame. Figure 13 shows a schematic of the burner exit. The pilot flame consists of a stoichiometric mixture of the main-jet fuel and air that was mixed well upstream of the combustor exit. This fuel-air mixture ratio (ξ_s = 0.43) results in the combustion products of the premixed flame having the same C/H/O ratios as the main fuel (LHC gas) when burned stoichiometrically, and simplifies the modeling of the flowfield by retaining the two-stream feature. The premixed annular burner has an open area five times that of the main jet. A flame arrestor consisting of 18 1-mm diameter holes is installed 4 mm upstream of the exit to anchor the premixed flame. The exit velocity of the premixed products is estimated to be 20 m/s, based on an estimated post-flame temperature of 2000 K. The coflowing air velocity in the tunnel was set at 5 m/s. Two flames at cold flow exit velocities of 25 m/s and 80 m/s, corresponding to Reynolds numbers of 5000 and 15,000, respectively, were studied. The pilot-stabilized burner is designed to provide a stable flame in the region of large strain near the exit, yet is devoid of gross unsteady features. The pilot flame results in reduced initial strain rates and provides radicals resulting in the stabilization of the main flame. Further downstream, the turbulence is fully developed, the strain rate is still high, and the effects of the pilot are not significant. The main jet flame at Re = 15,000 is approximately 50 diameters long (based on main jet diameters). The premixed pilot flame extends to about 5 to 6 diameters when lit without the main jet. It is estimated that the enthalpy content contributed by the pilot is less than 5% of that by the main jet because of its relatively low volumetric flow rate. Figure 14 shows a schematic of the flame identifying the various regions in the flame. The pilot flame, the main jet, and the region of maximum strain rate where the flame is narrow are also identified in the figure.

2.2.2 Measurements in Pilot-Stabilized Jet Flames

The Raman diagnostic system used for detailed measurements in the turbulent flame reported here is similar to that used for medium-Btu flame studies, with modifications to permit measurements in the more luminous LHC gas due to increased chemiluminescence. The joint Raman-Rayleigh diagnostic system is used to obtain instantaneous measurements of temperature and mole fractions of the major species (H_2, CO, CO_2, H_2O, O_2, N_2). A flash lamp pumped dye laser that provides pulses of $\approx$1 J in 2 to 4 μs, within a 0.2-nm bandpass at 488.0 nm at a repetition rate of 1 pps is used to excite the scattering processes. The light scattered at right angles is collected by two lenses, separated in

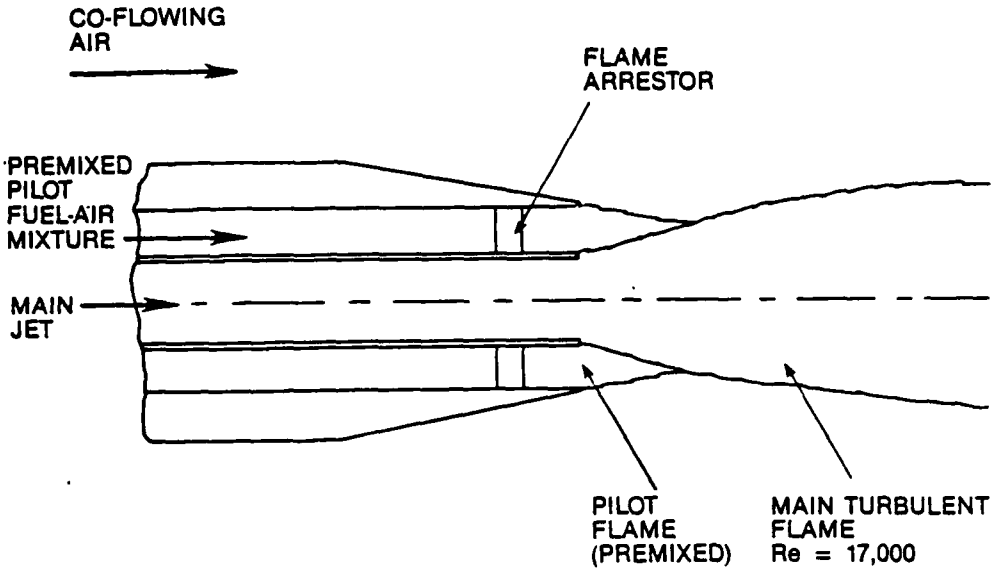

Figure 13. Schematic of the burner exit.

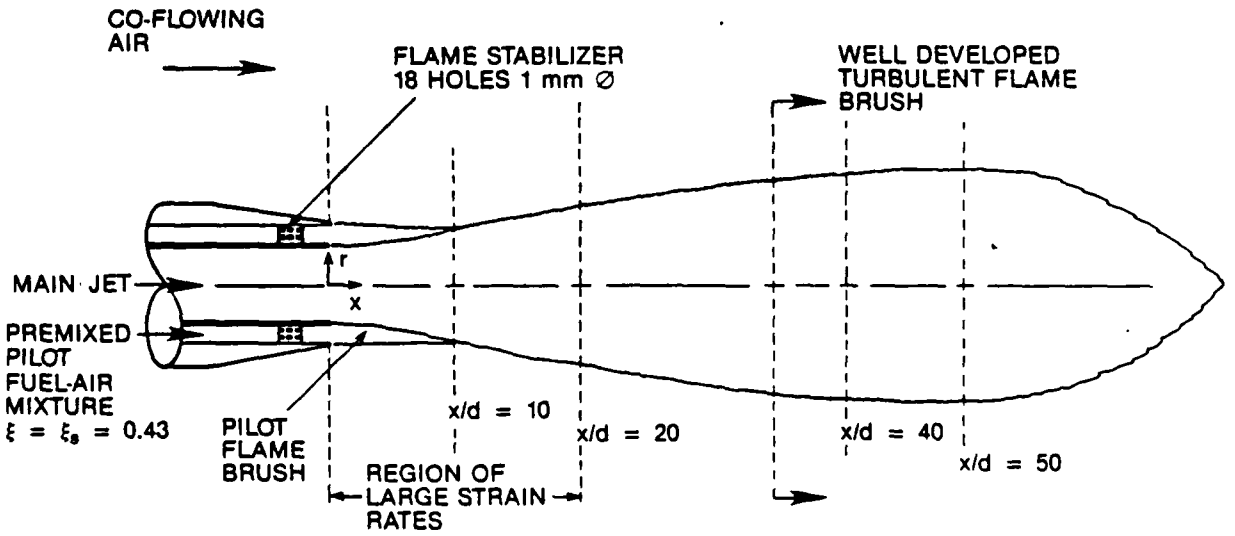

Figure 14. Schematic of premixed pilot-stabilized burner showing the regions of maximum strain rates and fully developed turbulent-flame brush.

frequency by a 3/4-m spectrometer, and is detected by eight photomultiplier tubes. The photomultiplier tubes detect anti-Stokes vibrational Raman scattering from N_2; Stokes vibrational Raman scattering from N_2, O_2, H_2, H_2O, CO and CO_2; and Rayleigh scattering. The temporal resolution (2 μs) of the technique is limited by the laser pulse length, the spatial resolution ($0.2 \times 0.2 \times 0.6$ mm), by the spectrometer entrance slit, and by the collection optics, while the data aquisition rate (1 pps) is limited by the laser-firing rate. The flame luminescence was found to be very broad- banded throughout the visible region. Three more photomultiplier tubes were added to the Raman system. One of the photomultiplier tubes is used to monitor Rayleigh scattered light for temperature measurements, whereas the other two are provided to monitor the chemiluminescence from the flame. A polarization filter was used in the collection optics system to reduce flame luminescence. The polarization vector was aligned to pass the horizontally polarized Raman and Rayleigh scattered light. Typically, 200 measurements were made at each flame location,although 2000 shots were also recorded at some locations for statistical purposes.

The joint Rayleigh-Raman data are obtained as follows. The photomultiplier tubes are gated electronically before and after the firing of the laser. The differential voltages, which correspond to the Raman signal minus the flame background at $t = 0$ are amplified and filtered before digitization using a 12-bit A/D convertor. The signals are then corrected for electrical and other background errors corresponding to each channel and are normalized by the laser energy for every shot. The subsequent signals are corrected for relative sensitivities of the photomultiplier tubes to obtain the final values corresponding to the vibrational intensities of Raman scattering (which is linearly proportional to the number density) in the bandpass of the exit slits of the spectrometer. The system was calibrated extensively using 100% pure gases and well-characterized premixed porous plug burners before the measurements reported here were made.

The instantaneous temperature at every shot was determined by using three independent methods. The Stokes-anti-Stokes (SAS) ratio method described in Drake (1985), based on the nitrogen element, yields the value of the temperature directly. The second method is based on the iteration scheme in which an initial temperature is guessed, based on which the mole fraction of all major species are calculated using their measured vibrational intensities. The mole fractions are then corrected using the high-temperature correction factors to account for changes in the fraction of the Raman band falling in the slit function provided for the respective photomultiplier tubes. The iteration process is repeated until the sum of the mole fractions is unity. This iteration procedure converges in two to three iterations since the correction factors are relatively weak functions of the temperature. The third method, Rayleigh scattering, is discussed below.

In this flame it was found that the chemiluminescence caused by $CO + O \rightarrow CO_2$ reaction was significant, and extra precautions had to be taken to improve the signal/noise ratio, such as inserting a polarization filter in the collection optics, reducing the entrance slit size, and adding two additional photomultiplier tubes (one in the Stokes region and one in the outer-Stokes region), etc. In addition, since the N_2 channel is affected most by the luminosity of the flame, the SAS measurements were susceptible. Hence, Rayleigh scattering was used to obtain an independent measurement of temperature. Since it is a diffusion flame, additional information about the Rayleigh cross section of the species involved is needed for Rayleigh scattering to be applicable. In this flame the Raman scattering signals from the major species were used to obtain information about changes in Rayleigh cross section of the mixture and thus measure temperature in an iterative manner. Some of the typical results obtained from Raman measurements in this flame are shown in Figures 15 through 18.

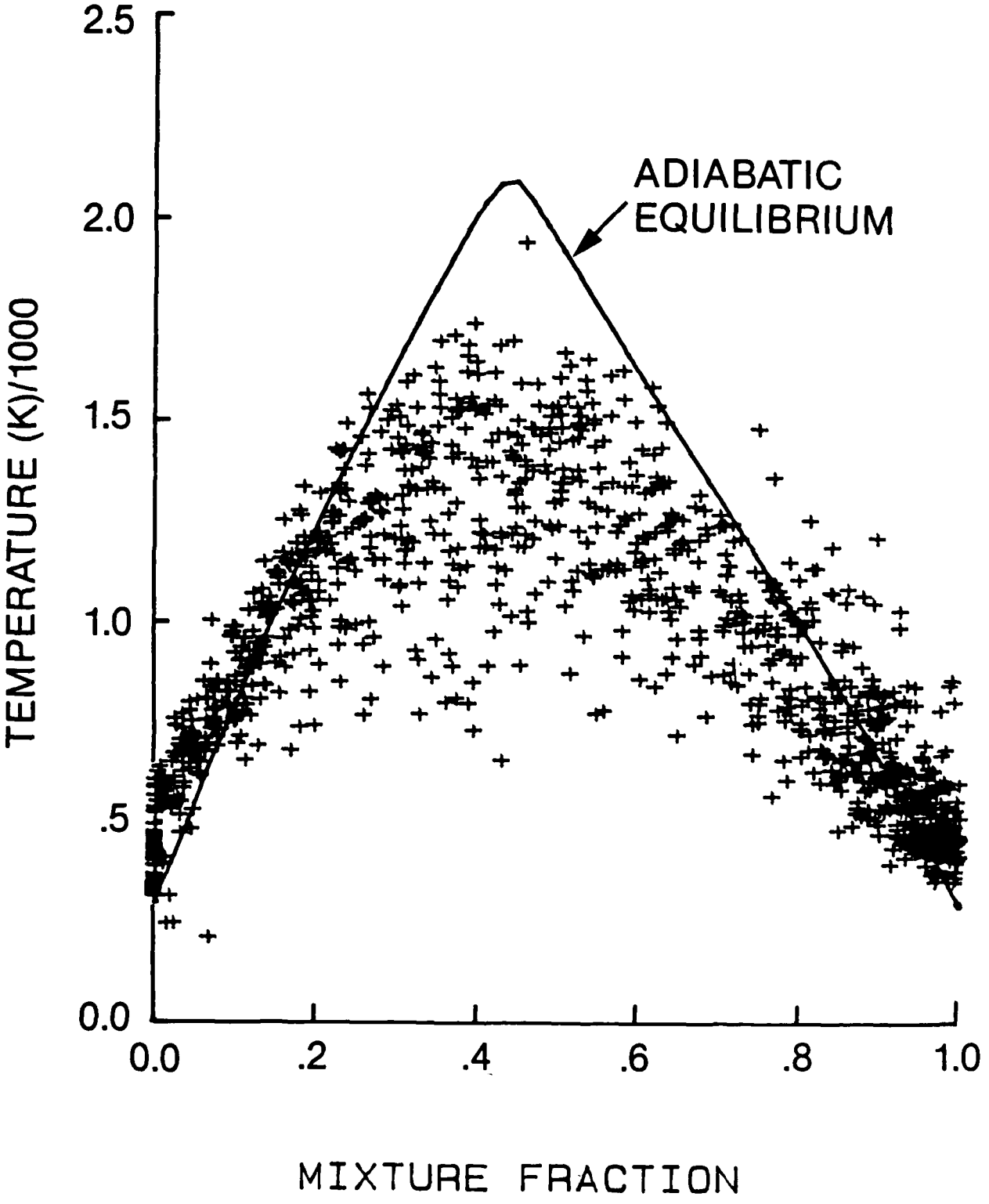

Figure 15. **Measured temperature-mixture fraction scattergram at $x/d = 10$; all radial positions.**

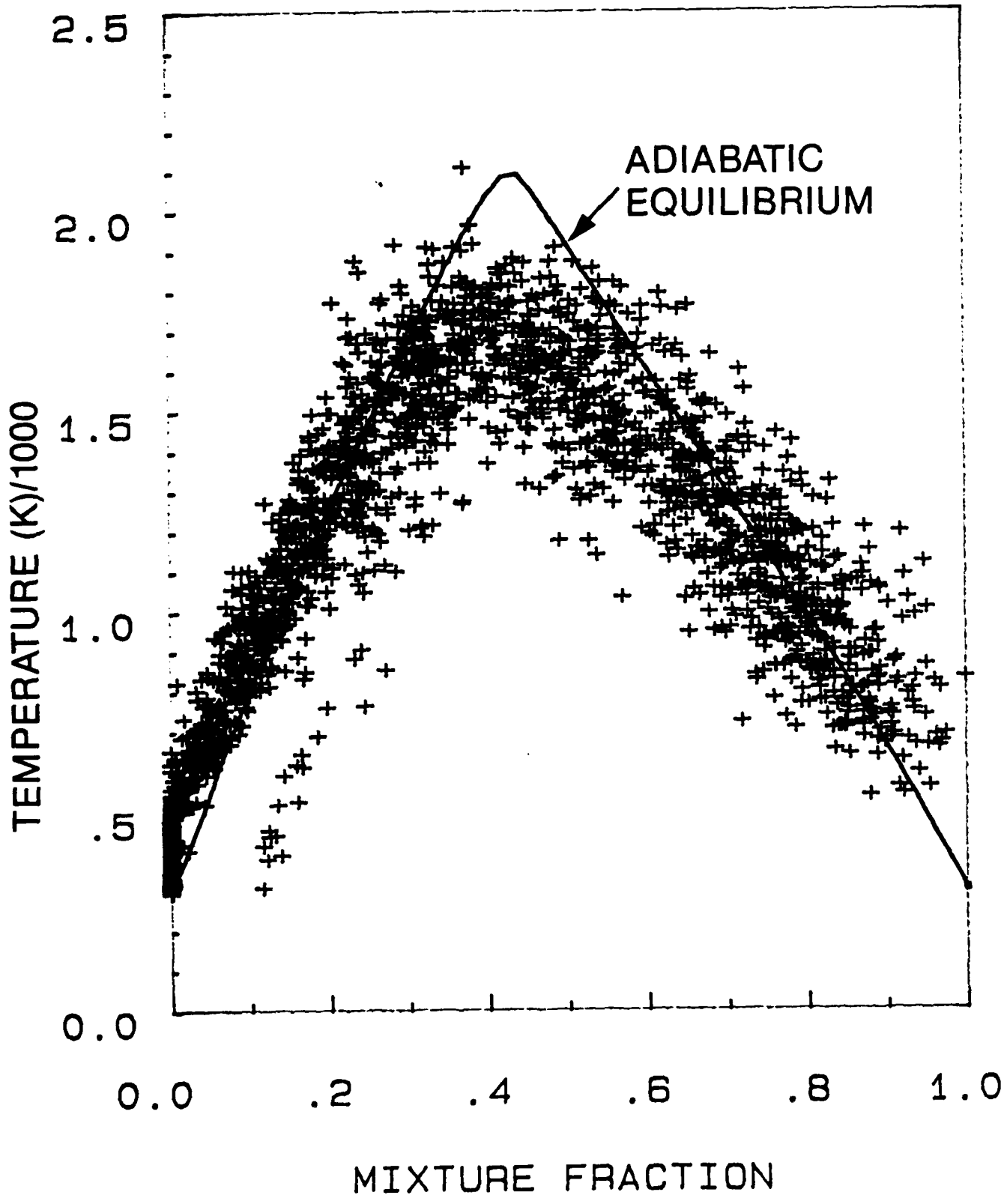

Figure 16. **Measured temperature-mixture fraction scattergram at $x/d = 20$; all radial positions.**

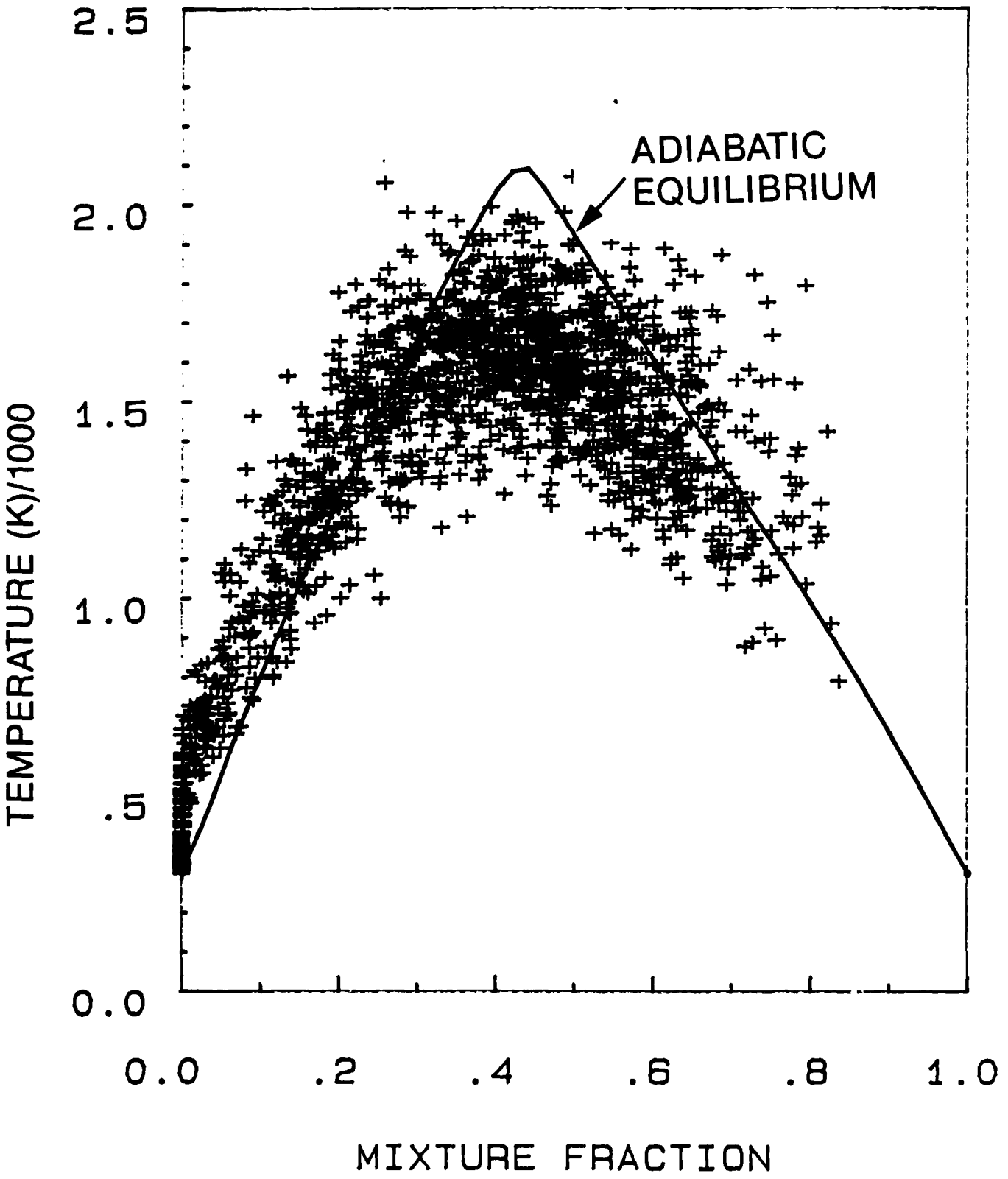

Figure 17. **Measured temperature-mixture fraction scattergram at $x/d = 30$; all radial positions.**

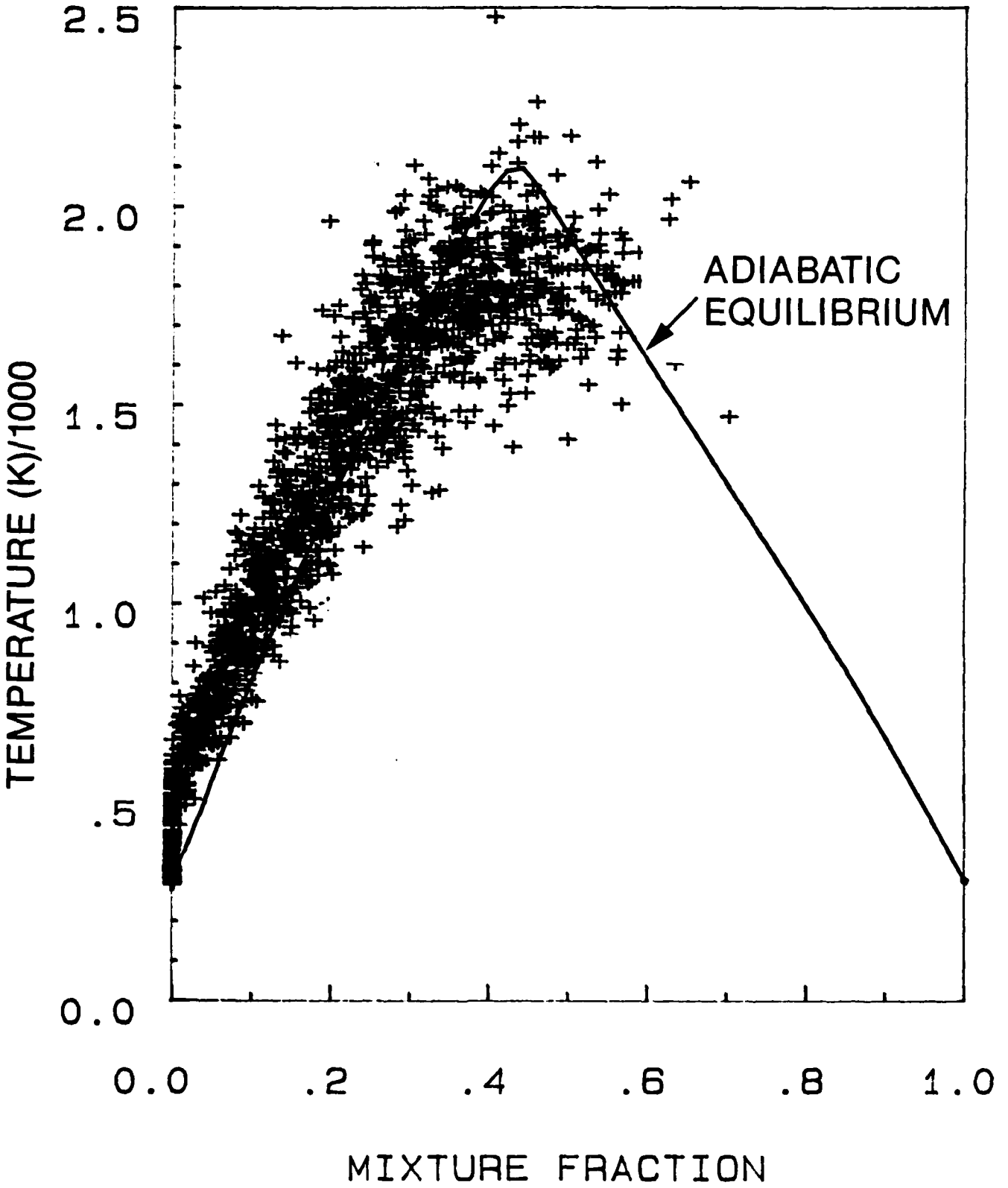

Figure 18. Measured temperature-mixture fraction scattergram at $x/d = 40$; all radial positions.

Figures 15 through 18 show the scattergrams of temperature vs. mixture fraction at four axial locations in the Re = 15,000 LHC gas flames. Each data point in the figures represents an instantaneous simultaneous realization of temperature and mixture fraction (based on carbon element). In each figure, data from all radial positions are included.

Figure 15 represents data obtained in the high Re = 15,000 flame at x/d = 10. This location is representative of a region of high strain rate. Figure 15 shows an enormous amount of scatter in the data (2000 points) and large departures from equilibrium values. The mixture fractions lie in the range 0.0 to 1.0, and temperature departures from equilibrium in the range 400 to 1500 K. The data points having mixture fraction values near stoichiometric and significantly low temperatures might be thought to represent locally extinguished flamelets. Local extinction refers to a flammable mixture of fuel and air that is unburnt or that has been extinguished; however, the data indicate no evidence of local extinction. The large deviations from adiabatic equilibrium are caused by finite rate radical pool chemistry. The scattergram at x/d = 20 (Figure 16), at which location the fuel and air are significantly mixed and the strain rates are significantly lower, shows most of the data to lie along the adiabatic equilibrium curve and the departures from equilibrium to be minimal. There is virtually no evidence at all of localized extinction at this axial location. Figures 17 through 19 confirm that this trend continues downstream.

2.3 Bimodal Laminar Flamelet Calculation

Under the assumption that the laminar flame thickness is small compared with the turbulent scales in the flow, the "laminar flamelet" analysis for turbulent diffusion flames has been advanced [Peters (1984)]. In this model, the instantaneous composition of the turbulent flow is assumed to correspond to that of an undisturbed laminar diffusion flame at the prevailing value of mixture fraction. It offers an alternative to explicit multivariable representations of the chemistry, such as those for turbulent H_2 diffusion flames[Janicka and Kollman (1979, 1982)] and CO/H_2 flames [Correa et al. (1984); Correa (1985)]. Turbulent flames are hypothesized to be ensembles of these laminar flamelets.

Numerical studies of the structure of laminar diffusion flames with full kinetics indicate a strong dependence on the strain rate [Miller et al. (1984)]. A configuration often studied is the counterflow diffusion flame burner [Tsuji and Yamaoka (1970)]. It is established that as the strain rate $2V/R$ – where V is the oxidizer velocity and R is the radius of the burner – is increased, the maximum temperature in the system decreases until an abrupt transition to inert flow occurs. The critical strain rate varies with fuel type ranging from about 12,000 s^{-1} for H_2 [Dixon-Lewis (1984)] to about 330 s^{-1} for methane [Miller et al. (1984)].

The sensitivity of the laminar flame to strain rate implies that the instantaneous composition in a turbulent flame will depend on the local scalar dissipation $X(\vec{x})$ as well as mixture fraction. In physical terms, the composition would correspond to that at the same mixture fraction in a laminar flame subjected to the same straining. In principle, a "library" of such strained flames could be generated computationally or experimentally; however, Liew et al. (1984) adopted the simpler approach of sampling the undisturbed flame (from experimental data) or inert flow, depending on X being less or more than an assumed quenching value of scalar dissipation rate, X_q. In highly turbulent flames where the local probability density function (pdf) of strain rate results in $X > X_q$ much of the time, the mean flow would be strongly biased towards the inert flow. Local extinction would therefore be very significant.

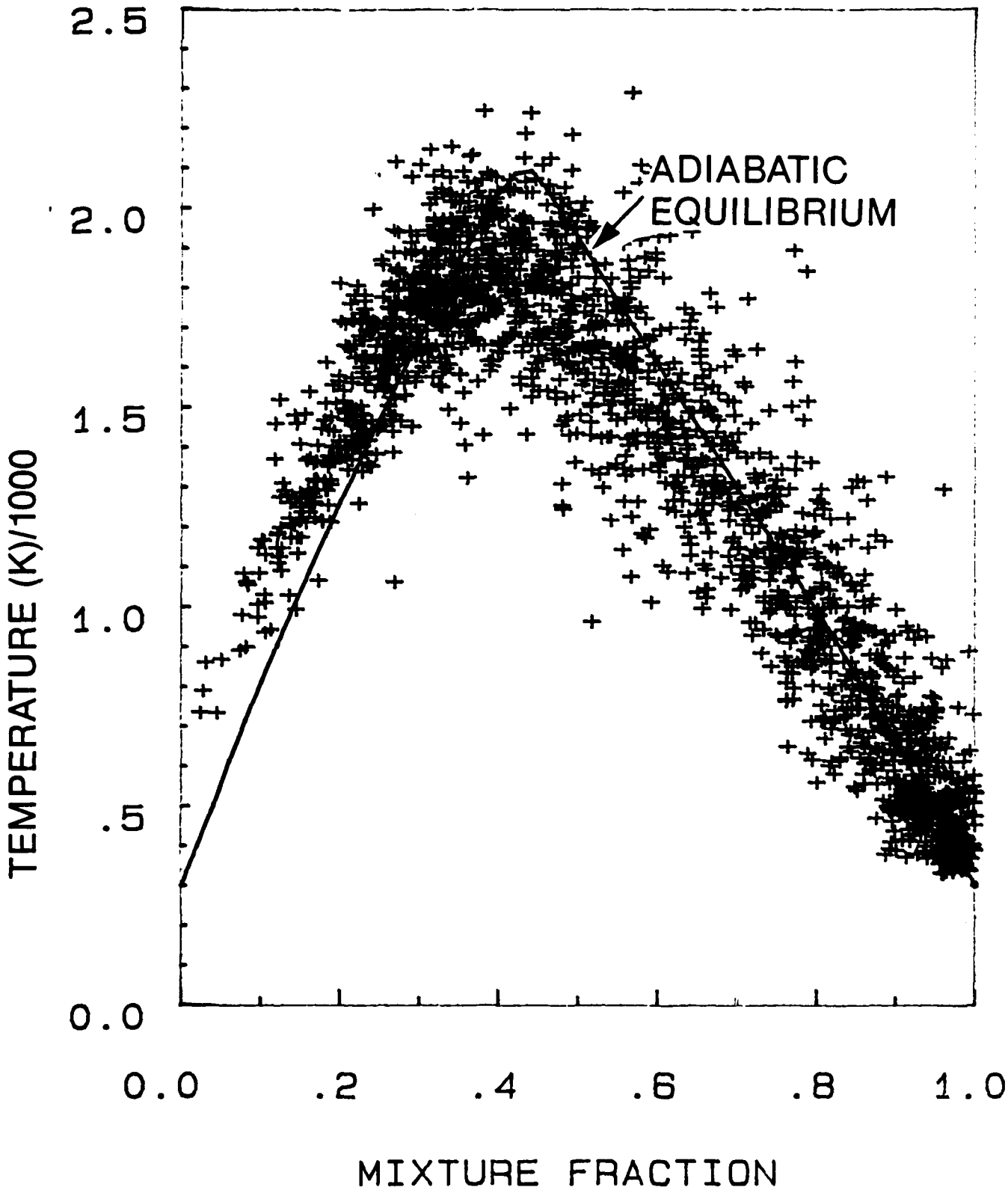

Figure 19. Measured temperature-mixture fraction scattergram along centerline; all radial positions.

The pilot-stabilized 40% CO, 10% H_2, 50% N_2 flame at Reynolds number 15,000 has been simulated by means of a laminar flamelet model in which equilibrium or inert flow are assumed for strains (X) less or greater than a critical level (X_q), respectively. In highly turbulent flames where the mean scalar dissipation rate is large, much of the time $X > X_q$ and then the flame is "extinguished." The laminar flamelet model follows the version of Liew et al. (1984), which was developed for a non-premixed turbulent jet flame [see also Liew et al. (1981)].

The argument by which the local distribution of scalar dissipation rate is obtained follows Liew et al. (1984). Kolmogorov's hypothesis of a log-normal distribution is made with the mean $\tilde{X}$ given by

$$\tilde{X} = c_{g_2} \tilde{\xi}''^2 \tilde{\epsilon}/\tilde{k} \tag{3}$$

which is the modeled term in the variance transport equation. The local pdf for X is

$$\tilde{P}(X) = \frac{1}{X} \frac{1}{\sigma} \frac{1}{(2\pi)^{1/2}} \exp[-(\ln X - \mu)^2/2\sigma^2] \tag{4}$$

where σ^2 is the variance of lnX. The pdf of X conditioned on the presence of zones of intense reaction (here we refer to two-body reactions) is assumed to be identical, and may be integrated to give the probability of being below a critical level X_q, i.e., the probability of "combustion" P_c (more precisely, the probability of two-body reaction equilibration:

$$P_c = 1 - \frac{1}{2} erfc\ [(\ln X_q - \mu)/\sqrt{2}\sigma]. \tag{5}$$

As the gas flows downstream, the strain rates decrease and the probability P_c of the gas being below the burning limit increases. Thus, more of the gas is equilibrated.

The pdf over thermochemical states is needed to obtain various quantities such as mean density. Since the flow is either inert (u) or in a state of equilibrium (e), the pdf is $P(\xi) = (1-P_c)\, P_u(\xi) + P_c \cdot P_e(\xi)$ where P_c is the fraction of gas that is burning. The pdf for the occurrence of values of the mixture fraction is needed. Such pdfs can be obtained directly from evolution equations based on the Navier-Stokes and species equations [Pope (1981)] or more simply by assumed-shape pdf methods as in Kent and Bilger (1976) for $P_e(\xi)$, which is taken to be a beta-function. Figure 20 shows the modeled probability of combustion P_c in the flame for three assumed values of X_q (the quenching parameter). The region of maximum probability of extinction of two-body reactions and the trend of its radial variation are predicted reasonably well by the model. Figure 20 shows the model predictions for X_q = 40, 100, and 1000 s^{-1}. X_q is the quenching rate parameter used in the model. The experimental data follow a similar trend, although the model predicts a slower temperature growth rate for all values of X_q. The deviations of experiment from data are greatest at x/d = 20. Further downstream (e.g., at x/d = 50), the strain rates are expected to be much lower and so the predicted profiles for all these values of X_q collapse and are much closer to the experimental results. This however, is not conclusive support of the model because if a flamelet is quenched in the large strain region (lower x/d values), it is premixed and cannot be described adequately by the model. This is because the model is applicable to strained flames of the diffusion type only, whereas extinguished flamelets lead to a premixed situation. Detailed comparisons between model and experimental results are presented in Gulati and Correa (1987).

Discrepancies in the region of greatest strain near the nozzle exit could be attributed to one or more of several possible causes. Exit conditions in the nozzle and pilot are difficult to characterize

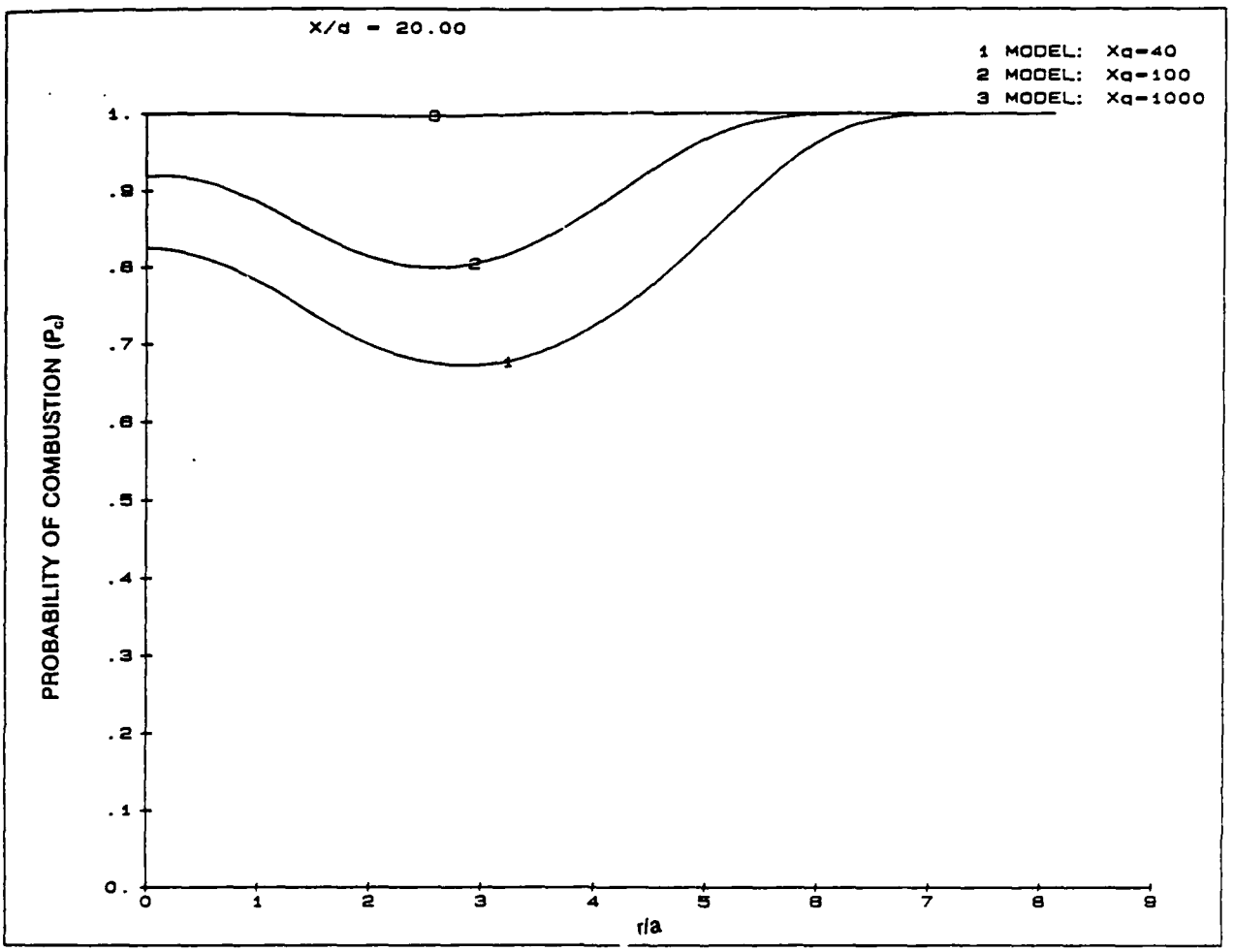

Figure 20. Radial profile of predicted probability of combustion based on stretched flamelet model at x/d = 20 for three values of X_q.

and may exert a nontrivial influence on the near-exit region despite the large shear. These conditions include turbulence quantities and the heat loss in the pilot. From model calculations, it was found that the results were sensitive to the temperature profile at the exit of the premixed pilot burner. Later, experiments were conducted to measure the velocity profiles at the exit of the pilot burner to provide more initial conditions.

These findings were summarized as follows; a more accurate model has been developed, as discussed next.

1. There is no firm evidence of local extinction (or frozen conditions) in the LHC gas Re = 15,000 flame, even in the regions of largest strain. It is observed that approximately 20% of data points have mixture fraction values close to stoichiometric, but have significantly lower temperatures than adiabatic equilibrium. These low temperature eddies could result from any of the following reasons: (a) they could represent eddies that were extinguished but are above 300 K as a result of mixing with surrounding hot products; (b) they could represent strained eddies with much lower temperatures (than AE) caused by large nonequilibrium chemistry effects; (c) they could represent mixed eddies that are partially burned (i.e., they were extinguished due to large strains after initial ignition). Past experience suggests large nonequilibrium chemistry effects to be the most plausible explanation of the departure from AE curve.
2. The theoretical predictions of the model show that the results are sensitive to the assumed value of X_q, the quenching value of dissipation rate, especially in the region of large strain, and are also sensitive to the assumed velocity and temperature profiles at the exit of the pilot burner.
3. Even though the model provides significant insight into the quenching and localized extinction phenomena in turbulent diffusion flames, there is significant disagreement between the data and calculations, especially at $x/d = 20$. The relatively better agreement at $x/d = 50$ may be fortuitous. The model suffers from serious drawbacks of (a) relying on an unknown quenching parameter X_q, (b) an inability to adequately describe flamelets after they are quenched (premixed strained flamelets), and (c) considering only two types of flamelets: equilibrium and unstrained. This suggests a need to improve the chemistry modeling and to combine partial-equilibrium models, which have been very successful in the past, with laminar flamelet models as discussed below.

2.4 Alternate Approach to Modeling Turbulent Extinction

An important shortcoming of the laminar flamelet analysis is that, in practice, laminar flames are not necessarily thin compared with turbulent scales. In H_2 and CO/H_2 flames, there are two distinct sets of scales associated with the chemistry: the set corresponding to two-body chain-branching or propagating reactions and the set corresponding to three-body recombination reactions. The large disparity between these scales has led to partial-equilibrium models that assume the two-body reactions are in equilibrium [Janicka and Kollman (1979), Bilger (1980), Correa et al. (1984), Correa (1985), Pope and Correa (1986)]. This disparity also implies that, in intense turbulence, the two-body reaction zones would remain comparatively thin while the three-body zones would overlap, leading to distributed reaction zones that are incompatible with the laminar flamelet hypotheses.

Thus, if independent control over the turbulent mixing was exercised, as the time-scale is progressively reduced from large values, the OH concentrations (to pick a radical) would first increase because the recombination reactions are no longer fast enough to realize equilibrium; the concentrations then abruptly drop as the two-body reactions are quenched and the gas is inerted. Temperature shows a monotonic decrease throughout this process with a more rapid decrease as extinction is ap-

proached. This behavior is consistent with the notion that the abrupt transitions in a stretched flamelet are characteristic of high-activation energy (shuffle) reactions, while well-distributed reaction zones are characteristic of low or zero activation-energy (recombination) reactions.

The large difference in the rates of the two-body and the three-body reactions is apparent from experiments at relatively low Reynolds numbers. Correa et al. (1984) used the partial-equilibrium model for CO/H_2 in an Re = 8500 (based on jet exit) flame. The data indicated negligible or no local extinction, i.e., none of the Raman data showed low temperature in flammable gas, but the data did indicate large amounts of superequilibrium OH, up to factors of 5. The model agreed well with these data. One may conclude that the time-scales of turbulence in such flames are short enough to interfere with three-body recombination chemistry, i.e., a Damkohler number based on the recombination reactions is of O(1). The time-scales are still too long to disturb the two-body reactions ($D_{2\text{-}body} >> 1$), and so there is little or no local extinction.

Here it is proposed to retain the partial equilibrium model – successful in the studies discussed above – but with the quenched flamelet approach to the two-body reaction zone. The two-body reaction zone is assumed to be either in partial equilibrium or quenched (i.e., leading to inert flow), depending on the local dissipation X being less or more than the quench level, X_q.

The kinetic mechanism adopted consists of fast shuffle reactions (S1) to (S5), which are considered to be in partial equilibrium, such as

$$H + O_2 = OH + O \quad \text{(S1)}$$

$$O + H_2 = OH + H \quad \text{(S2)}$$

$$H_2 + OH = H_2O + H \quad \text{(S3)}$$

$$2OH = H_2O + O \quad \text{(S4)}$$

$$CO + OH = CO_2 + H \quad \text{(S5)}$$

and relatively slow three-body recombination reactions, (R1) to (R4), such as

$$H + OH + M \rightarrow H_2O + M \quad \text{(R1)}$$

$$H + O + M \rightarrow OH + M \quad \text{(R2)}$$

$$H + H + M \rightarrow H_2 + M \quad \text{(R3)}$$

$$H + O_2 + M \rightarrow HO_2 + M \quad \text{(R4)}$$

Kinetic data are taken from Baulch et al. (1972).

In the model, combustion chemistry is represented by two-body shuffle reactions, taken to be infinitely fast or frozen, and three-body recombination reactions. The scalar dissipation rate field is examined for critical values, below which the two-body reactions are assumed to be in partial equilibrium and above which they are assumed to be frozen and the gas therefore unburned. The kinetics of the recombination reactions are activated for the former fraction of the gas. This approach is implemented in a shear-layer finite-volume averaged Navier-Stokes model with k-ϵ/assumed shape pdf submodels for turbulence. The model is applied to the Re = 15,000 pilot-stabilized 40% CO/10% H_2/50% N_2 jet flame for which laser-based spectroscopic data on major species and temperature have been obtained. The fuel is chosen to maximize the probability of local extinction. The model is useful for moderate to high Reynolds number diffusion flames.

Flamelet Approach

Since the mean scalar dissipation rate decreases as the jet fluid flows downstream, the region of intense stretch experiences a transition through the critical strain rate. The two-body reactions are assumed to be colocated with this region and are further assumed to immediately reach partial equilibrium. This is analogous to the approach used by Liew et al. (1984), who assumed a burnt flamelet state for the flamelets, which were below a critical scalar dissipation rate. In the present case, only the 2-body reactions are assumed to reach (partial) equilibrium; the recombination reactions commence and drive the system towards full chemical equilibrium. Thus this model has both flamelet features and partial equilibrium features. The argument by which the local pdf of scalar dissipation rate is obtained was described in the previous reaction.

The model is easily visualized in one dimension. If the pdf's for local dissipation rate X at an upstream and downstream location are denoted by $P_u(X)$ and $P_d(X)$, respectively, and the probabilities of 2-body reaction equilibration are $P_u(X < X_q)$ and $P_d(X < X_q)$, then it follows that the probability that the recombination reactions "just" started is $P_d\ (X<X_q)$ - $P_u\ (X<X_q)$. The gas which undergoes this transition is added to the gas described by the "reactedness" ($\tilde{\eta}$) transport equation [Correa et al. (1985)] with an initial value of $\tilde{\eta} = 0$. The increments are calculated by evaluating the differential change in the probability $P(X<X_q)$ along the mean streamlines. This contribution enters the mean reactedness equation as a source term S

$$S = - \frac{dP_c}{P_c} \cdot m \tag{6}$$

where P_c represents $P(X<X_q)$ and m is the mass flux along the stream tube.

The pdf over thermochemical states is needed to close the chemical source terms and obtain various quantities such as mean density. Since the flow is either inert (denoted by subscript i) or in a state of partial equilibrium (denoted by subscript b), the pdf is

$$P(\xi,\eta) = (1\text{-}P_c)P_i(\xi,\eta) + P_c \cdot P_b\ (\xi,\eta) \tag{7}$$

For the fraction of gas that is burning, the joint pdf for the occurrence of values of the two thermochemical variables is needed. Here occurrences of the two variables are assumed to be uncorrelated, and so the joint pdf may be assumed to be separable. [Pope and Correa (1986)] solved the evolution equation for $P(\vec{u},\xi,\eta;\vec{x})$ with a Monte Carlo technique and showed that ξ and η *were* correlated, but the results were qualitatively quite similar to those obtained using the assumed-shape model, at least on mean quantities. Here the pdf in the direction of mixture fraction is taken to be a beta-function that can be parameterized in terms of its lowest moments, i.e., the mean and variance, for which standard modeled transport equations are available. The influence of the shape of the pdf in the reactedness (η) has been studied previously and suggests that a single delta-function at the mean reaction $\tilde{\eta}$ is sufficient, because negligibly weak contributions are made by delta-functions at $\eta=0$ and $\eta=1$.

The calculation procedure is similar to that used previously [Correa et al (1984)], except that the pdf described above is used for closure. The shear-layer equations are solved numerically in axial distance-stream function coordinates [Patankar and Spalding (1972)]. They consist of the axial velocity, turbulence kinetic energy k, dissipation rate ε, mean and variance of mixture fraction, and mean (reactedness progress variable). Boundary conditions on the variables correspond to fully developed turbulent fuel flow with appropriate assumed intensity and length-scale of turbulence.

The computational model was run for the LHC gas flame at Re = 15,000. Raman data were taken at $x/d = 10$, 20 and beyond (d = fuel tube diameter, $a = d/2$). Since the region of maximum strain rates is within the first 20 diameters, the comparisons reported here are restricted to the axial planes $x/d = 10$ and 20.

Figures 21 through 24 compare the computed mass-averaged mean mixture fraction ($\tilde{\xi}$)and conventionally averaged temperature ($\overline{T}$) at $x/d = 10$ and 20 with the data. The agreement on $\tilde{\xi}$ is reasonable at $x/d = 10$, although the computed jet has spread too rapidly. This is more pronounced at $x/d = 20$ and shows that the model overpredicts the jet spread. The mixture fraction data have been obtained by averaging mixture fractions based on C, H and O. Errors in measuring the corresponding molecular species contribute in part to the differences from predicted values. The temperatures obtained by two methods (sum of mole fractions, Rayleigh) agree well. The mean temperature at $x/d = 10$ is predicted well except for the cool fuel-rich core of the flame, where partial equilibrium is expected to break down. [Correa et al. (1984); Correa (1985)]. The comparisons at $x/d = 20$ are very similar, with a generally higher predicted temperature particularly in the core.

The overprediction of the jet spread rate is due in part to the sensitivity to initial conditions. Generally, jet flames are studied in the fully developed region far downstream (e.g., $x/d = 50$ to 200 for H_2 flames in which the stoichiometric mixture fraction ξ_s is 0.0283). Here, however, the near-exit high strain rate region is of interest because of the local extinction issue and because the flame is shorter ($\xi_s = 0.43$). Further measurements are being made to adequately characterize the initial conditions. Given the difficulty of probing the annular pilot, a numerical sensitivity analysis may be the only practical approach. For present purposes, however, the results are adequately accurate.

The computed "probability of combustion," P_c (Figure 25), defined above, is higher in the regions of greater strain rate. Note that, strictly speaking, this probability refers to the radical pool and not to the overall system. The turbulence is not intense enough to cause widespread extinction. These results are somewhat sensitive to the choice of quench scalar dissipation rate X_q (here taken as 35 s^{-1} on the basis of prior work [Gulati and Correa (1987)]; X_q is related to, but not the same as, the critical strain rate α_c measured in counterflow diffusion flame burners). Indirect evidence of the probability of combustion is available from mixture-fraction vs. temperature scattergrams constructed from the Raman data (Figures 15 through 19). The large variations of the temperature data (up to 1200 K) from the adiabatic equilibrium curve indicate that local temperature-decreasing mechanisms are active. There is, however, no evidence of local extinction even at this location ($x/d = 10$) where the strain rates are high; extinction would have manifested itself in low temperatures in the flammable range of samples. The temperature scatter is due to the slowness of recombination reactions, as suggested by the computed mean reaction progress variable (Figure 26).

2.5 Strain in Compressible Flow

Critical values of strain corresponding to flame extinction in a cylindrical counterflow diffusion flame burner are approximately 330 s^{-1} for CH_4 [computed, Miller et al. (1984)], 950s^{-1} for a mixture of 40% CO, 10% H_2, and 50% N_2 [measured as discussed above] and 12,000 s^{-1} [computed, David et al. (1984)]. The large critical strain for fuels with significant H_2 implies that, for cylinders of reasonable size (R = 2 cm.), the critical air velocity (V = 120 m/s, for H_2 fuel) is in the compressible flow range. Velocities this high suggest the need for a compressible analysis of the flow. In particular, the strain rate at the forward stagnation point in cylinder flow is needed, since cylindrical sector burners [Tsuji (1970)] are routinely used to measure flame extinction limits [e.g., Section 2].

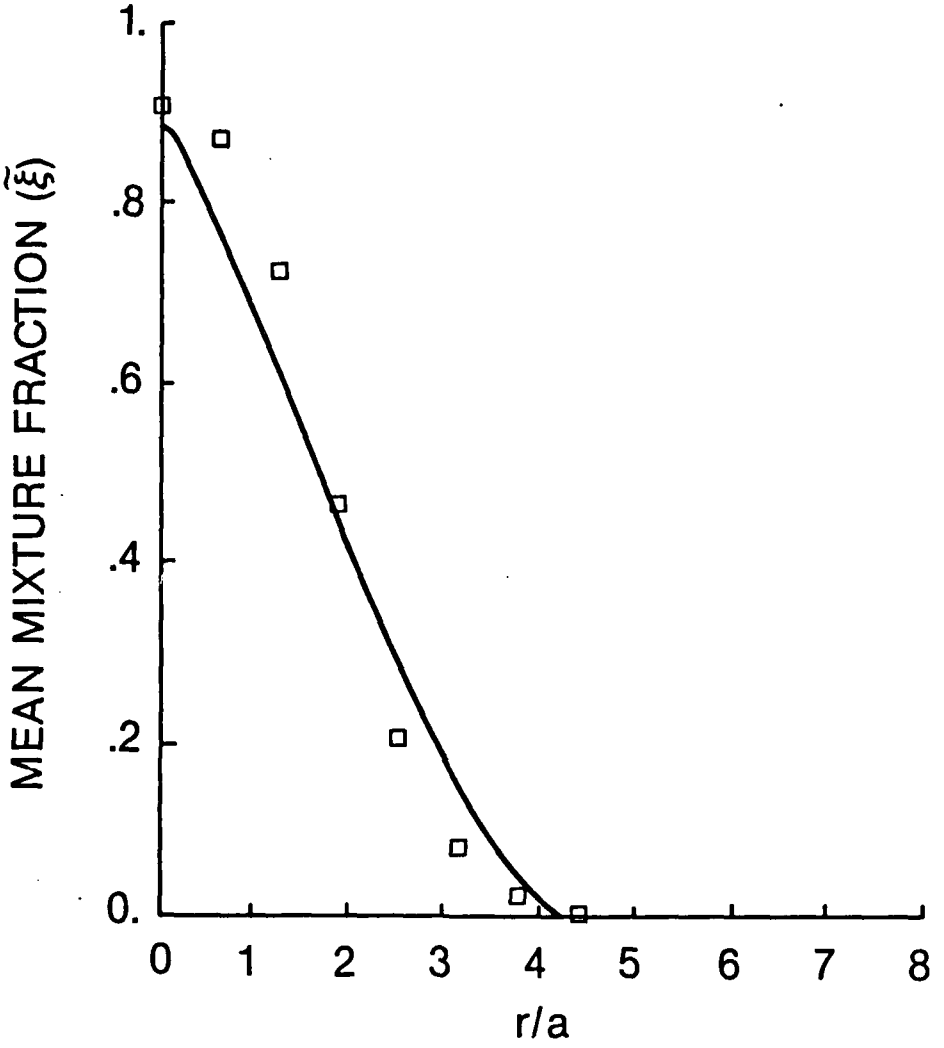

Figure 21. Radial profiles of mass-averaged mean mixture fraction at $x/d = 10$

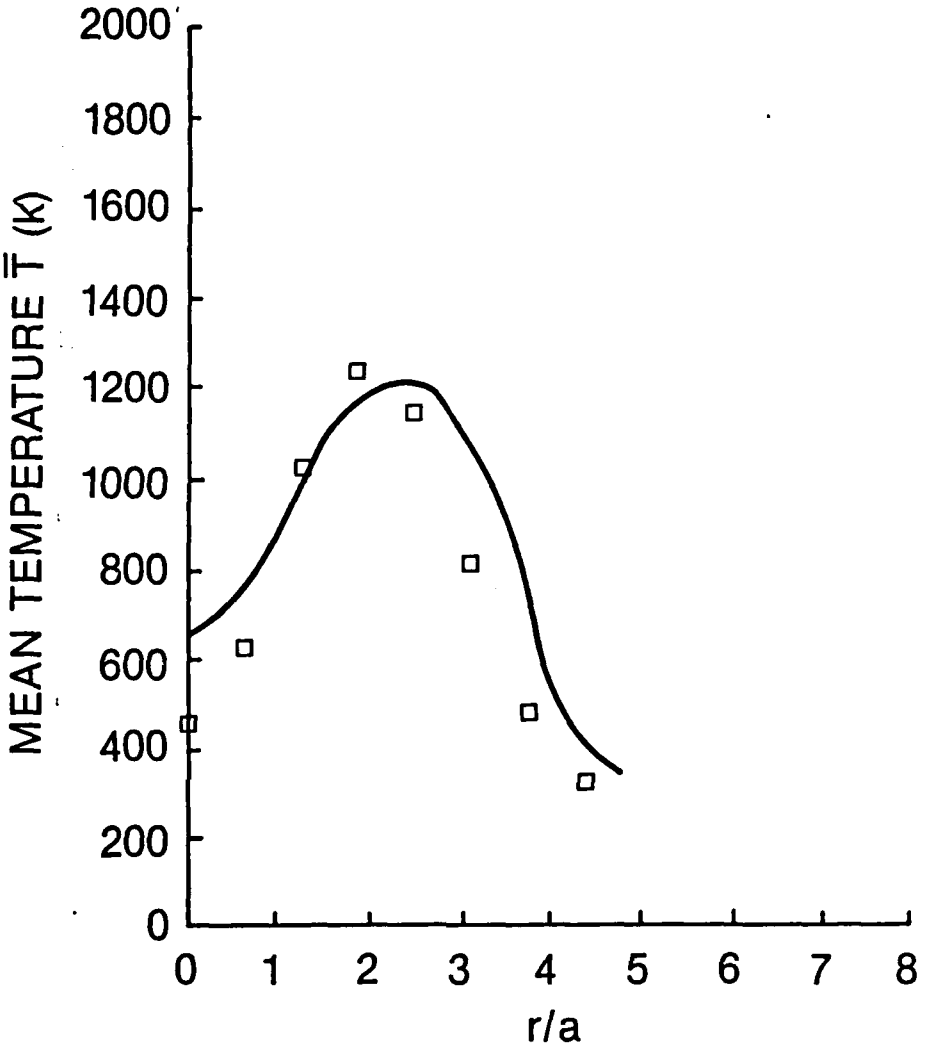

Figure 22. Radial profiles of mean temperature at $x/d = 10$

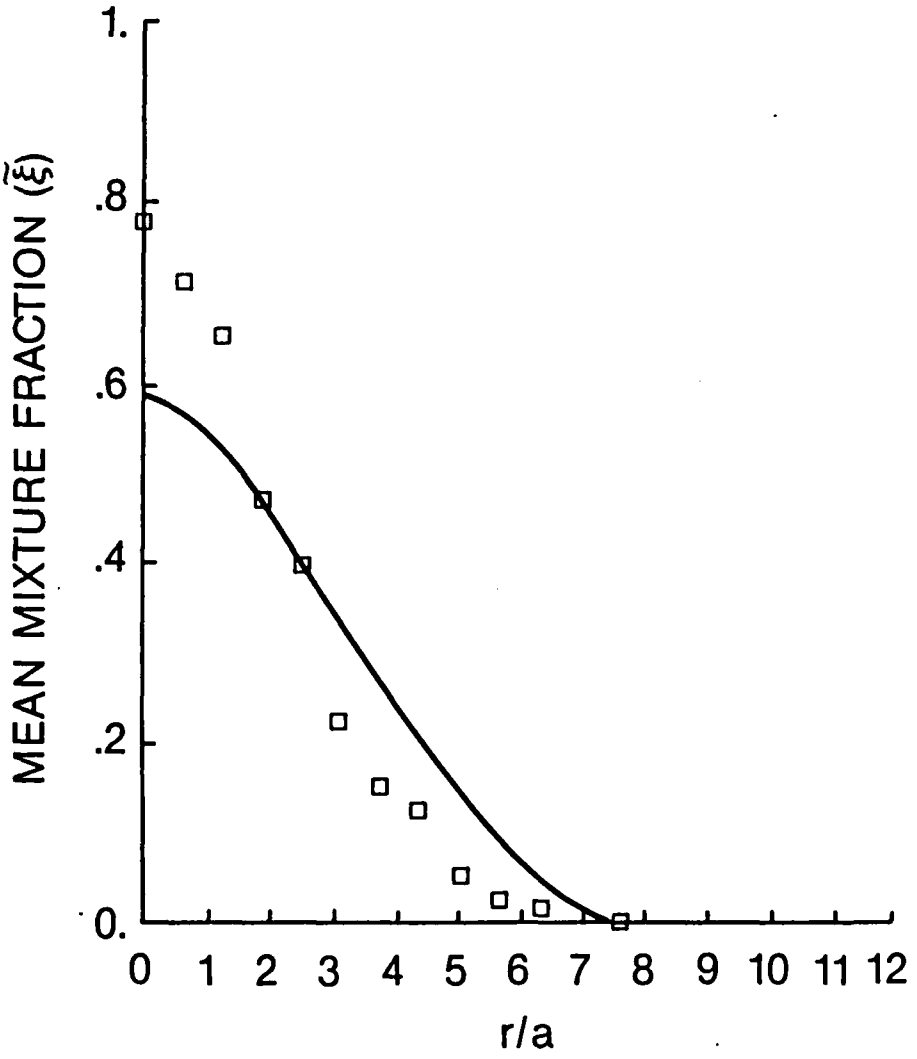

Figure 23. Radial profiles of mass-averaged mean mixture fraction at $x/d=20$

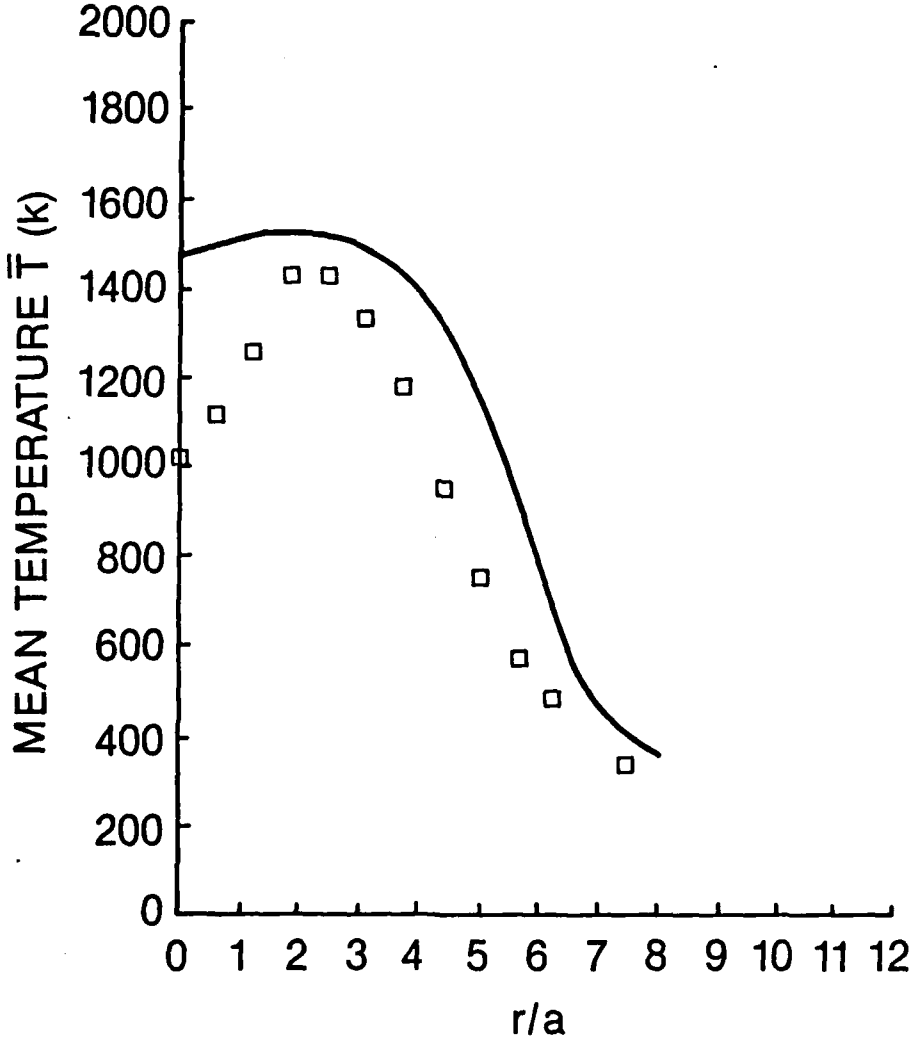

Figure 24. Radial profiles of mean temperature at $x/d=20$

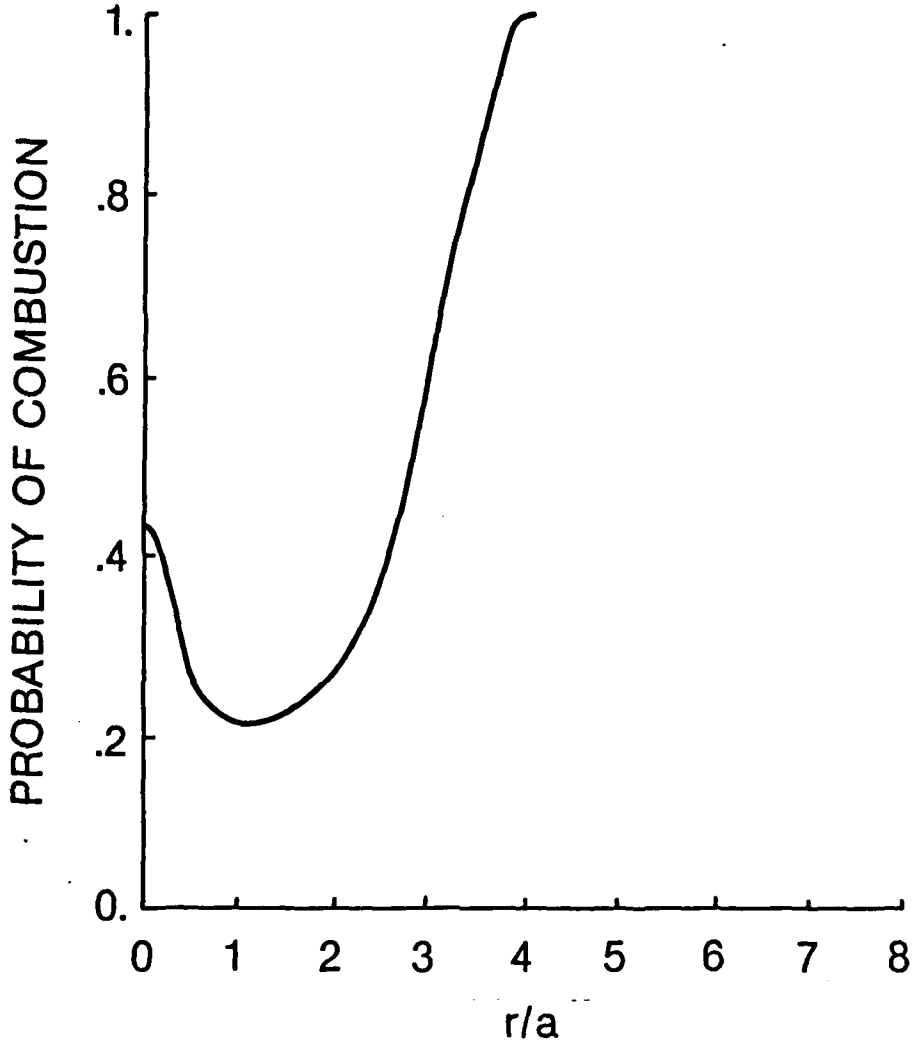

Figure 25. Radial profiles of probability of combustion at $x/d = 10$

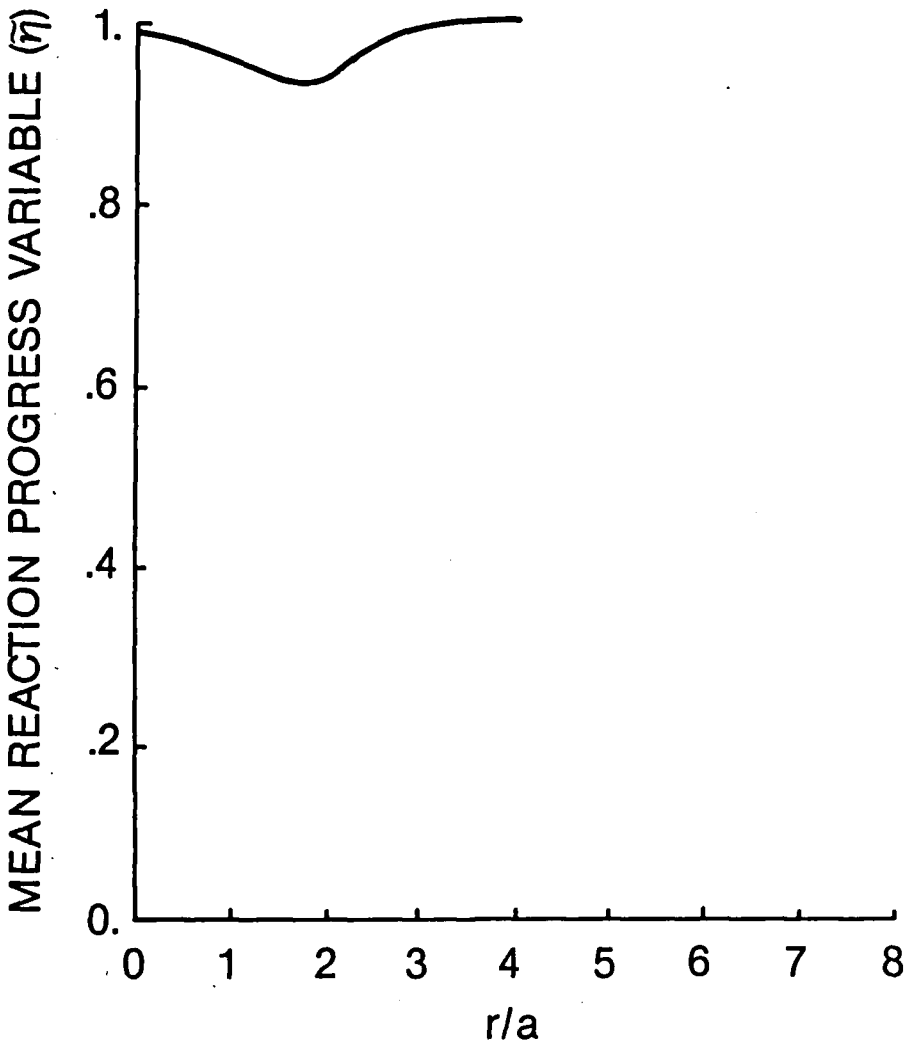

Figure 26. Radial profile of mass-averaged mean reaction progress variable at $x/d = 10$

The incompressible flow about a cylinder resembles the Hiemenz plane stagnation flow, in the region of the forward stagnation point, $s/R << 1$ where s is an arc coordinate starting at the stagnation point. This flow consists of an outer potential flow and an inner boundary layer flow (Figure 27). The characteristic normal strain (α) can be obtained from the solution for the cylinder – a doublet plus a uniform flow – evaluated at the forward stagnation point on the cylinder surface, as

$$\alpha = \frac{2V}{R} \tag{8}$$

where V is the approach velocity. In physical terms, this strain is due to the velocity going from V to zero (at the cylinder surface) over a region whose extent is on the order of R [O(R)]. This result is incorrect when applied to extinction of flames of fuels containing significant amounts of H_2, as shown next.

The concept of an inner incompressible region within which the flame resides and the corresponding incompressible calculations [e.g., Miller et al. (1984)] are still valid; the present analysis will show how compressibility in the free stream affects the strain in the inner incompressible region of a cylinder in uniform flow.

The incompressible flow solution cited above can be extended to the (subsonic) compressible regime using the Rayleigh-Janzen method of successive approximations. The method is tedious, becoming impractical for generating terms past second-order. Van Dyke and Guttmann (1983) automated the procedure and (symbolically) computed a 29-term solution for the velocity potential. Because the resulting expressions were too lengthy to be presented, these authors discussed only the numerical results for the maximum tangential speed. Their interest lay in the structure of the flow when locally sonic speed was first attained – specifically, whether a continuous range of shock-free potential flow solutions existed. This information is not sufficient to calculate the strain field. Hence the calculation was repeated in this study and the expression for the potential function was obtained to six terms. As will be seen, higher-order terms were not needed for an adequate level of convergence.

The equation for the velocity potential ϕ for steady, two-dimensional, planar inviscid flow about a right circular cylinder is

$$\phi_{rr} + \frac{1}{r}\phi_r + \frac{1}{r^2}\phi_{\theta\theta} = M^2 \cdot C(\phi_r, \phi_{rr}, \phi_{r\theta}, \phi_{\theta\theta}, \phi_\theta, \gamma, r) \tag{9}$$

where C is a function which contains terms due to compressibility. The subscripts denote differentiation with respect to polar (r,θ) coordinates. The cylinder radius R and uniform-stream velocity V have been used to nondimensionalize the variables. M is the free stream Mach number and γ is the ratio of specific heats.

The boundary conditions on the velocity potential are that the normal velocity is zero on the cylinder surface

$$\phi_r = 0 \text{ at } r = 1 \tag{10}$$

where the subscript denotes differentiation and the far-field velocity is V

$$\phi_r \to r\cos\theta \text{ as } r \to \infty \tag{11}$$

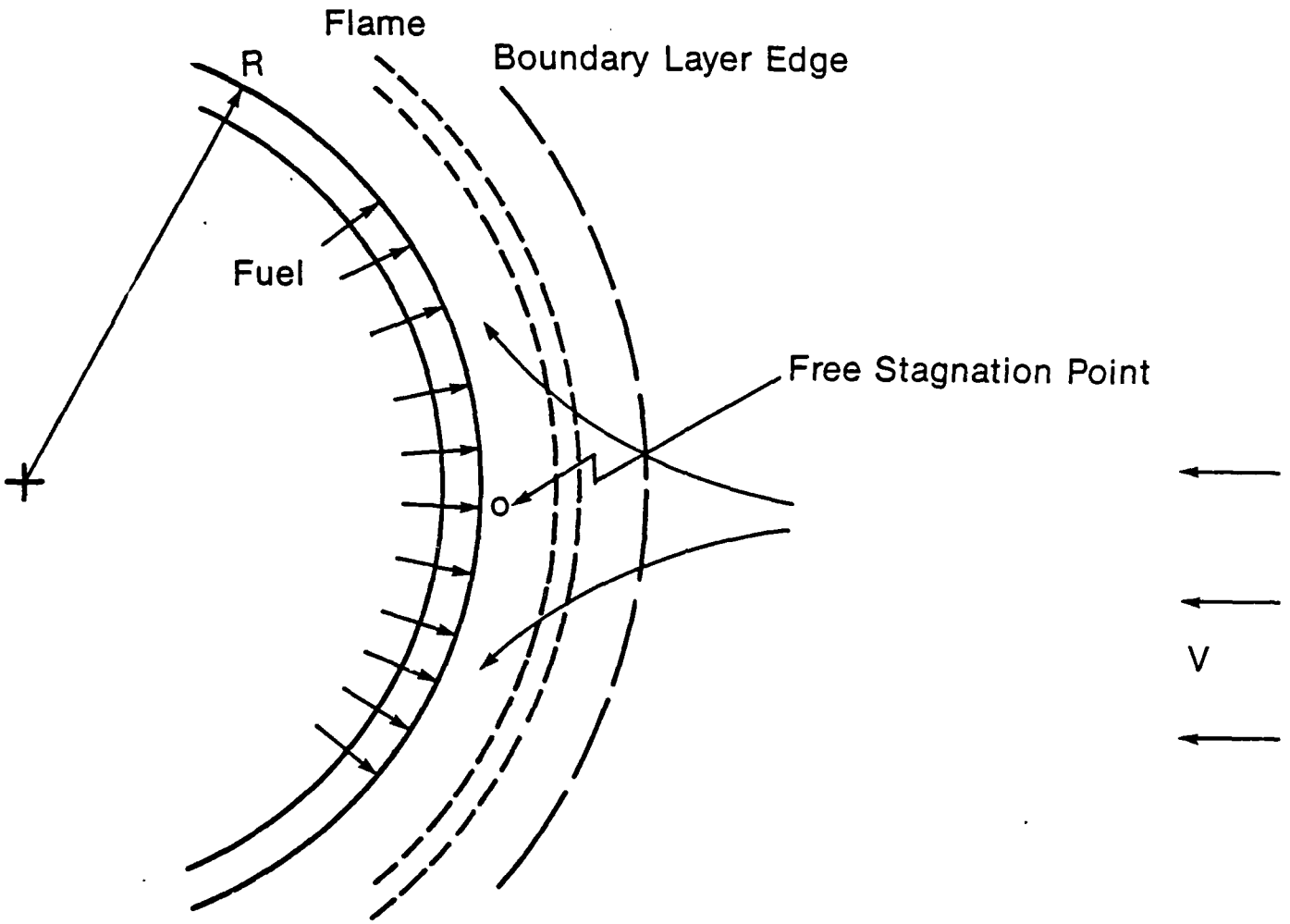

Figure 27. Counterflow diffusion flame in forward region of cylinder.

Moreover, there is no circulation about the cylinder so that only solutions that are symmetric in the polar angle θ can be allowed.

For $M = 0$ (the incompressible case), Equation 9 becomes linear, and the solution can also be derived by the superposition of a uniform stream and a doublet. This leads eventually to the strain given by Equation 8. In the compressible case, the nonlinearity of Equation 9 precludes superposition or other methods of solution in closed form. A method of successive approximations is used to solve Equations 9 through 11.

By expanding the solution for ϕ in a series,

$$\phi = \sum_{n=1}^{\infty} \phi_n M^{2n-2} \tag{12}$$

and substituting the series into Equation 9, a sequence of Poisson equations for each of the coefficients ϕ_i, in turn, is obtained. The $(i\text{-}1)^{th}$ solution is substituted into the right side of Equation 9 to obtain a Poisson equation for the term of order i. This iterative procedure starts with the incompressible solution, ϕ_1, which is

$$\phi_1 = (r + \frac{1}{r}) \cos\theta \tag{13}$$

Because the effort required to generate higher-order solutions in analytical form rapidly exceeds reasonable (manual) bounds, the procedure was automated using a symbolic manipulation language [Moses (1967)].

The solution was obtained up to the term of fifth (zero'th to fifth) order; here the first three terms are presented to show the form of the solution

$$\phi = (r+\frac{1}{r}) \cos\theta + M^2 \left[(\frac{13}{12}\frac{1}{r} - \frac{1}{2}\frac{1}{r^3} + \frac{1}{12}\frac{1}{r^5}) \cos\theta + (\frac{1}{12}\frac{1}{r^3} - \frac{1}{4}\frac{1}{r}) \cos 3\theta \right]$$

$$+ M^4 \left[(225r^8 + 315r^6 - 234r^4) \cos 5\theta + (-1425r^8 - 741r^6 + 945r^4 - 186r^2 + 25) \cos 3\theta \right.$$

$$\left. + (6573r^8 - 4980r^6 + 3045r^4 - 1215r^2 + 183) \cos\theta \right] / (3600\, r^9) + O(M^6) \tag{14}$$

The higher-order terms are too lengthy to be included here.

The solution for the velocity potential is differentiated twice to obtain the equation for the normal strain as an analytic function of r, θ and M^2. It is evaluated at the forward stagnation point ($r = 1$, $\theta = \pi$), to produce a series for the normal strain of interest here. Retaining terms to fifth order, the result is

$$\alpha = \frac{2V}{R} (1 - 0.8333M^2 - 0.3283M^4 - 0.7237M^6 - 1.6106M^8 - 4.2178M^{10}) \tag{15}$$

The ratio of specific heats (γ) appears in terms past second-order, and was taken to be 1.4. Note that the coefficients of the higher-order terms remain of order unity.

The radius of convergence of the series for the maximum surface speed is estimated as $M = 0.403$ (to three significant figures) by Van Dyke and Guttmann (1983). This series

$$\left[\frac{u(1,\theta)}{V}\right]_{\max} = \sum_{n=1}^{\infty} k^n M^{2n-2} \tag{16}$$

has coefficients k^n which grow with n; for example, $\alpha_1 = 2.0$, $\alpha_6 \simeq 96.3$, $\alpha_{12} = 7.26 \times 10^5$, $\alpha_{20} = 2.95 \times 10^{11}$. On the other hand, the coefficients of the series for the normal strain, as given in Equation 15, remain of order unity.

Equation 15 may seem surprising because the higher-order terms, which are due to compressibility, reduce the strain in the region of interest. Figure 28 shows that this reduction can be quite significant. To investigate this phenomenon, the strains corresponding to the first three terms are plotted along the stagnation streamline. These strain terms are

$$\alpha_0(r) = -\frac{2}{r^3}\frac{V}{R} \tag{17}$$

$$\alpha_1(r) = -\left(\frac{5}{3}\frac{1}{r^3} - \frac{5}{r^5} + \frac{5}{2}\frac{1}{r^7}\right)\frac{V}{R} \tag{18}$$

and

$$\alpha_2(r) = -\left(\frac{2.985}{r^3} - \frac{18.020}{r^5} + \frac{31.300}{r^7} - \frac{21.793}{r^9} + \frac{5.200}{r^{11}}\right)\frac{V}{R} \tag{19}$$

where, to second-order,

$$\alpha(r) = \alpha_0(r) + \alpha_1(r)M^2 + \alpha_2(r)M^4 \tag{20}$$

The signs in Equations 17 through 19 are consistent with the coordinate system. (The strains in Equations 8 and 15 are the absolute values of sums of series similar to Equation 20.)

Figures 29 through 31 show the variation of these strain terms. The leading term decays monotonously (Figure 29), while the higher-order terms each display a zero-crossing. From Equation 18 it can be shown that the term α_1 crosses zero at $r = 1.538$. Thus, the reduction in strain due to compressibility exists only within this location. Outside $r = 1.538$, this first order strain term becomes negative (Figure 30) and so increases the strain, agreeing with the intuitive notion that compressibility ought to reduce the forward influence of the stagnation point. These regions will be referred to as the near- and far-fields, respectively.

Equation 11 also shows that the near-field reduction of strain is due to the r^{-5} term. The r^{-3} term corresponds to a doublet, as discussed earlier, and has the same sign as the leading strain term, α_1. Thus, the near-field reduction in strain is due to the localized effects of higher-order singularities, which enter the solution due to the source terms in Equation 9. Equation 19 and Figure 31 show that the second-order term α_2 expands the near-field region of reduced strain (the zero crossing occurs further upstream, at $r = 1.925$) and the overall size of the region affected by compressibility (the asymptotic approach to zero occurs further upstream).

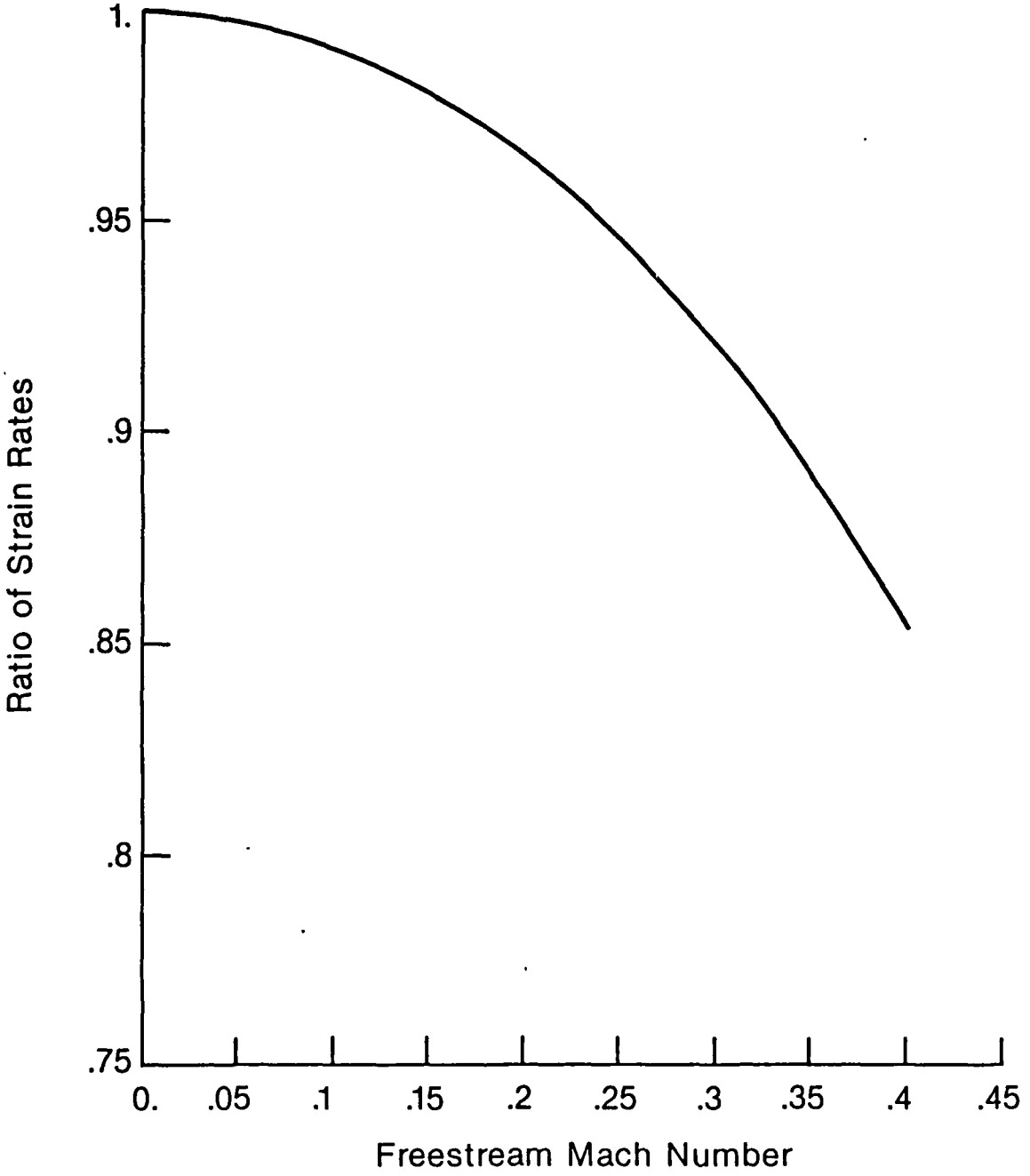

Figure 28. **Variation of strain rate due to compressibility, normalized by incompressible strain rate.**

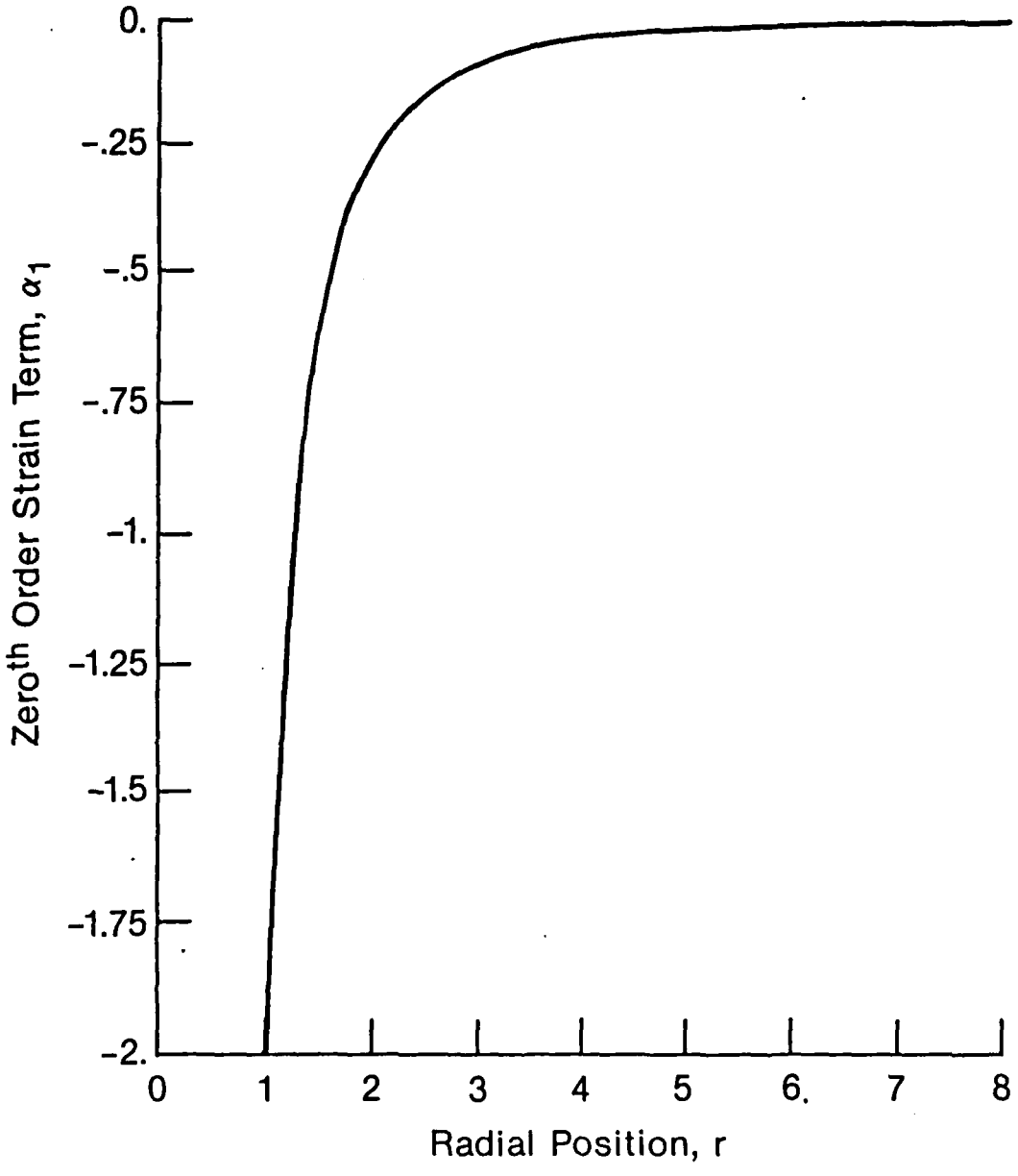

Figure 29. Variation of zero'th order strain term along stagnation streamline.

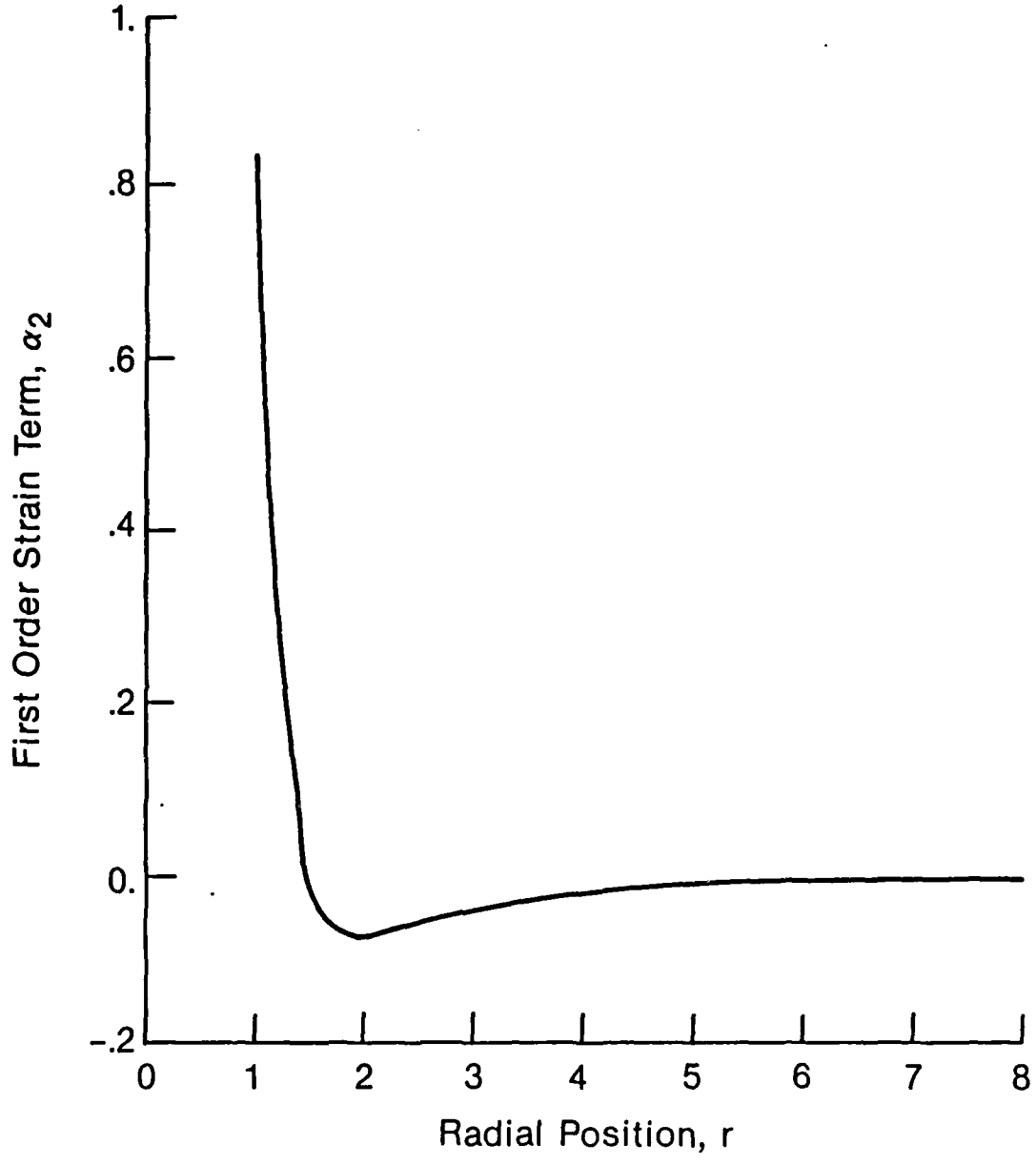

Figure 30. Variation of first order strain term along stagnation streamline.

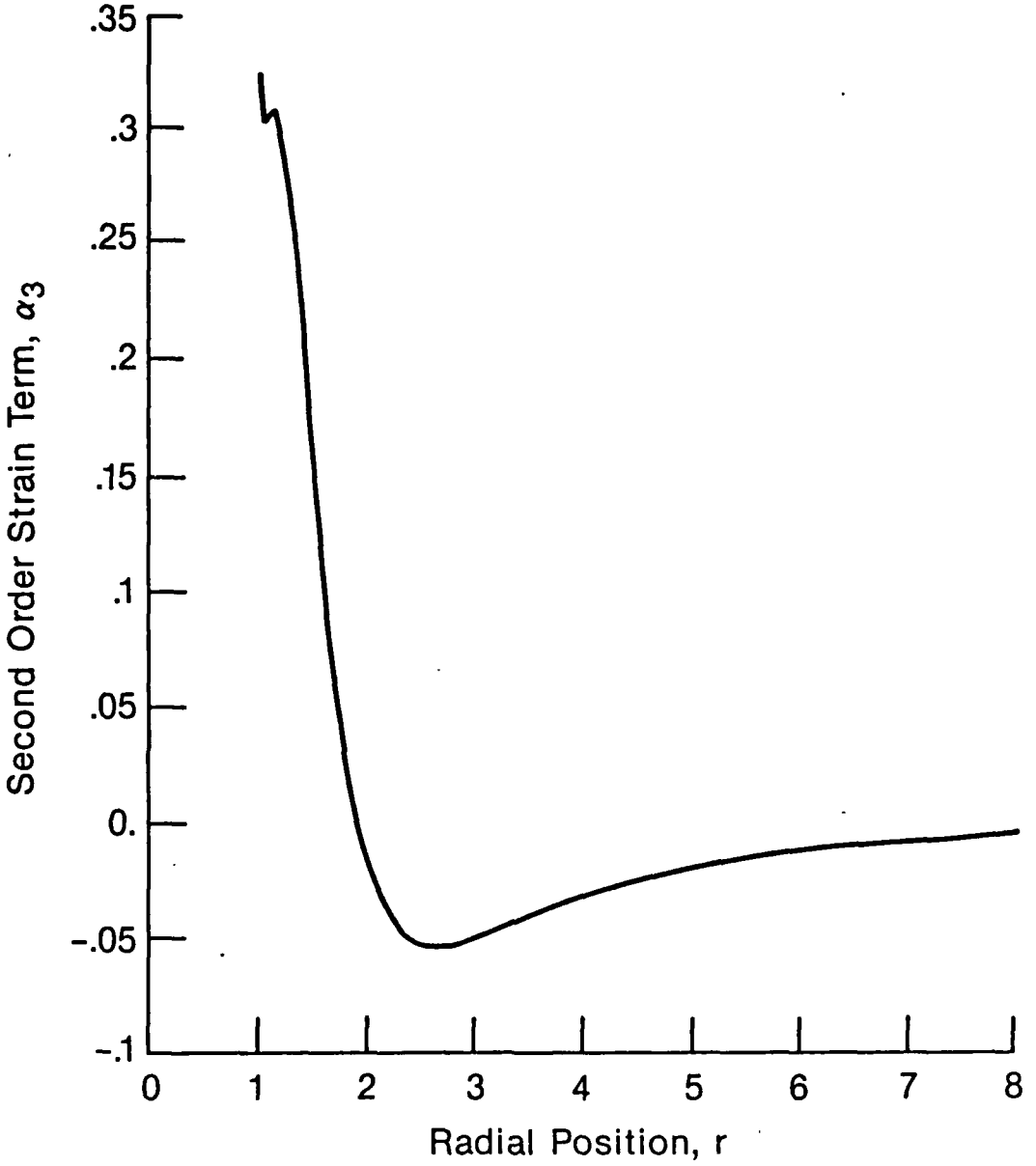

Figure 31. Variation of second order strain term along stagnation streamline.

Assuming a cylinder radius of 2 cm, the free stream velocity corresponding to an extinction strain of 12,000 s^{-1} is 120 m/s which is equivalent to a free stream Mach number of approximately 0.34, within the scope of this analysis. (A free stream air sonic speed of 347 m/s has been assumed).

Figure 32 shows the critical velocity required to produce the (critical) strain of 12,000 s^{-1} as a function of the cylinder radius. The deviation from the linear relation of Equation 8 at higher velocities (Mach numbers) is clear. The velocity range is chosen to emphasize the regime where compressibility is first noticed. These results should be used to correct laboratory measurements of critical strain for extinction of hydrogen flames and suggest an alleviation of strain in compressible turbulence.

2.6 Extended Partial-Equilibrium Model

In the partial-equilibrium model for CO/H_2 flames just described, CO is considered to be in partial equilibrium with the radical species by assuming the reaction (S5)

$$CO + OH \rightarrow CO_2 + H \qquad (S5)$$

to be fast enough. This assumption has been relaxed in other studies [Correa (1985)]. Denoting the partial equilibrium CO levels with the superscript *pe*, a third variable ψ can be defined to account for CO kinetics

$$\psi \equiv \frac{Y_{CO} - Y^{pe}_{CO}}{Y^{u}_{CO} - Y^{pe}_{CO}} \qquad (21)$$

ψ varies between 0 (when CO kinetics are sufficiently fast for CO to be in partial equilibrium with the radical pool) and 1 (when the CO is completely frozen). Thus the two-variable partial equilibrium model is a special case ($\psi = 0$) of the current model. Similarly, full chemical equilibrium is realized when $\eta \rightarrow 1$ and $\psi \rightarrow 0$.

Eleven equations are required to solve for the concentrations, temperature, and density. The mixture fraction provides five of these via the four elemental concentrations and total enthalpy. Using equilibrium relationships for the radical pool, three more equations are obtained while specification of η yields a fourth equation. Another equation results from Equation 21 for given ψ and the equation of state completes the set. The three-dimensional space defined by the three variables ξ, η, and ψ is then covered with a uniform mesh and the above equations solved for each point of interest (ξ,η,ψ), thus generating a thermochemical "library" for the instantaneous state of the fluid as in the two-variable approach.

Application of the model, with k-ϵ/assumed-shape pdf closure, to the above 40% CO/ 30% H_2/ 30% N_2 jet flame at a Reynolds number of 8500 shows that CO kinetics are significant only in the initial region of the jet [Correa (1985)]. Within 30 diameters, the CO attains partial equilibrium with the radical pool, and the entire pool reaches full chemical equilibrium via relatively slow three-body recombination reactions by about 50 to 75 diameters. Once the CO is in partial equilibrium, $\psi = 0$, and the two-variable model discussed earlier would apply. In flames at higher Reynolds numbers, however, the CO may not reach partial equilibrium as rapidly, and the entire flame might be influenced by CO kinetics. Full details of this thermochemical model and the transport equations are presented in Correa (1985).

2.7 Bluff-Body-Stabilized Flame

A bluff-body-stabilized combustor that employs recirculating flow in the near-exit region of the jet

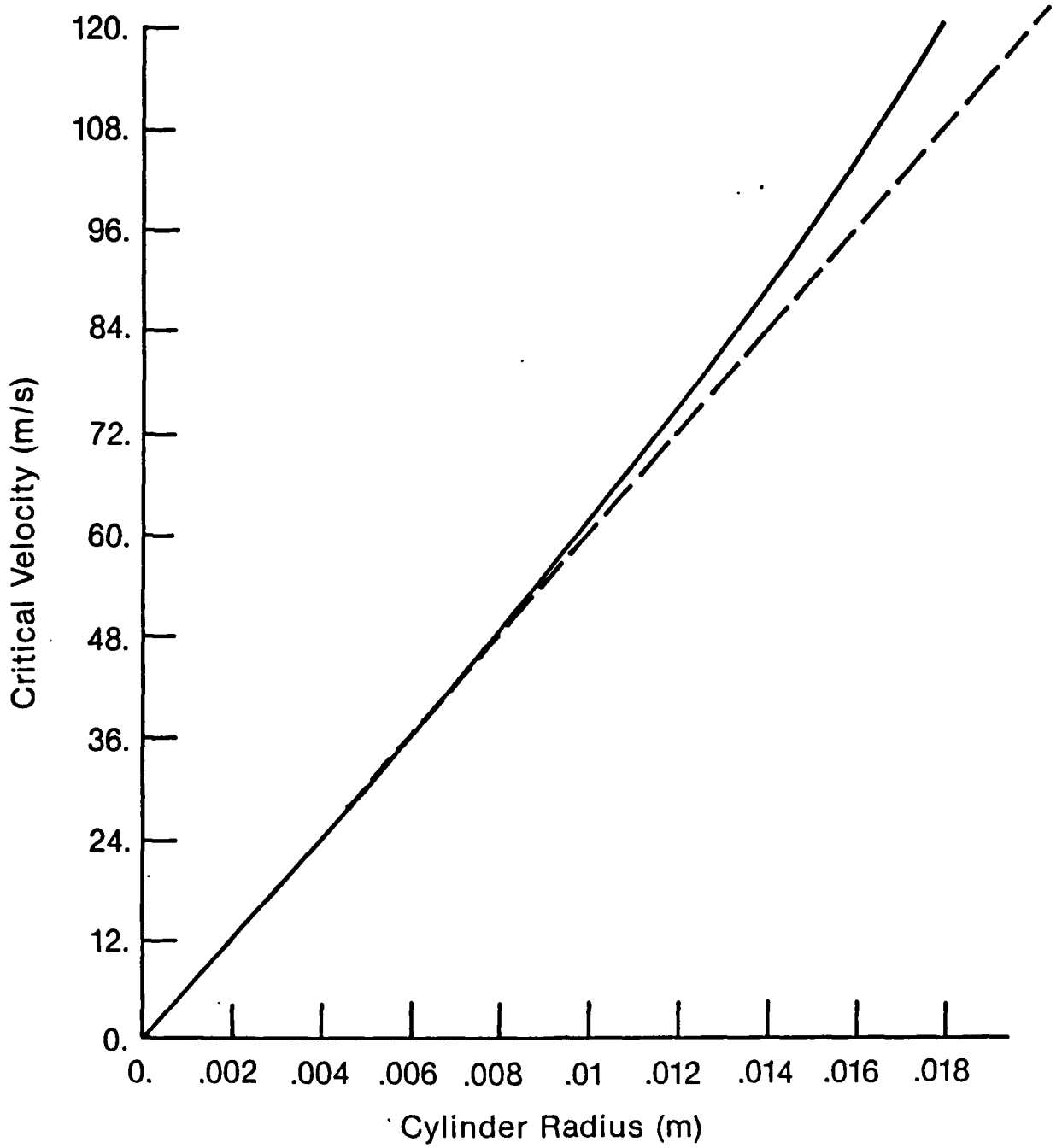

Figure 32. Variation of critical velocity with cylinder radius allowing for compressibility.

----------incompressible _____compressible

to stabilize the flame was designed and used to provide flame stabilization at higher Reynolds numbers. A schematic of the apparatus is shown in Figure 33. Preliminary results with different fuels are reviewed here. The bluff-body combustor has an outer diameter of 38.1 mm and is installed in the tunnel such that the exit plane is fairly downstream from the contraction zone. The bluff body has a jet of diameter 3.18 mm located in its center. The flame is stabilized by the recirculation zone provided by the bluff body. The ratio of the bluff-body diameter to the central jet diameter is 12:1 as opposed to the 28:1 design studied by Roquemore and coworkers [1980, 1982]. The blockage ratio provided by the bluff body is less than 5%. Hence, the flowfield can be assumed to be axisymmetric. Different fuels such as CH_4 and CO/H_2 mixtures were used to stabilize the flame in the tunnel at various Reynolds numbers. It was found that the flowfield was jet-dominated for most of the cases studied. Despite this, modeling would be complicated by recirculation for reasons of numerical accuracy and less reliable models of turbulence [Correa (1984)], as discussed briefly below.

The data discussed above (for Re = 15,000 LHC turbulent flame) indicates a low (or zero) probability of local extinction in pilot-stabilized jet flames. Attempts to increase the Reynolds number of the jet beyond Re = 17,000 were unsuccessful. Thus, there is a need to change the strain rate field by altering the mechanism of stabilization. The following discussion deals with our experiments (in a limited manner) with bluff-body-stabilized flames.

Bluff-body stabilized flames have two advantages over jet flames, but have one very serious drawback. The first advantage is that the wake behind the bluff body and the shear layer adjacent to it on both sides provide a region of large strain rates, which increase up to the forward stagnation point. Thus, the region of maximum strain rate (the region of interest) is located sufficiently downstream of the lip of the flameholder so that inlet perturbations there should not affect the strain field dramatically. In jet flames the maximum strain rate is at the lip of the jet and is very sensitive to the inlet free stream conditions. Secondly, there is no need for pilot stabilization, and thus there is no interference from the premixed pilot as suspected in jet flames. The major drawback in studying bluff-body-stabilized flames is that the recirculation zone is very difficult to model because of the mathematically elliptic nature of the flowfield and the lack of a sufficiently reliable turbulence model. Thus, the modeling of turbulence-chemistry effects may become overshadowed by the problems associated with the turbulence model and computational scheme [Correa (1984)], thus making the interpretation of the results difficult.

Figure 34 shows the bluff-body combustor installed in the 6 in. × 6 in. tunnel. Three different fuels were used: (a) H_2/N_2 mixtures, (b) LHC gas, and (c) methane. Figure 35 shows a turbulent flame at Re = 31,600 (based on cold flow jet conditions) with fuel composition of 78% H_2, 22% N_2. The jet velocity is estimated to be 340 m/s, whereas the coflowing air speed is 20 m/s. The flame is seen to be completely jet-dominated and is stabilized in the recirculation zone behind the bluff body. The flame brush appears very turbulent even in this time-averaged photograph. The flame has negligible luminosity as expected in H_2/N_2 flames. At higher Reynolds numbers and higher nitrogen concentrations, the flame was found to begin to lift off and eventually blow off.

Figures 36 through 38 show the effect of the bluff-body stabilizer in a 20% H_2, 80% CO turbulent flame. The jet velocity in all cases is 40 m/s and the Reynolds number is estimated to be 7400. Figures 36, 37, and 38 correspond to coflowing air speeds of 10, 20, and 30 m/s, respectively. At low air velocities the flame is quite jet-like since the ratio $\frac{U_j}{U_a}$ is $>> 1$. As the air velocity is increased, the flame appears more wake-like and eventually appears totally wake-dominated. The flame appears more luminous because of the $CO + O \rightarrow CO_2$ chemiluminescence. Figure 39 shows a 15% H_2, 60%

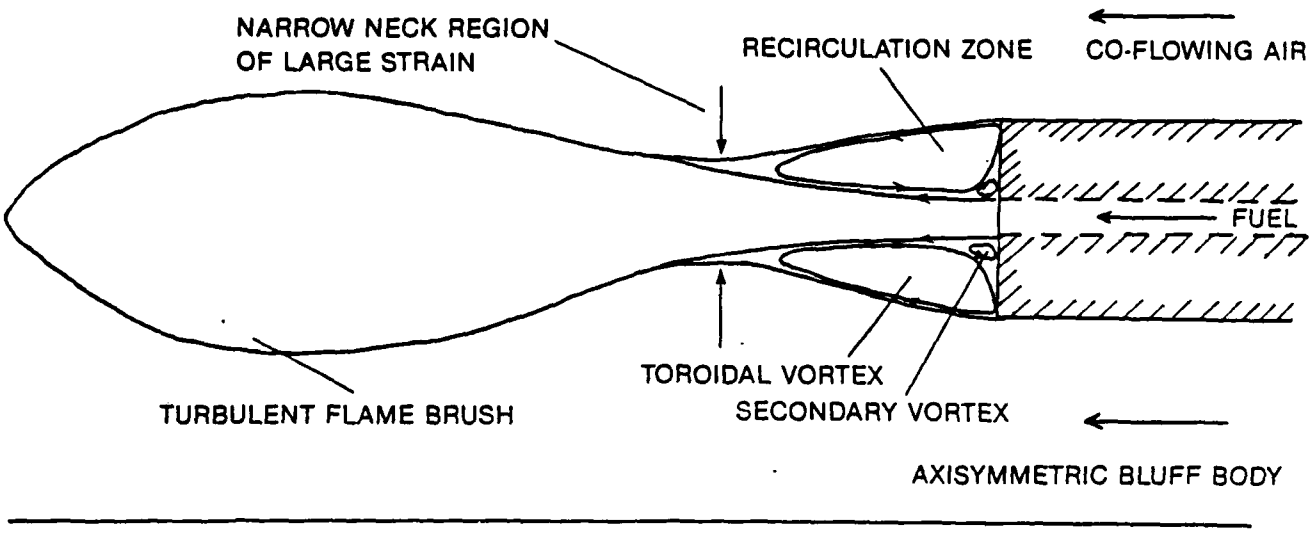

Figure 33. Schematic of a jet-dominated bluff-body stabilized turbulent diffusion flame.

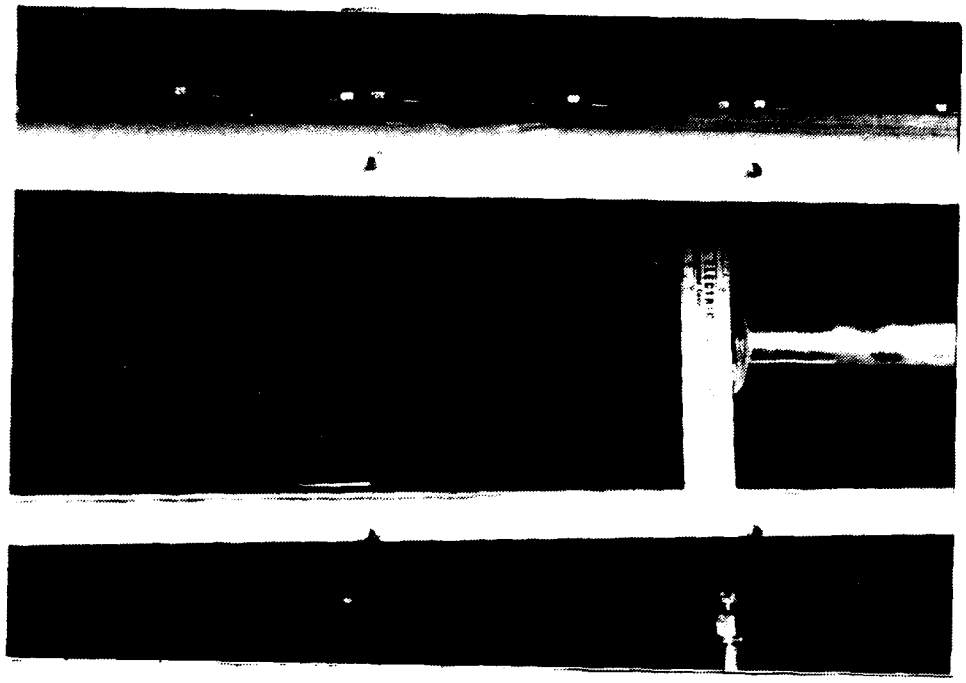

(a)

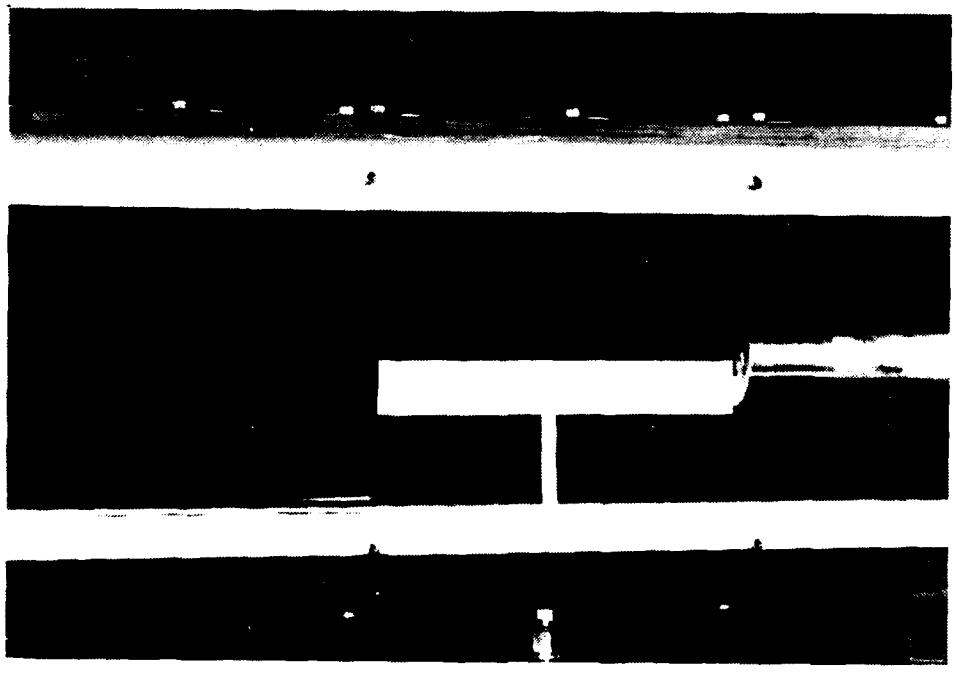

(b)

Figure 34. **Photograph of bluff-body combustor installed in the 6 in. × 6 in. combustion tunnel.**

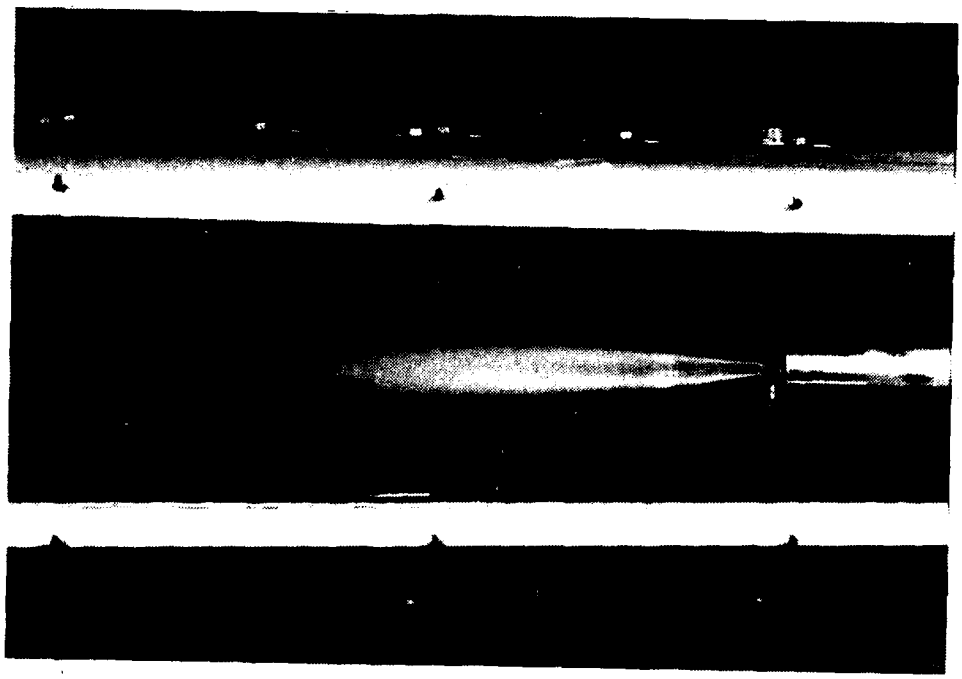

Figure 35. **Bluff-body stabilized turbulent flame Re = 31,000 (78% H_2, 22% N_2). The jet velocity is 340 m/s; co-flowing air is 20 m/s.**

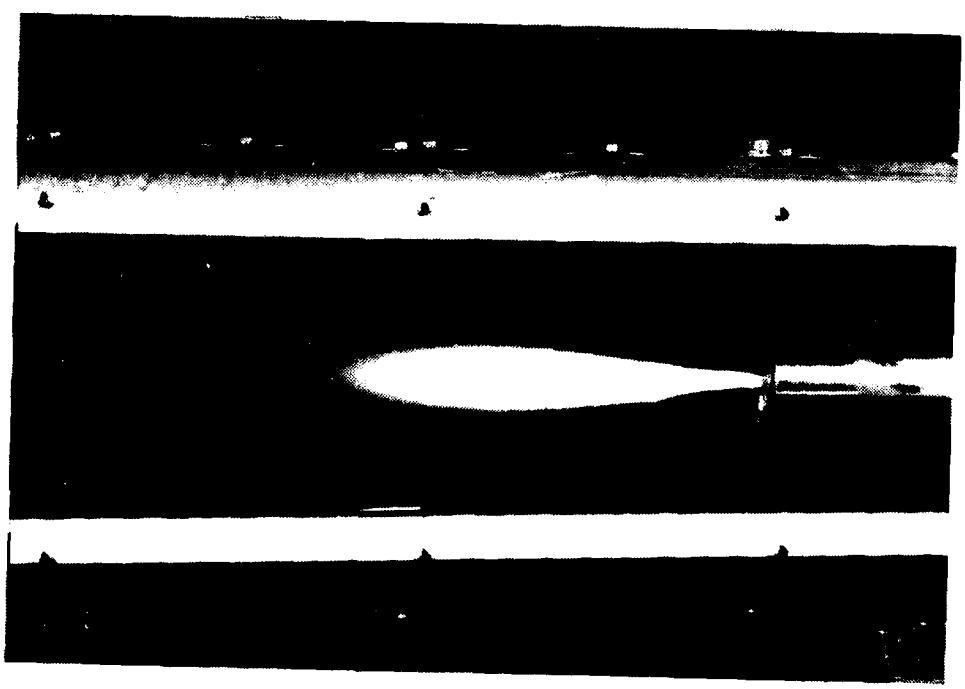

Figure 36. **Bluff-body stabilized turbulent flame Re = 7400 (20% H_2, 80% CO, V_j = 40 m/s, V_a = 10 m/s).**

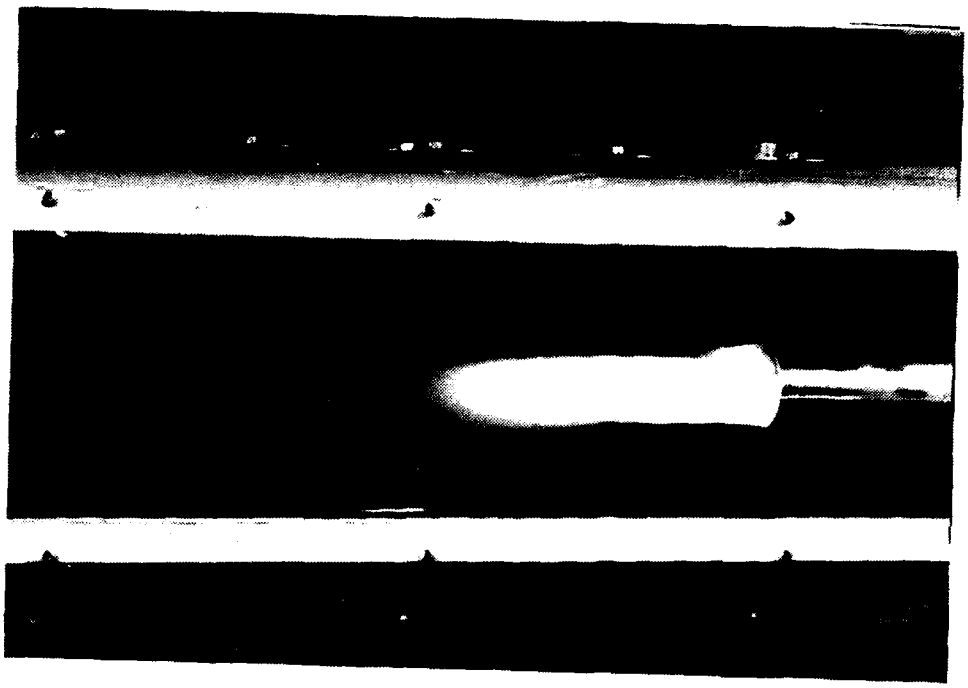

Figure 37. Turbulent flame, Re = 7400 (20% H_2, 80% CO, V_j = 40 m/s, V_a = 20 m/s).

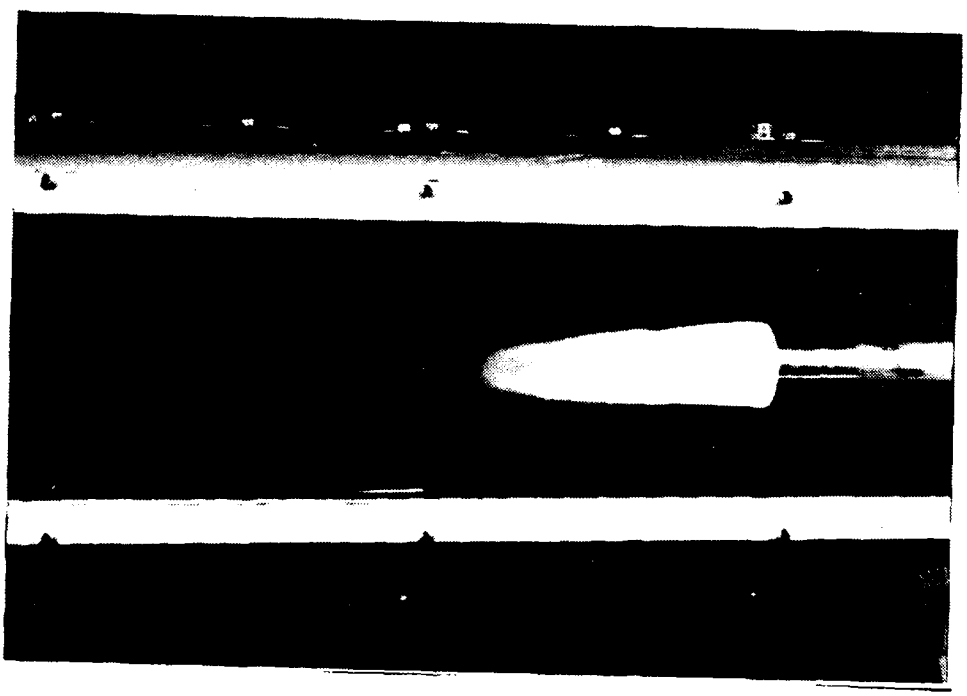

Figure 38. Turbulent flame, Re = 7400 (20% H_2, 80% CO, V_j = 40 m/s, V_a = 30 m/s).

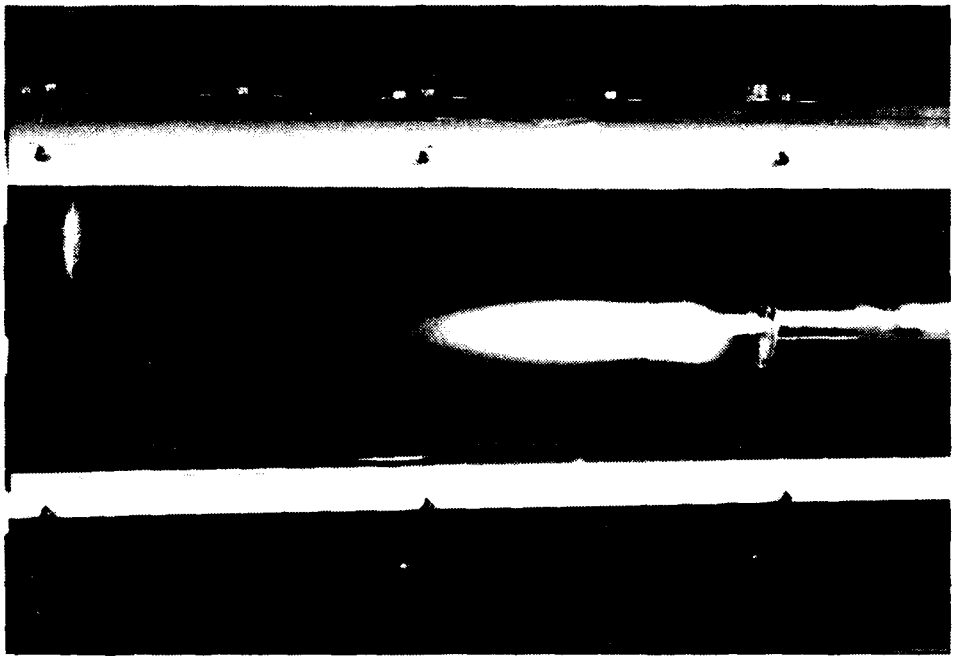

Figure 39. **Turbulent flame Re = 10,500; 15% H_2, 60% Co, 25% N_2, V_j = 55 m/s, V_a = 30 m/s.**

CO, 25% N_2 flame at Re = 10,500 (U_j = 55 m/s) with coflowing air at 30 m/s. Even though the flame is jet-dominated, the effect of the wake and the adjoining shear layer is clear in this photograph. Up to the forward stagnation point, the flame appears jet-dominated, but in the intense shear zone there, the turbulent brush appears highly convoluted and is broadened by the recirculation zone. The flame there looks quite different from a jet. Finally, Figure 40 shows the same 10% H_2, 40% CO, 50% N_2 (LHC) Re = 15,000 flame brush stabilized by the bluff body instead of a premixed pilot. The flame is jet-dominated, but the recirculation results in a broadening of the flame front and makes it look more turbulent. The probability of local extinction should be greatest in the region near the stagnation point where the brush appears to be most turbulent.

The most dramatic effect of bluff-body stabilization is apparent in the case of the methane flame. Figures 41 through 43 illustrate the effect of increasing the jet Reynolds number of a 100% methane flame in coflowing air at 20 m/s. At a jet velocity of 65 m/s (Re = 12,600), the flame (Figure 41) assumes the appearance of a traditional bluff-body-stabilized flame. The flame narrows progressively from the exit plane and is narrowest at the end of the recirculation zone, where the strain field should be maximum. In this region the flame appears to be significantly stretched. As the jet velocity is increased to 75 m/s (Re = 15,000, Figure 42), the flame starts to blow off intermittently in the narrow neck region. Apparently, the strain in this region causes the flamelets to be locally extinguished in this region but as the strain field diminishes exponentially further downstream, these flamelets reignite because there are still sufficient radicals and hot products from the wake region to provide sources of ignition. The main flame region is downstream of the narrow neck and appears to the eye to be connected to the wake only in an intermittent fashion. As the jet velocity is further increased (U_j = 90 m/s, Re_j = 17,000) in Figure 43, the flame downstream of the neck eventually blows off and is no longer able to reignite. This is probably because, for fixed coflowing air, as the jet velocity is increased, the flame gets stretched enough so that eventually it is extinguished and blows off. The flame near the wake of the flameholder remains in the recirculation zone.

This dramatic effect of interaction between the jet, recirculation zone, and the coflowing air is most apparent in methane flames because the flame speed is low and the stoichiometric mixture fraction value (ξ_s = 0.058) is low, which implies that the stoichiometric contour extends significantly downstream of the exit plane and is thus affected by the intense shear zone at the stagnation point. The LHC gas has a similar value of flame speed, but the value of ξ_s is 0.43 such that the flame brush is very small, and most of the fuel is burned upstream of the region of largest strain. The hydrogen flame shows no effect (ξ_s = 0.028) for a different reason; its flame speed is extremely high, and hence it is very difficult to induce local extinction in H_2 flames even with significant nitrogen dilution. A further difference between H_2 (and CO/H_2) flames versus methane flames is that, in the latter, radicals are consumed by alkyl species. If not continuously produced by reactions, therefore, these radicals disappear and the flame is extinguished.

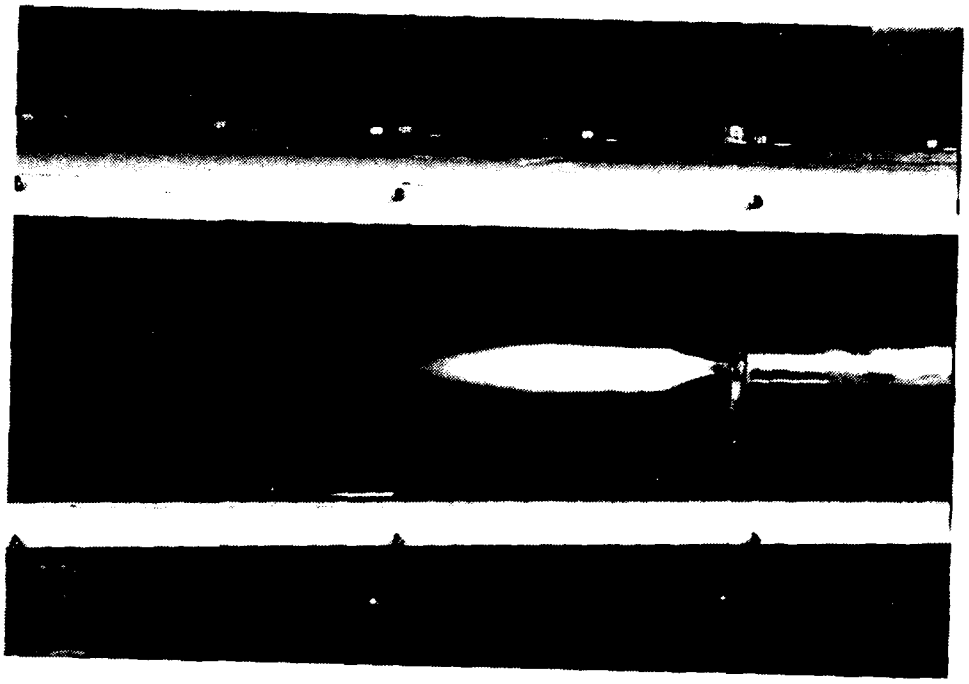

Figure 40. Turbulent flame, Re = 15,000, 10% H_2, 40% CO, 50% N_2, (LHC), V_a = 30 m/s, v_j = 80 m/s.

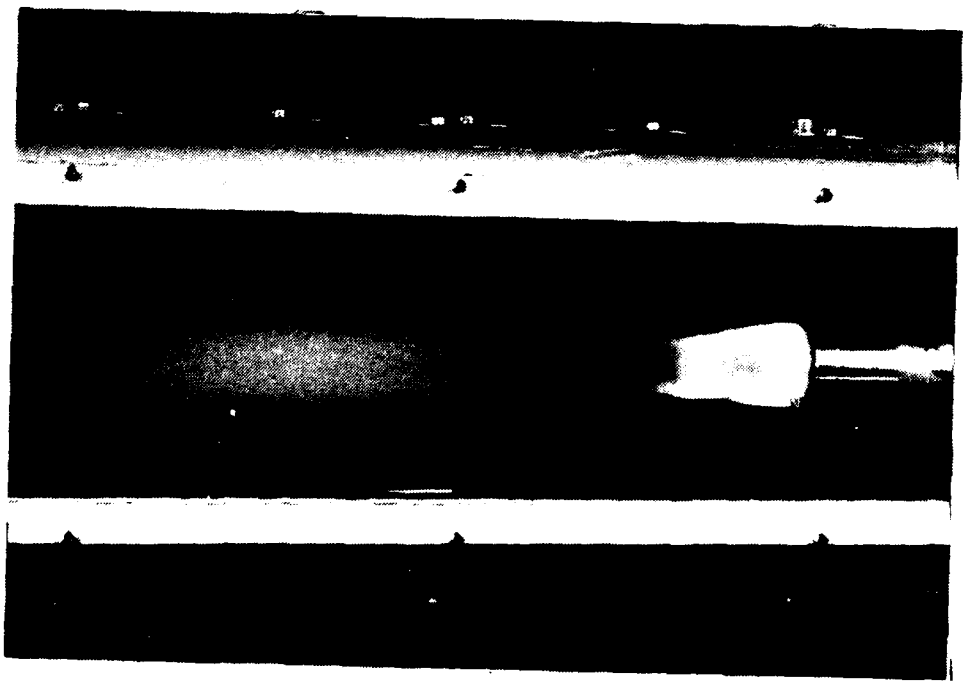

Figure 41. Turbulent methane flame, Re = 12,600, V_j = 65 m/s, V_a = 20 m/s.

Figure 42. Turbulent methane flame, Re = 15,000, V_j = 75 m/s, V_a = 20 m/s.

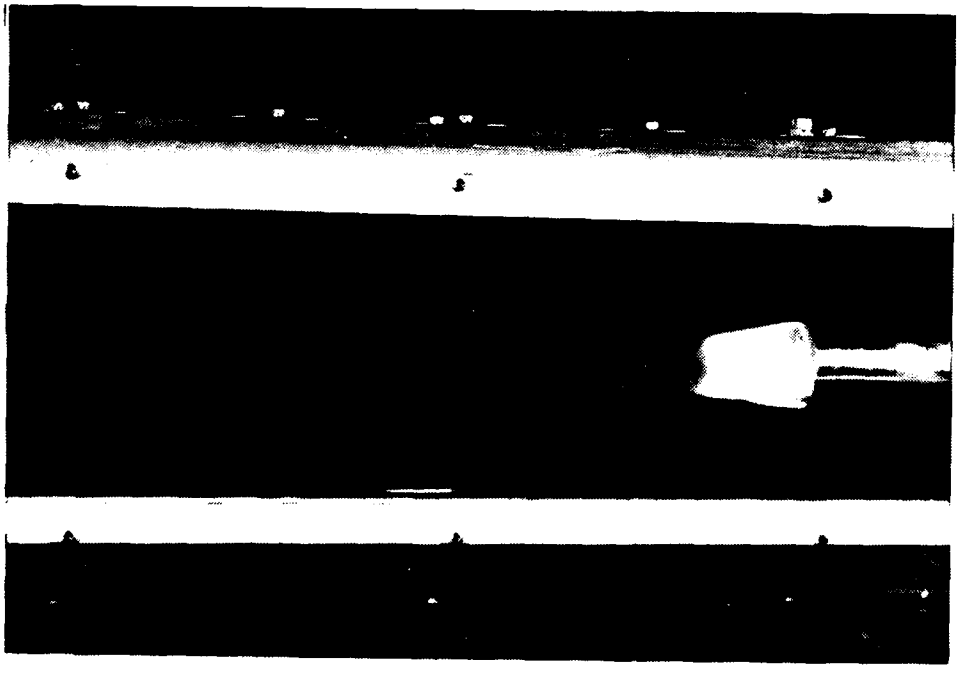

Figure 43. Turbulent methane flame, Re = 17,000, V_j = 90 m/s, V_a = 20 m/s.

3. NOMENCLATURE

a,b	Parameters in beta function
$c_1 - c_3$	Parameters in pdf
c_{g2}	Constant in variance transport equation
C_1, C_2, C_μ	Constants in $k-\epsilon$ model
D	Diffusion coefficient
d	Diameter
f	pdf of conserved scalar
Fr	Froude number
g	pdf of reactive scalar
h	Total enthalpy
I	Intermittency
j	Turbulent flux
J	Jacobian
k	Turbulence kinetic energy, reaction rate, coefficients in series
M	Number of chemical elements, Mach number
M_i	Molecular mass of species i
N	Number of species
p	Pressure
P	Joint pdf of two scalars
Pe	Peclet number
Pr	Prandtl number
q	Twice the turbulence kinetic energy
q_{ij}	Metric terms in coordinate transformation
R	Universal gas constant, turbulence time-scale ratio
R	Cylinder radius
Re	Reynolds number
$\dot{r}$	Reaction rate per unit volume
S	Swirl ratio
Sc	Schmidt number
T	Temperature
u,v	Velocity components in Cartesian coordinates
V	Velocity of approach flow

u_i	Velocity component in i direction
$\dot{w}_i$	Rate of reaction i
X	Scalar dissipation rate
x_i	Cartesian coordinate i
Y_i	Mass fraction of species i
Z_i	Elemental mass fraction of species i
α	Strain rate
β	Beta function
Γ_i	Diffusion coefficient for quantity i
δ	Dirac delta function
δ_{ij}	Kronecker delta
ε	Dissipation rate
η	Reaction progress variable, coordinate
μ	Viscosity
μ_{ij}	Mass of ith element in unit mass of jth species
ν	Kinematic viscosity
θ	Polar angle
ξ	Mixture fraction, coordinate
ρ	Density
σ_i	Turbulent Prandtl number for quantity i
τ	Time
τ_{ij}	Turbulent stress
ϕ	Scalar variable, generalized variable, velocity potential function
ψ	Deviation variable for CO kinetics

Subscripts

r,θ	Derivative with respect to coordinate r,θ
c	Critical
i	Cartesian component
s	Species index

Superscripts

l	Laminar

a	Air
e	Equilibrium
f	Fuel
s	Stretched
t	Turbulent
u	Unburned (frozen)
$\tilde{(\,)}$	Density-weighted mean
$(\,)''$	Density-weighted fluctuation
$*$	Transformed variable
$\overline{(\,)}$	Conventional mean
$(\,)'$	Conventional fluctuation

4. BIBLIOGRAPHY

Baulch, D. L., Drysdale, D. D., Horne, D. G., Lloyd, A. C., (1972), *Evaluated Kinetic Data for High Temperature Reactions 3,* London, Butterworths.

Bilger, R.W., (1980), *Comb. Sci. Tech. 22,* 251-262.

Bilger, R.W. and Kee, R.J., (1987), "Simplified Kinetics for Diffusion Flames of Methane in Air," submitted to Western States Section of Combustion Institute.

Burke, S.P. and Schumann, T.E.W., (1928), *Indust. Eng. Chem. 20,* 998.

Chandrasudra, C., Mehta, R.D., Weir, A.D., and Bradshaw, P., (1978), *J. Fluid Mech. 85,* 693-704.

Correa, S.M., Drake, M.C., Pitz, R.W., and Shyy, W., (1984), *Twentieth Symp. (Int.) on Comb.,* The Combustion Institute, Pittsburgh, PA, 337-343.

Correa, S.M., (1984), *AIAA Journal 22,* 1602-1608.

Correa, S.M., (1985), *Archivum Comb. 5, 3-4,* 223-242.

Correa, S.M. and Mani, R., (1987), "A Non-Equilibrium Model for Hydrogen Combustion in Supersonic Flow, " *AIAA 23rd Joint Propulsion Conference,* San Diego, CA.

Correa, S.M., Gulati, A., and Pope, S.B., (1987), *Comb. Flame 72,* 159-173.

Correa, S.M., and Gulati, A. (1988), "Non-Premixed Turbulent CO/H_2 Flames at Local Extinction Conditions," *Twenty-second Symp. (Int.) Comb.,* Seattle, August 14-19.

Dahm, W.J.A. and Dimotakis, P.E., (1987), *AIAA Journal 25,* No. 9, 1216.

David, T., Gaskell, P.H., and Dixon-Lewis, G. (1986), *Twenty-first Symp. (Int.) Comb.,* The Combustion Institute, Pittsburgh, PA,.

Dibble, R.W. and Magre, P., (1987) *SANDIA Report 85-8601.*

Dibble, R.W., Masri, A., and Bilger, R.W., (1987), *Comb. and Flame 67,* 189.

Dixon-Lewis, G., David, T., Gaskell, P.H., Fukutani, S., Jinno, H., Miller, J.A., Kee, R.J., Smooke, M.D., Peters, N., Effelsburg, E., Warantz, J., and Behrendt, F., (1984), *Twentieth Symp. (Int.) on Comb.,* The Combustion Institute, 1893.

Dixon-Lewis, G., Goldsworthy, F.A., and Greenberg, J.B., (1975), *Proc. Roy. Soc. London A 346,* 261-278.

Drake, M.C. and Kollmann, W., (1985), "Slow Chemistry Nonpremixed Flows," *Evaluation of Data*

on Simple Turbulent Reacting Flows (W.C. Strahle, ed.), AFOSR TR-85 0880.

Drake, M.C., (1985), "Kinetics of Nitric Oxide Formation in Laminar and Turbulent Methane Combustion," *Report GRI-85/0271,* Gas Research Institute, Chicago, Ill.

Drake, M.C., Correa, S.M., Pitz, R.W., Shyy, W., and Fenimore, C.P., (1987), *Comb. Flame 69,* 347-365.

Drake, M.C., Pitz, R.W., Correa, S.M., and Lapp, M., (1984), *Twentieth Symp. (Int.) on Comb.,* 1983-1990.

Drake, M.C., Bilger, R.W., and Starner, S.H., (1982), *Nineteenth Symp. (Int.) on Comb.,* The Combustion Institute, Pittsburgh, 459-467.

Gulati, A. and Correa S.M., (1987), "Local Extinction Due to Turbulence in Non-Premixed Flames," *AIAA Paper 87-1717.*

Hornung, H.G., and Schoeler, H., (1985) *AIAA J. 23,* 7, 1121.

Janicka, J. and Kollmann, W., (1982), *Combust. Flame 44,* 319-336.

Janicka, J. and Kollmann, W., (1979), *Seventeenth Symp. (Int.) on Comb.,* The Combustion Institute, Pittsburgh, 421-430.

Kent, J.H. and Bilger, R.W., (1976), *Sixteenth Symp. (Int.) on Comb.,* The Combustion Institute, Pittsburgh, PA, 1643-1656.

Koochesfahani, M.M., Dimotakis, P.E., and Broadwell, J.E., (1985), *AIAA J. 23-8,* 1191-1194.

Lapp, M., Drake M.C., Penney, C.M., Pitz, R.W., and Correa, S.M., (1983), "Turbulent Combustion Experiments and Modeling," *General Electric Company Report 83CRD049,* DoE Contract DE-AC04-78 ET 13146.

Launder, B.E., Reece, G.J., and Rodi, W., (1975), *J. Fluid Mech. 68,* 537-566.

Libby, P.A. and Williams, F.A., (1980), ed., *Turbulent Reacting Flows,* Springer-Verlag, New York.

Liew, S.K., Bray. K.M.C., and Moss, J.B., (1984), *Comb. Flame 56,* 199-213.

Liew, S.K., Bray. K.M.C., and Moss, J.B., (1981), *Comb. Sci. Tech. 27,* 69-73.

Miller, J.A., Kee, R.J., Smooke M.D., and Grear J.F., (1984), "The Computation of the Structure and Extinction Limit of a Methane-Air Stagnation Point Diffusion Flame," *Western States/CI Paper 84-20.*

Monat, J.P., Hanson, R.K., and Kruger, C.H., (1979), *Seventeenth Symp. (Int.) on Comb.,* The Combustion Institute, Pittsburgh, 543-552.

Moses, J., "Symbolic Integration," PhD Thesis, Massachusetts Institute of Technology, Cambridge, MA, (1967).

Peters, N. *Progress in Energy and Combustion Science, 10* p. 319 (1984).

Pope, S.B., (1985), *Progress in Energy and Combustion Science 11*, 119-192.

Pope, S.B. and Correa, S.M., (1986), *Twenty-First Symp. (Int.) on Comb.,* The Combustion Institute, Pittsburgh, 1341-1348.

Pope, S.B., (1981), *Phys. Fluids 24,4*, 588-596.

Patankar, S.V. and Spalding, D.B. (1972), "Heat and Mass Transfer in Boundary Layers," Intertext books, London.

Roquemore, W.M., Bradley, R.P., Satutrud, J.S., Reeves, C.M., and Krishnamurthy, L., (1980), "Preliminary Evaluation of a Combustor for Use in Modeling and Diagnostics Development," *ASME Paper No. 80-GT-93.*

Roquemore, W.M., Britton, R.L., and Sandhu, S.S., (1982), "Investigation of the Dynamic Behavior of a luff-Body Diffusion Flame Using Flame Emission," *AIAA Paper No. 82-0178.*

Tsuji, H. and Yamaoka, I., (1970), *Thirteenth Symp. (Int.) on Comb.,* The Combustion Institute, Pittsburgh, PA, 723-731.

Westbrook, C.K. and Dryer, F.L., (1981), *Eighteenth Symp. (Int.) on Comb.,* The Combustion Institute, Pittsburgh, 749-767.

Schlicting, H. (1979), "Boundary Layer Theory," McGraw Hill, New York, NY.

Van Dyke, M.D., and Guttmann, A.J.,*J. Austral. Math. Soc., Ser. B, 24,* 243, (1983).

5. PUBLICATIONS RELATED TO WORK PERFORMED UNDER THIS CONTRACT

Excepting [5], the following were wholly or partially funded by this contract. [5] draws on the partial equilibrium model assessed in the course of this contract.

[1] Correa, S.M. and Gulati, A.,"Non-premixed Turbulent CO/H_2 Flames at Local Extinction Conditions," accepted in Twenty-Second Symposium (International) on Combustion, Seattle, WA, August 1988.

[2] Correa, S.M., Gulati, A. and Pope, S.B., "Assessment of a Partial-Equilibrium Monte-Carlo Model for Turbulent Syngas Flames," Combust. Flame, 72, pp. 159-173, (1988).

[3] Correa, S.M. and Shyy, W., "Computational Models and Methods for Continuous Gaseous Turbulent Combustion," Prog. Eng. and Comb. Sci., 13, pp. 249-292, (1987).

[4] Drake, M.C., Correa, S.M., Fenimore, C.P. and Shyy, W., "Superequilibrium and Thermal Nitric Oxide Formation in Turbulent Diffusion Flames," Comb. and Flame, 69, pp. 347-365, (1987).

[5] Correa, S.M. and Mani, R., "A Non-Equilibrium Model for Hydrogen Combustion in Supersonic Flow," AIAA Paper No. 87-1961, (1987).

[6] Gulati, A. and Correa, S.M., "Local Extinction Due to Turbulence in Non-premixed Flames," AIAA Paper No. 87-1717, (1987).

[7] Pope, S.B. and Correa, S.M., "Joint PDF Calculations of a Non-Equilibrium Turbulent Diffusion Flame," Twenty-First (International) Symposium on Combustion, The Combustion Institute, Pittsburgh, PA, pp. 1341-1348, (1986).

[8] Correa, S.M., "A Model for Non-Premixed Turbulent Combustion of CO/H_2 Jets," IX International Symposium on Combustion Processes, Archivium Combustionis, 5, Nos. 3-4, pp. 223-242 (1985).

6. PROFESSIONAL PERSONNEL

DR. SANJAY M. CORREA

Aerospace Engineer

EDUCATION

BSE, MSE, and PhD, University of Michigan, 1977, 1979, and 1981.

EXPERIENCE

Dr. Correa's fields of research are turbulent combustion and computational fluid mechanics. Following a theoretical doctoral study of the group behavior of liquid drops forming a cloud, he joined the GE Research and Development Center in 1981. He is currently developing numerical models based on fundamental studies in turbulent diffusion flames. The work, on physical models for turbulence and turbulence-chemistry interactions and on advanced numerical techniques, has led to models for combustion phenomena such as pollutant formation, local extinction, scramjet performance, and so on. Other research areas have included the prediction of transitional and turbulent plasma jet flows, natural convection and halogen chemistry in lamps, computational studies of Marangoni and magnetohydrodynamic flows in liquid metals, the development of comprehensive kinetic models for "dirty" and off-stoichiometric combustion of methane and optical sensors for compressible flows. He was instrumental in the development of the supersonic wind-tunnel facility at the Center and is the principal investigator on internally and externally funded programs involving combined modelling/laser diagnostics studies. He was a member of the GE National Aerospaceplane team and has continued to work on company-funded scramjet propulsion programs.

Dr. Correa has authored or coauthored over 25 scientific papers and holds one U.S. patent. He serves on the Propellants and Combustion Technical Subcommittee of the AIAA.

DR. ANIL GULATI

Aeronautical Engineer

EDUCATION

B. Tech., Mechanical Engineering, Indian Institute of Technology Kanpur, India, 1981; M.S., Mechanical Engineering, Pennsylvania State University, 1983; Ph.D., Aerospace Engineering, University of Michigan, 1986.

EXPERIENCE

Dr. Gulati joined GE Research and Development Center in July 1986 after completing his PhD at the University of Michigan. His doctoral thesis involved simultaneous measurement of density and velocity in a premixed turbulent flame using Rayleigh scattering and laser velocimetry. These measurements, obtained for the first time in premixed flames, were used to assess the Bray-Moss-Libby model for premixed flames. His current research interests at GE involve the study of blowout and extinction due to turbulence in high Reynolds number diffusion flames using Raman diagnostics. He is responsible for all laser based diagnostics including PLIF, Raman and Laser Velocimetry for subsonic and supersonic flow applica tions, and he is co-principal investigator on externally funded programs involving combined laser diagnostics/modeling studies. He is also currently working on exploring passive and active means to control unsteady combustion oscillations.

Dr. Gulati has published several papers in combustion-related journals and the AIAA Journal.

7. INTERACTIONS

Information and insights obtained in these studies have been communicated at

- Sandia Cooperative Group on Aerothermochemistry of Turbulent Combustion (March and October, each year).
- National Aerospace Project Quarterly Review (DARPA/USAF) meetings and technical workshops (October 1986; January, February, May 1987) at General Electric Aircraft Engine Group. The scientific implications of this work to high-altitude combustion were discussed.
- Open technical meetings and journals as per Section 5.